CRUSTAL MAGNETISM

Michael E Purucker
SGT at Planetary Geodynamics Laboratory, Code 698
Goddard Space Flight Center/NASA
Greenbelt, MD 20771
U.S.A.
Michael.e.purucker@nasa.gov
+1 301 614 6473

Kathryn A. Whaler
School of GeoSciences
Grant Institute
West Mains Road
Edinburgh EH9 3JW
Scotland, U.K.
Kathy.whaler@ed.ac.uk
+44 (0)131 650 4904

Chapter 6
Volume 5: Geomagnetism
M. Kono (ed.)
Elsevier Treatise on Geophysics
3 July 2013
Version 1.8

8. Separation of Induced and Remanent Magnetization

Abstract

Crustal magnetic fields were first measured systematically by airborne surveys in the 1930s. Today, crustal magnetic fields are also measured in boreholes, from ships and balloons, and from terrestrial and planetary spacecraft. Metamorphism, petrology, and redox state all have important effects on the magnetism of crustal materials. Mapping of the crustal magnetic field provides a 3rd dimension to surface observations of the Earth's composition and geologic structure, and a suite of mathematical tools has been developed to assist with this interpretation. Studies of crustal magnetism have contributed to geodynamic models of the lithosphere, geologic mapping, and petroleum and mineral exploration. Inferences from crustal magnetic fields, interpreted in conjunction with other information, can locate geologic features which have a magnetic contrast with their surroundings. Present-day efforts are focused on 1) the enhancement of a global, near-surface map of the crustal magnetic field that integrates airborne and satellite coverage, 2) developing the techniques at other planets and moons of our solar system, and 3) extending regional and detailed mapping as an exploration and reconnaissance tool.

Keywords

Crust Lithosphere Magnetism Magnetic fields Mathematical techniques

Nomenclature

P	Pressure
τ	Temperature
t	time
Ma	Million Years
μ_0	permeability of free space
v	volume
v_f	volume fraction of magnetite
F	Non-crustal magnetic field
M	magnetization
$\mathbf{M}_r$	Remanent magnetization
$\mathbf{M}_i$	Induced magnetization
B	magnetic induction
H	magnetic field intensity
Q	Koenigsberger ratio
V	scalar potential
d	magnetic source-observation distance
χ	magnetic susceptibility
ΔT	Total field anomaly
T	Total field
s_i	Structural index or attenuation rate
g_n^m, h_n^m	spherical harmonic coefficients

$P_n^m(\cos\theta)$ Schmidt quasi-normalized associated Legendre functions of degree n and order m

a	radius of Earth
A	Analytic signal
G	Green's function
Γ	Gram matrix
ϕ	Longitude
θ	Colatitude

6.01.1 INTRODUCTION

6.01.1.1 *Definition*

Crustal magnetism is defined as magnetism originating from rocks below their Curie temperature, in the Earth's crust and uppermost mantle. The dominant magnetism is associated with igneous and metamorphic rocks, whereas sedimentary rocks generally have subordinate, but measurable magnetism. Magnetism of these ferri- and ferro-magnetic materials is a function of temperature, with a loss of magnetism as the materials approach their Curie temperature (typically 200-700 deg C). The increase of temperature with depth in the Earth means that rocks below a certain depth, termed the Curie depth, will be nonmagnetic. This depth is typically in excess of 20 km in stable continental regions.

6.01.1.2 Measurement

The measurement of crustal magnetism is done utilizing total and vector field magnetometers, and associated gradiometers. The total field magnetometers exploit fundamental resonances (Primdahl 2000) to measure the magnitude of the field, whereas the vector instruments typically utilize fluxgate magnetometers (Ripka 2000). The magnetometers measure these fields from borehole, ground-based, marine, aerial, balloon, or satellite platforms.

6.01.1.3 Governing equations

The magnetic induction $B^{(\eta)}(\mathbf{r_j})$ of the η component of the magnetic field due to a magnetization distribution **M** is given by:

$$B^{(\eta)}(\mathbf{r}_j) = -\hat{\mathbf{l}}_j^{(\eta)} \cdot \nabla_{\mathbf{r}_j} \int_v \left\{ \frac{\mu_0}{4\pi} \nabla_s \frac{1}{|\mathbf{r}_j - \mathbf{s}|} \right\} \cdot \mathbf{M}(\mathbf{s}) dv \qquad (6.1.1)$$

where $\hat{\mathbf{l}}_j^{(\eta)}$ is the unit vector in the η direction, v is the volume of the magnetized crust, and the quantity in brackets is the Green's function relating magnetization **M** to magnetostatic potential V. The subscript on the gradient (∇) operator indicates whether derivatives are with respect to observation point coordinates ($\mathbf{r}_j$) or locations within the magnetized crust (**s**). The magnetization **M** is the vector sum of remanent magnetization $\mathbf{M}_r$ and induced magnetization $\mathbf{M}_i$.

$$\mathbf{M} = \mathbf{M}_i + \mathbf{M}_r \qquad (6.1.2)$$

In the case of terrestrial crustal magnetic field observations, what is often measured is the total field, the magnitude of the total magnetic field without regards to its vector direction. The total field anomaly (ΔT) is then

$$\Delta T = |\mathbf{T}| - |\mathbf{F}| \tag{6.1.3}$$

where $|\mathbf{T}|$ is the magnitude of the magnetic field, and $|\mathbf{F}|$ is the magnitude of the (largely) non-crustal field, determined from a global or regional model. If vector data are available, the total field anomaly is calculated as

$$\Delta T = \hat{\mathbf{F}} \cdot \mathbf{T} \tag{6.1.4}$$

where $\hat{\mathbf{F}}$ is the unit vector in the direction of **F**. The geometry of a total field anomaly of a magnetic body dominated by induced magnetization is dependent on the geometry of the inducing field. At high latitudes an induced magnetization will give a total field anomaly high (positive) over the source, whereas at low latitudes an induced magnetization will yield a total field anomaly low (negative).

6.01.1.4 Previous reviews

Book length reviews include those of Langel and Hinze (1998), Blakely (1995), Lindsley (1991), Hahn and Bosum (1986), Grant and West (1965), the Encyclopedia of Geomagnetism and Paleomagnetism (Gubbins and Herrero-Bervera, 2007) and Hinze, von Frese and Saad (2013). Shorter articles, within books or encyclopedias, have included Shive et al. (1992), Frost (1991a,b,c), Reynolds et al. (1990c), Blakely and Connard (1989), Harrison (1987), Bosum et al. (1985), Haggerty (1976), Zietz and Andreasen (1967), Purucker and Clark (2011), Langlais et al.(2009), Thébault et al. (2010) and Schott and Thébault (2011). Reviews in journals include those of Mandea and Purucker (2005), Nabighian *et al*. (2005), Nabighian and Asten (2002), Clark (1997, 1999), Phillips *et al.* (1991), Keller (1988), Mayhew and LaBrecque (1987), Paterson and Reeves (1985), Grant (1985), Mayhew et al. (1985), Haggerty (1979), Hinze (1979), Zietz and Bhattacharyya (1975) and Robinson et al. (2008) Bibliographies include Langel and Benson (1987) and Hill (1991), and online at http://crustal.usgs.gov/geophysics/North_America.html.

6.01.1.5 Computer software and applications

Computer software for crustal magnetic field applications includes a collection of Fortran subroutines in Appendix B of Blakely (1995). Another software resource is the potential field software programs of the U.S. Geological Survey (Phillips, 1997). Matlab and Fortran routines for the evaluation of spherical harmonic models are described in Olsen et al. (2006a). Other Fortran-based tools for working with spherical harmonics include SHTOOLS (cf. Wieczorek et al., 2012), an archive of Fortran 95 based software that can be use to perform spherical harmonic transforms and reconstructions, rotations, and multitaper spectral analyses. The transforms are demonstrated to be accurate through spherical harmonic degree 2800, and have been optimzed for speed. Transforms are calculated using quadrutures, either via the sampling theorem of Driscoll and Healy (1994) or Gauss-Legendre quadrature. Programs for high degree spherical harmonic analysis and synthesis (Adams and Swarztrauber, 1997) are associated with Spherepack. Occasionally, the journal *Computers and Geosciences* includes articles of relevance. The

'Numerical Recipes' books (Press et al., 1992, 1996, 1997) are another resource for inverse codes, sparse matrix theory, wavelets, interpolation, and Fourier and spectral applications. The publicly available Generic Mapping Package (GMT) is useful for both producing maps, and for analysis of potential field data. It is documented in Wessel and Smith (1998). Commonly used commercial codes include Geosoft, Matlab, and IDL.

Online applications include those for the evaluation of terrestrial and planetary magnetic fields of the Solar System (Nicholas et al., 2011), the International Geomagnetic Reference Field (Maus and Macmillan, 2005), and the Atlas of Structural Geophysics (Jessel, 2002).

6.01.1.6 Structure of the remainder of the chapter

The remainder of this chapter begins with a summary of the salient points of magnetic petrology. We then outline the utility of crustal magnetism through a series of case studies, and discuss compilations to produce models at continental or larger scale. This is followed by details of the processing, transformation and modeling methods that are applied to crustal magnetic data to facilitate interpretation. The issue of the separation of the various contributions to the measured magnetic field is then addressed, and we conclude with one of the key outstanding questions, identifying the induced and remanent components of magnetization. We have included within the references both papers which we have cited within the text of the review, and others, which, while important, we were unable to discuss because of space limitations.

6.01.2 MAGNETIC PETROLOGY

An understanding of the processes that create, alter, and destroy magnetic minerals in rocks is the province of magnetic petrology (Lindsley, 1991; Clark, 1997; Purucker and Clark, 2011). This field integrates rock magnetism (see Chapter 8) and petrology to address questions such as the effects of metamorphism, hydrothermal alteration, rock composition, and redox state on magnetic properties. Magnetic minerals of major importance to an understanding of crustal magnetism are the Fe-Ti spinel group (magnetite and titanomagnetite), the rhombohedral titanohematites, and monoclinic pyrrhotite. These minerals can possess remanent (permanent) or induced (in response to an inducing field) magnetizations. Induced magnetization is, to first order, proportional to, and parallel to the direction of, the inducing field. The proportionality constant χ is called the magnetic susceptibility, and the governing relationship is of the form $|\mathbf{M}| = \chi|\mathbf{H}|$. Magnetic susceptibility in many rocks is strongly controlled by their magnetite content and the empirically determined relationship (Shive et al., 1992) is

$$\chi \approx 0.2 \times 4\pi v_f \qquad (6.1.5)$$

where χ is the susceptibility and v_f is the volume fraction of magnetite. Many authors use k for susceptibility.

Magnetic remanence, on the other hand, while also correlated with titanomagnetite content, is strongly dependent on the grain size, shape, and microstructure of the magnetic minerals. The Koenigsberger ratio (Q) measures the relative strengths of the induced and remanent magnetizations. It is given by $|\mathbf{M_r}|/|\mathbf{M_i}|$. Hence, Q's greater than unity indicate dominance by remanent magnetization; Q values of less than unity indicate dominance by induced magnetization. Representative tables and values of susceptibility and Q can be found in Clark (1997).

The magnetic properties of igneous and metamorphic rocks are a reflection of the partitioning of iron between oxide and silicate phases, and do not correspond to standard petrologic classifications. This partitioning occurs in the near-surface realm (Clark, 1997) and probably also within the deep lithosphere (cf. Wasilewski and Mayhew, 1992). Standard sedimentary rock classifications, on the other hand, do show a correspondence with magnetic properties. Fe-rich chemical sediments (e.g. Banded Iron Formations) and immature clastic sediments with abundant magnetite are two strongly magnetic sedimentary rock types, for example. Iron sulphide minerals, possibly associated with hydrocarbon migration or abiologic processes, may also produce subtle magnetic anomalies over sedimentary basins (Reynolds et al. 1991, 1994), but the processes are still controversial and an active area of research (Stone et al., 2004).

Igneous and metamorphic rock types (e.g. granodiorite, rhyolite, gabbro) often exhibit bimodal susceptibility distributions, a reflection of ferromagnetic and paramagnetic populations (cf. Figure 7 in Clark, 1999). This was first recognized as a consequence of the very large petrophysical sampling program conducted on the Fennoscandian shield

(cf. Korhonen et al., 1993). Iron in the paramagnetic population is incorporated into silicate phases, whereas iron in the ferromagnetic population is typically in magnetite.

The magnetic petrology of granitic rocks provides an example of this bimodal distribution, with the relatively oxidized, magnetite-rich, I-type granitoids contrasting with the relatively reduced, ilmenite-rich, S-type granitoids (Clark, 1999). These granitoid-types can often be distinguished by the presence of common minor minerals. Hornblende-biotite granodiorites are usually ferromagnetic, whereas muscovite-biotite granodiorites are not (Clark, 1997). Economic mineralization (Cu, Au, Mo, Sn) also shows patterns (Ishihara, 1981) that are controlled in part by this classification.

Although the rule of thumb that basic rocks are more magnetic than silicic rocks is often violated, rocks from within a single igneous province are more likely to show this tendency than are larger population samples. Hence, interpretation of magnetic surveys should include investigation of the magnetic properties of representative rock samples when possible. Within-province generalizations also find that basalts have slightly higher susceptibilities than related andesites, but phonolites are weakly magnetic. Rhyolites also exhibit a bimodal susceptibility distribution. Rhyolites which are under- or over-saturated with respect to alumina, or which contain iron-rich olivine, are likely to be weakly magnetic (Clark, 1999).

Rapidly chilled basaltic rocks are characterized by high Q values, and the Q-ratio is strongly correlated to the distance from the chilled margin. As long as the primary remanent magnetization has not been chemically or thermally modified, even relatively thick sills and dikes have high Q values.

Hydrothermal alteration generally destroys magnetite, and replaces it with paramagnetic phases like zeolites, clays, or more weakly magnetic minerals like titanohematite (Criss and Champion, 1984). One major exception to this generalization is that serpentinization of olivine-rich ultramafic rocks produces abundant magnetite with low Q values (Saad, 1969). Other notable exceptions include potassic alteration associated with magnetic felsic-intermediate intrusives (Sexton et al., 1995) and potassic and sodic alteration in deeper levels of iron-oxide copper-gold systems (Hitzman et al., 1992). Production of hydrothermal magnetite is enhanced in mafic protoliths.

Prograde and retrograde metamorphism can produce marked changes in magnetic properties, and these changes are dependent on the composition of the protolith, and the pressure (P), temperature (τ), and time (t) path of the metamorphism. For mafic igneous protoliths undergoing regional metamorphism, primary magnetite remains unchanged during zeolite to prehnite-pumpellyite grade metamorphism in the absence of hydrothermal fluids. Subsequent metamorphism to greenschist-grade converts the magnetite to chlorite, epidote, and hematite. In turn, these minerals give way to biotite and amphibole in the amphibolite facies of regional metamorphism. Magnetite is again created during granulite-grade metamorphism. At the highest metamorphic grade (eclogite), the iron returns to silicates such as clinopyroxene and garnet. For sedimentary protoliths the redox conditions prevailing during sedimentation and diagenesis, and the

iron content of the protolith, constrain the mineral assemblage produced during metamorphism.

The magnetic state of the lower crust remains poorly known. Although P and τ can be predicted, the protolith's history and current compositions are the subject of speculation. Because of the lower crust's elevated temperature, induced and viscous remanent magnetizations are expected to be strong (Shive et al., 1992). Inferences from deep drilling and seismic constraints (Prodehl and Mooney, 2012) suggest a generally mafic composition. A host of mineralogic and magnetic changes may occur, with maximum magnetizations in the granulite facies zone. Stable large remanence in ilmenite-hematite intergrowths (McEnroe et al., 2001a,b; McEnroe and Brown, 2000) within granulite-facies rocks provides another mechanism for producing magnetic rocks within the lower crust.

Two mechanisms have been suggested for large-scale magnetizations within the mantle. The conversion of metabasalt to eclogite within subducting oceanic crust releases large amounts of water into the surrounding upper-mantle peridotite, and may produce serpentinite (Hyndman and Peacock, 2003). As long as the mantle wedge in the subduction zone is cooler than the Curie temperature, it is possible that a significant magnetization may form. Blakely et al. (2005) have explained the long-wavelength aeromagnetic and gravity fields above the Cascadia forearc as an example of this process, using matched filters (Sec. 6.01.5.5.2.1) to establish the depth of the source, and a pseudo-gravity transform (Sec. 6.01.5.4.3) to center the magnetic fields over their source. Satellite magnetic anomalies over subduction zones are also common (cf. Clark et al. 1985; Vasicek et al., 1988, Purucker and Ishihara, 2005; Maus et al., 2006), and may have a similar explanation. A second mechanism for magnetizations in the mantle invokes the presence of metallic alloys, which have been detected in xenoliths originating from the upper mantle (Toft and Haggerty, 1988). Significant amounts of metal alloys in the upper mantle could impart magnetic behaviors to depths of almost 100 km. But questions remain about how representative of the upper mantle these metal alloys are (Frost and Shive, 1989, Toft and Haggerty, 1989).

While magnetic petrologic approaches have provided significant insights into the interpretation of crustal magnetism, there still remains the problem of extrapolating from field observations at micron- to hand-sample scale to scales appropriate for aeromagnetic or satellite observation. For example, even within the ferromagnetic population, the distribution of magnetization or susceptibility is usually log normal, and exhibits high variability. Parker (1991) has developed an inverse approach, which incorporates this variability into the creation and testing of a magnetization model. Some of this high variability can also be ascribed to surface processes, such as lightning (Verrier and Rochette, 2002) and weathering, which may not be observable from non-ground-based platforms.

6.01.3 CONTINENTAL AND OCEANIC MAGNETIC ANOMALIES

Because magnetic oxide or sulphide-bearing phases are commonly associated with other economic mineral phases, magnetic measurements play a significant role in mineral exploration. Mapping of the crustal magnetic field is a geologic and exploration tool in the terrestrial environment, and provides a 3rd dimension to surface observations of composition and structure. The magnetic method also contributes to plate tectonic theory, oil and gas exploration, structural geology, and geologic mapping. The generation of new seafloor at the ridge crest was established via the magnetic method. The symmetry of the magnetic patterns (Vine and Matthews, 1963) about the ridge crest is often cited as the breakthrough which led to the widespread acceptance of plate tectonics. The magnetic time scale (Heirtzler et al., 1968), suitably calibrated with numerical ages, serves many purposes in the Earth sciences. In particular, readers are referred to Chapter 12 for further details of crustal magnetism within the oceanic realm. Inferences from crustal magnetic fields, interpreted in conjunction with other geological and geophysical information, can locate kimberlite pipes, impact structures, plutons, ophiolites, and other geologic entities which have a magnetic contrast with their surroundings. This permits extrapolation from, or interpolation between, outcrops, drill holes, or regions of localized geophysical measurements into areas where surficial materials may obscure the feature. Magnetic studies can locate faults, folds, and unconformities, and describe their geometrical properties. Magnetic measurements provide constraints on the amount of sediment in a depositional basin by characterizing its depth and dimensions. Magnetic measurements can be used to infer heat flux, and the depth to the bottom of the magnetic crust, because magnetic properties are temperature dependent. Finally, crustal magnetic fields can help delineate suture zones or terrane boundaries, and unravel the history of volcanic terranes.

In the sections that follow, we use a case study approach to illustrate the utility of the magnetic method. We begin with the Chicxulub impact structure, showing how it was first recognized using a combination of aeromagnetic and gravity data, and how these data sets have been used to produce 3-dimensional (3-D) models of the structure. We proceed then to review geodynamical interpretations of aeromagnetic data that have been derived from dike swarms, and some of the caveats that must be considered. We then discuss structural and tectonic interpretations of aeromagnetic maps over forearc basins with Cenozoic to Recent faulting, and their role in assessing earthquake risk. We next illustrate how magnetics has been used to infer heat flux under the Antarctic ice cap, and how this may have applications in modeling ice flow, and in identifying undiscovered volcanic regions under the ice. In the exploration arena, we summarize the role of aero- and ground magnetic surveys in identifying diamond-bearing kimberlites from northern Canada. Finally, we review the structural inferences drawn from magnetic and gravity surveys over the West Siberian basin, and their relation to the world's largest gas field, the Urengoy. A case study approach such as this might also have included a demonstration of the utility of magnetics in determining the depth to basement in sedimentary basins, and its relevance in petroleum exploration. The proprietary nature of this kind of work means that while there are no shortage of articles discussing depth to basement techniques (e.g. Peters, 1949; Li, 2003; Thompson, 1982; Thurston et al. 2002; Thurston and Smith, 1997; Hsu et al., 1998; Ku and Sharp, 1983; Mushayandebvu et al., 2001, 2004; Naudy, 1971; Salem and Ravat, 2003; Silva et al., 2001,2003; Nabighian et

al., 2005), there is only a single volume (Gibson and Millegan, 1998) which focuses on the role of magnetics in an integrated hydrocarbon exploration program.

6.01.3.1 Chicxulub

Located below, and straddling the coastline of the northwest Yucatan, Mexico, the Chicxulub impact structure (Figure 1) is the world's most widely known impact, and produced major biologic and environmental changes at the end of the Cretaceous Period 65 Ma. The enhanced porosity associated with the collapse of nearby structures (Grieve and Therriault, 2000) from Chicxulub's associated seismic events has been linked to the development of large hydrocarbon deposits in the Campeche Bank region immediately to the NW. The impact site is now covered by up to1 km of carbonate rock. First recognized by its circular and coincident magnetic (Figure 1) and gravity signatures in the aftermath of a 1978 survey (Penfield and Camargo, 1981), the impact was subsequently tied to other diagnostic signatures such as an iridium anomaly and shocked quartz grains by direct drilling into the structure, and dating of the crystallization age of the melt rocks (Hildebrand et al. 1991; Sharpton et al 1992).

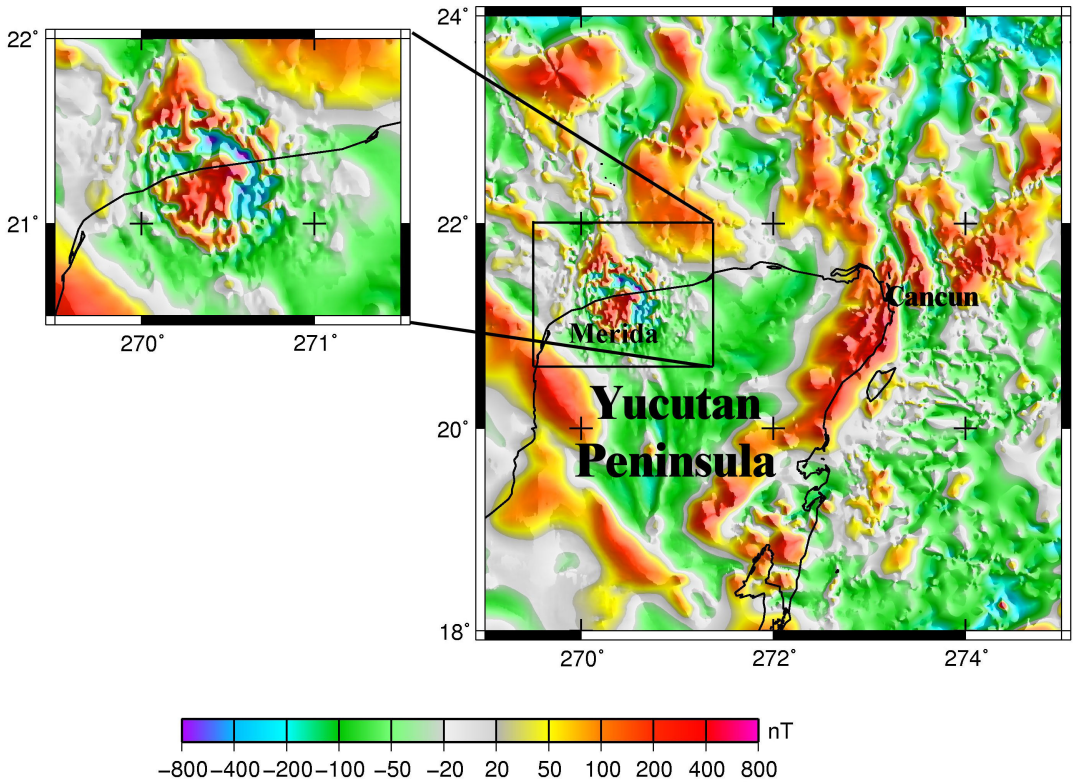

Figure 1. Total field anomaly (ΔT) over Chicxulub impact structure (Pilkington and Hildebrand, 2000), shown in an expanded view in the inset. Coastline shown as a solid line. Data interpolated to a 1 km grid from digital data grids of the magnetic anomaly map of North America (Bankey et al., 2002). Artificial illumination from the NNE and ESE. Mercator projection.

The magnetic signature consists of three concentric zones (Pilkington and Hildebrand, 2000) with radii of 20, 45, and 80 km. The impact occurred in a carbonate sequence several kilometers thick characterized by much longer (hundreds of kms) and weaker amplitude magnetic anomalies. The innermost zone is characterized by a single, high amplitude anomaly indicative of a single source. The middle zone consists of numerous, intermediate amplitude dipolar anomalies. The outermost zone consists of short-wavelength, low amplitude anomalies. The outermost zone is better defined by its gravity signature, and associated cenotes (fresh-water caves), than by its magnetic signature. In their recent interpretation of the aeromagnetic survey data, Pilkington and Hildebrand (2000) perform 3-D modeling of the crater structure by inversion using a two-layer model. The layers, at depths corresponding to the melt sheet and the basement surface, are inverted individually subsequent to separation via a wavelength filter (see 6.01.5.5.2.1 for the related concept of matched filter). The inner magnetized zones within the melt sheet are interpreted to result from hydrothermal activity at the edge of the central uplift and the collapsed disruption cavity. Although some lines of evidence (Snyder et al., 1999) suggest that Chicxulub may be a multi-ring impact structure, the magnetic data as currently modeled resolve only a single ring with a central peak. Although the magnetic signature of Chicxulub is distinctive, a variety of magnetic signatures are encountered in other terrestrial impact structures (Pilkington and Grieve 1992; Grieve and Therriault 2000; Shah et al 2005; Goussev et al., 2003; Grieve et al., 2008), dependent on the target rocks, impact magnetizations, and subsequent evolution of these metastable assemblages. A magnetic low is frequently encountered, due to a reduction in magnetic susceptibility. Large structures such as Chicxulub tend to exhibit a central high-amplitude anomaly. Imaging techniques that emphasize the edges of magnetic bodies via derivatives, or via artificial illumination in one or more directions (Wessel and Smith, 1998) are commonly employed adjuncts to magnetic survey interpretation of impacts. Specific extensions to impact, and other circular features (e.g. kimberlite pipes) within magnetic data, include circular sunshading as described by Cooper (2003) and Cooper and Cowan (2003), and fractional derivatives (Cowan and Cooper, 2005) for better matching to the available data. Finally, impact structures on extra-terrestrial bodies, such as the Moon and Mars, often have a magnetic signature (Purucker and Clark, 2011).

6.01.3.2 Dike Swarms

The Earth hosts hundreds of radiating, arcuate or linear mafic dike swarms (Ernst et al., 1996) whose mapping has contributed to improved geodynamic models of the Earth. In southern Africa alone, one digital database (Mubu, 1995) has enumerated 14000 dikes, mapped in large part because of their magnetic expression. While some of these dikes are exposed, most are not, and hence the magnetic method has played a crucial role in their understanding. These magnetically defined dike swarms have been used in global plate reconstructions, and locally to understand the kinematics of rifting. In addition, dikes define fractures and shear zones (Figure 2), along which economic mineralization is often found.

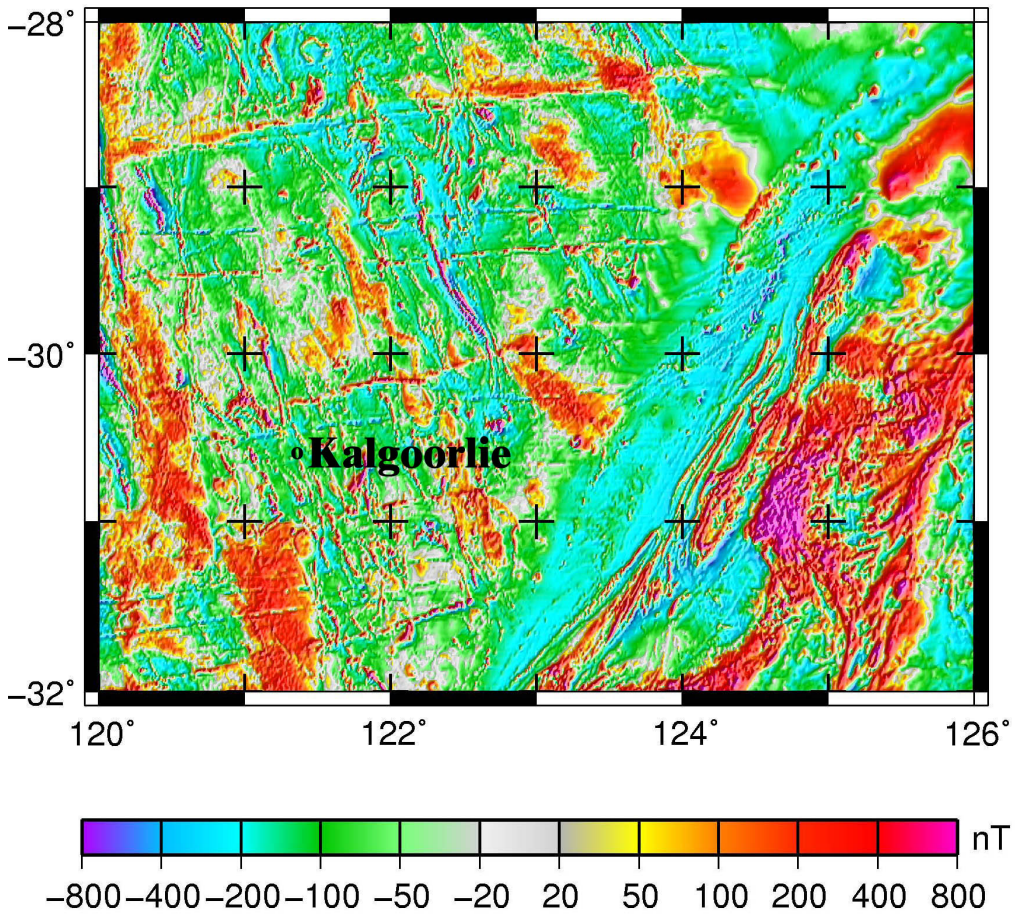

Figure 2. Total field anomaly (ΔT) over Australian dikes of the Archean Yilgarn craton. The E-W trending set seen here is part of the Widgiemooltha dike swarm, dated at 2410 Ma. Map based on a 1 km grid rendition of the Magnetic Anomaly Grid Database of Australia (Milligan et al., 2005). Artificial illumination from the East and Southeast. The Kalgoorlie gold and precious metal district is located in the central portion of the figure. Many of the ore deposits in this district are localized along fractures and shear zones (Weinberg et al., 2004). Mercator projection.

Mafic dikes provide evidence for magmatic activity, large igneous provinces, and mantle plumes (Ernst and Buchan, 2001; Soederlund et al., 2010), and are especially useful in older rocks where erosion has removed much of the other evidence for igneous activity. In these older rocks it is frequently only the dikes, representing the igneous plumbing system, that survive. Although dikes are often interpreted as paleo-stress markers they can also reflect the pre-existing structure of the lithosphere. The Jurassic dikes of southern Africa (Reeves, 2000; Chavez Gomez, 2001; Marsh, 2005), one of the manifestations of the Karoo large igneous province, have been used to enumerate plate motion associated with the break-up of Gondwana. For example, Ernst and Buchan

(1997) make the case that the convergence point of these Jurassic dikes defines the location of a paleoplume. The dikes here consist of four distinct swarms, the Okavango, the Save-Limpopo, the Olifants River, and the Lebombo. Dikes of both Jurassic and Proterozoic age have been identified within the ESE-trending Okavango dike swarm (Jourdan et al., 2006), suggesting that the Jurassic events represent the reactivation of a pre-existing trend, and calling into question Jurassic kinematic reconstructions made using these dikes. Many older dike swarms are now dismembered, as in the well-documented Central Atlantic dike swarm of Africa, North and South America (May, 1971). Magnetic identification of dikes relies on simple pattern matching from contour maps generated from simple source geometries (Vacquier et al., 1951). The depth to the top of dikes can be a valuable indicator of the kinematics of post dike faulting (Modisi et al., 2000). In Modisi et al.'s (2000) study, determinations of the depth to the tops of dikes were made using Euler's homogeneity equation (see section 6.01.4.7). Although the magnetic signature of a dike is usually easy to recognize, little attention has been directed to the important problem of magnetically recognizing dikes of common trend but dissimilar ages from within a single swarm. There are likely to be significant differences in magnetic signature, although the identification and mapping of these differences will require inputs from both field and laboratory studies. Dike swarms are also common on other planets and satellites within the solar system, and in at least one case, within the South Pole-Aitken basin of the Moon, they possess a signficant magnetic contrast with the host rock (Purucker et al., 2011).

6.01.3.3 Cenozoic-Recent faulting in forearc basins

Forearc basins around the Pacific Rim are the site of devastating earthquakes because of their proximity to large population centers (Olsen et al., 2007). Three types of earthquakes (mega thrust contact, deep intra-slab, and shallow) are commonly encountered in these basins (Saltus et al., 2005). The faults that host earthquakes occurring along shallow crustal faults in the overriding continental plate can sometimes be located with high-resolution magnetic surveys. The Seattle fault zone, an east-trending zone of reverse faulting extending through Seattle, Washington, was the site of a M 7 earthquake about 1100 years ago (Bucknam et al., 1992), and is an example of such a fault. Mapped geologically and with an aeromagnetic survey (Blakely et al. 2002), and studied along several profiles with seismic reflection surveys, this region hosts a tripartite package of rocks in close proximity to the fault zone. The package has a distinct magnetic signature, and allows the fault zone to be traced in areas of poor exposure, or where it is covered. From north to south, the package consists of a magnetic Miocene volcanic conglomerate, a thick sequence of nonmagnetic marine and fluvial rocks, and variably magnetic volcanic and sedimentary rocks of Eocene age. After accounting for remanent magnetization, the magnetic contacts were picked objectively (Blakely and Simpson, 1986). Near-surface features of this magnetic survey have also been enhanced using a matched filter approach (Syberg, 1972; Phillips, 1997, and see Section 6.01.5.5.2.2). The deformation front of the Seattle fault zone, as revealed by the seismic reflection data, lies immediately north of, and locally coincident with, the magnetic conglomerate. The aeromagnetic survey can also provide information on individual strands of the fault zone, and whether it is segmented (Blakely et al., 2002). The longer wavelength information within these aeromagnetic surveys (Finn, 1990; Blakely et al., 2005, Wells et al., 1998)

can be used to provide a regional context for the tectonics of the Cascadia forearc region that hosts these basins.

6.01.3.4 Heat flux beneath the Antarctic ice sheet

Using magnetic data to infer heat flux is possible because the magnetic properties of rocks are temperature dependent, and at the Curie temperature rocks lose their magnetism. The geothermal heat flux is an important factor in the dynamics of ice sheets, the occurrence of sub glacial lakes and ice streams, and may affect the mass balance. Direct heat flux measurements in ice covered regions are difficult, thus Fox Maule et al. (2005) developed a method using first-order features of the satellite magnetic data to estimate the heat flux underneath the Antarctic ice sheet. They found that it varies from 40 to 185 mW/m^2, that areas of high heat flux coincide in part with known current volcanism, sub glacial lakes, and ice streams, and that some areas landward of the Ronne ice shelf near the shoulder of the West Antarctic rift system may host active, but undiscovered, sub-ice volcanic regions.

Traditional methods for inferring heat flux, or the related magnetic problem of inferring the bottom of the magnetic crust, have relied on the shape of radially averaged spectra from gridded aeromagnetic data sets (Spector and Grant, 1970; Maus et al., 1997; Bouligand et al., 2009). To quote Blakely (1995), 'this calculation ranks among the most difficult in potential field inversion'. At all wavelengths the contribution from the bottom of the magnetic source is dominated by contributions from the top. The top of the source must be also be known, in itself a difficult problem. The estimate of the bottom focuses on the lowest wave numbers, which overlap with poorly known regional fields that may be unrelated to the bottom of the magnetic bodies. There also exists a dependence on the characteristic shape of the magnetic bodies, and an assumption about the magnetization distribution. Assuming the magnetization is spatially uncorrelated ('white') is common, although magnetic susceptibility distributions are often correlated (Pilkington and Todoeschuck, 1995).

The method of Fox Maule et al. (2005, 2009) uses a self-consistent compositional and thermal model of the mantle and crust (Nataf and Ricard, 1996) as a starting point, which is then modified in an iterative fashion with the satellite data until the magnetic field predicted by the model matches the observed magnetic field within some specified error. At the scale of the surveys used (400+ km wavelength), a unique solution is guaranteed by assuming that induced magnetizations dominate over remanent magnetizations in continental crust, and that vertical crustal thickness variations dominate over lateral susceptibility variations (Purucker and Ishihara, 2005). The resulting magnetic crustal thickness is then used as one boundary condition in a thermal model of the continental crust, assuming 1D heat conduction, and using a simple model to account for radioactive heat production in the crust. The largest complications and uncertainties in this approach are 1) uncertainties in determining the magnetic field model in the dynamic, high-latitude auroral, sub-auroral, and polar cap region, 2) the starting seismic and thermal model, 3) uncertainties in the upper and lower temperature boundary conditions, 4) lateral

variations in thermal conductivity, and 5) lateral variations in (viscous) remanent magnetization.

6.01.3.5 Northern Canadian Kimberlite province

Diamond-bearing kimberlites were first recognized in rocks of cratonic North America more than 150 years ago. Exploration interest focused on the Slave Craton in Canada beginning in the 1970s, and the discovery of diamond-bearing kimberlites in the early 1990s set off a mineral staking rush (Krajick, 2001). By 2004 these deposits accounted for 15% of global diamond output by value. The exploration program relied on a complementary suite of geochemical and geophysical techniques, of which the magnetic technique was one (Reed and Witherly, 2007). Exploration usually proceeded from a program of indicator mineral sampling, to one of geophysical surveys in favorable regions, and finally to drilling in order to prove the deposits (Power et al., 2004). Airborne total magnetic field and electromagnetic surveys, and follow-up ground surveys, were the most common geophysical surveys performed (Jansen and Witherly, 2004), although sometimes gravity, ground-penetrating radar, and seismic techniques were used. The kimberlite host rock often exhibits a positive magnetic susceptibility contrast, and a strong remanence, compared to the surrounding country rock, commonly a high-grade metamorphic rock, or granite, in the Slave craton. Kimberlite pipes are often found in geographically localized groups, frequently under lakes because of differential erosion, and the remanence directions within those groups is often similar. Kimberlite pipes are often associated with diabase dikes (see previous section for a discussion of their magnetic signature), and are also commonly intruded along pre-existing zones of weakness (regional faults, geological contacts), many of which will have magnetic signatures. A completely preserved kimberlite pipe may be several hundred meters wide, and is often pipe or carrot shaped (Macnae, 1979). The resulting magnetic anomalies are usually circular in form (because the area is near the magnetic pole; see section 6.01.5.4.2), and data enhancement techniques are similar to those used for impact craters (see section 6.01.3.1). The use of the analytic signal (see section 6.01.4.6), and a pattern recognition technique (Keating and Sailhac, 2004), has been shown to be of some use in identifying possible kimberlite target rocks.

6.01.3.6 Structural control of the Urengoy gas field

The West Siberian Basin, one of the world's largest sedimentary basins developed on continental crust, hosts a super giant gas accumulation in the Urengoy field (Littke et al., 1999). The hydrocarbons in the Urengoy are found in an anticlinal trap defined by rejuvenated graben faults (Gibson, 1998a; Grace and Hart, 1990). Aeromagnetic (Makarova, 1974) and gravity (Arctic Gravity Project, 2002) mapping (Figure 3) over this region reveals north-south trending positive anomalies that are fundamentally lithologic, originating in Permo-Triassic basalt now found in rift basins. The basalt in these buried grabens is of the same age (Reichow et al., 2002) as the bulk of the Siberian traps exposed further east on the Siberian platform.

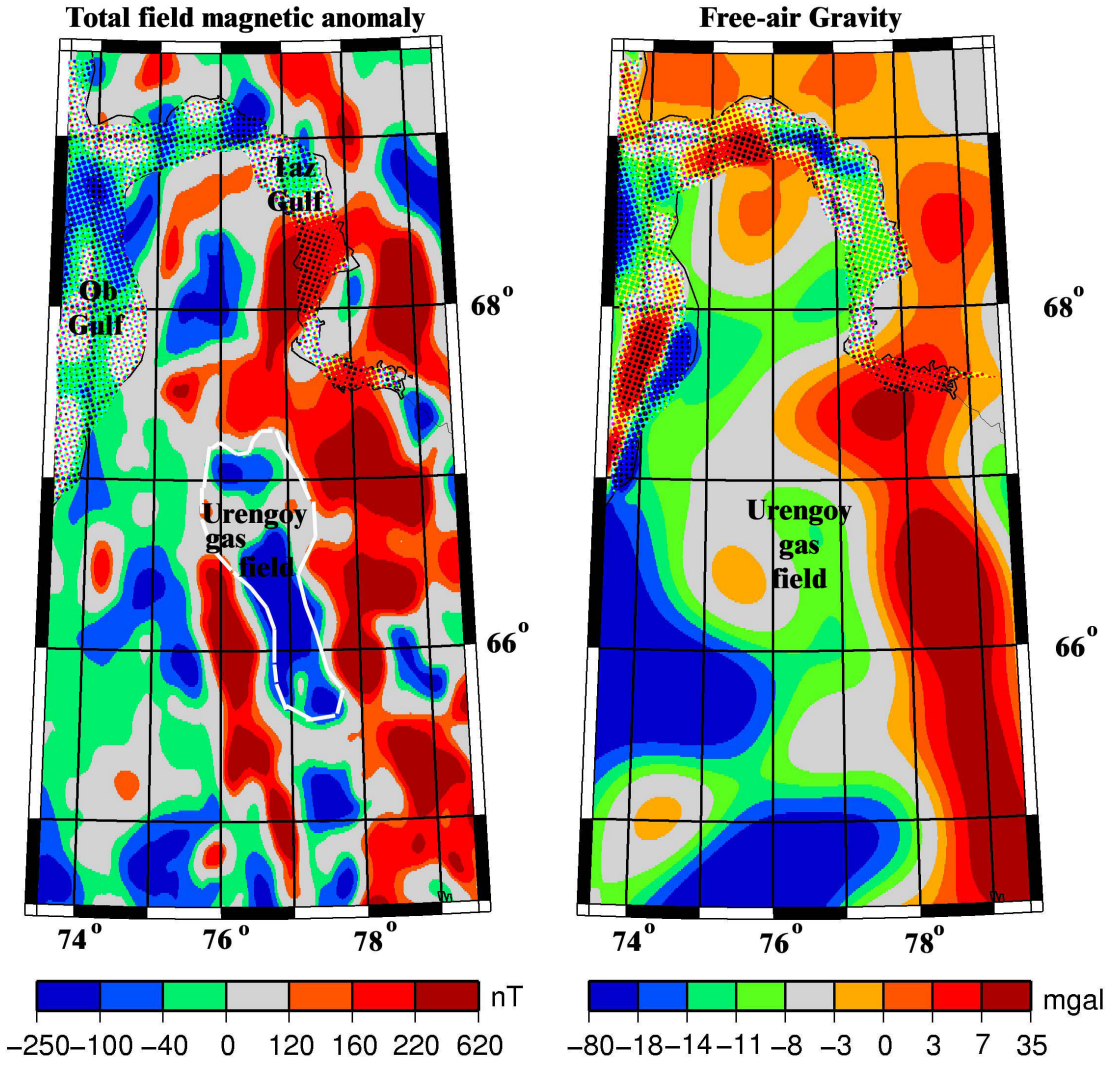

Figure 3. Aeromagnetic total field anomaly (ΔT) and free-air gravity maps of a portion of the West Siberian basin showing the correspondence of magnetic and gravity lows with the Urengoy gas field. This coincidence is a consequence of both lithologic and structural factors (Gibson, 1998b). The magnetic data are extracted from compilations of Makarova (1974), and Geol. Sur. Canada (1995), the gravity data come from the Arctic Gravity Project (2002), and the field boundaries of the Urengoy field are from Grace and Hart (1990). Lambert projection.

The Siberian traps, part of the largest recorded terrestrial flood basalt province, is contemporaneous with the end-Permian extinction (Erwin, 1994), the largest mass extinction of the Phanerozoic, although a causal relation between the two has not yet been established (Elkins-Tanton and Bowring, 2006). The West Siberian rift basins define the base of the sedimentary column, and subsequent post-rift deposition from the Jurassic to the Cretaceous consists of fluviatile and marginal marine sediments. The boundary faults of these basins were reactivated later, and hence the magnetic and gravity anomalies serve to reveal indirectly the faults that define the hydrocarbon trap. The graben faults were rejuvenated in the Early Cretaceous, and created broad arches in the

Cretaceous sediments. Maturation of Jurassic source rocks was followed by migration of hydrocarbons into traps located within the Pokur Formation of Cenomanian age.

6.01.4 Compilations and Models

Because maps of the crustal magnetic field are so useful for regional geologic understanding, and because magnetic surveys are usually acquired over small regions, there is a need to assemble the individual magnetic surveys into larger compilations. This assembly is often assisted by the addition of longer, higher altitude magnetic surveys that serve to tie the individual surveys together, and ameliorate the discontinuities that occur at survey boundaries. Perhaps the best known of these higher altitude surveys are a series of surveys flown in Australia (Tarlowski et al., 1996) for the purpose of leveling the Australian magnetic map, and the Project Magnet surveys (Coleman, 1992) of the US military. In North America, the 1970s saw the first regional compilations, followed by partial compilations of the entire continent in the 1980s, and more complete compilations by 2003. Similar scenarios have played out in Australia, the Former Soviet Union, China, South Asia, Australia, the Arctic and Antarctic, in Europe, and over the world's oceans. In contrast, Africa and South America are less advanced in terms of magnetic compilations, most of which have been led by industrial consortiums. The longest wavelengths of the crustal magnetic field can be measured from satellites in near-Earth orbits, and beginning in the 1960s, Russian and US satellites began to measure those magnetic fields. This effort continues today as an international effort, with the imminent launch of the ESA Swarm mission (Friis-Christensen et al., 2009). Earlier comparisons (Schnetzler et al., 1985) suggested a difference in amplitude between the crustal field measured at or near the surface and from satellites when the data sets were compared at the same altitude, with the satellite amplitude lower, but the two approaches are beginning to converge (e.g. Ravat et al., 2002). Upcoming satellite missions will use a gradiometer configuration to go to spherical harmonic degree 130 and beyond, and the wavelength content of near-surface surveys is being enhanced at both ends of the wavelength spectrum. There still remains a gap in our knowledge of magnetic anomalies with wavelengths from about 200 to 400 km. Only in Australia (Ravat et al., 2005) is this gap partially filled. The upcoming missions will provide data for an updated World Digital Magnetic Anomaly Map (WDMAM), the first edition of which was released in 2007. (see section 6.01.4.2).

In parallel with the development of compilations has been the development of larger and more elaborate models of the magnetic field, built on a deepening understanding of the sources of the magnetic field. These models utilize both forward and inverse approaches, and are frequently tested, and enhanced, using data from the compilations.

6.01.4.1 Continental-scale compilations

The first experimental airborne total field magnetometer was flown in the U.S.S.R. in 1936 (Gibson, 1998b) and in 1974, the Ministry of Geology of the U.S.S.R. published a mosaic series of 18 sheets at 1:2.5 million scale showing the residual magnetic intensity (Makarova, 1974) over the U.S.S.R. and surrounding waters. These sheets were digitized

in 1982 by the U.S. Naval Oceanographic Office, Stennis Space Center Mississippi in order to produce four regional one-arc-minute grids of magnetic anomaly values covering the entire Former Soviet Union. These digital data were provided to the National Geophysical Data Center (NGDC, 1996) for archival and public dissemination. The digitized data were made available on a 2.5 km grid.

The first continental-scale compilation, of North America (Hinze et al. 1988), was completed in preliminary form as part of the Decade of North American Geology, and released by the Committee for the Magnetic Anomaly Map of North America in 1987. Consisting of the aeromagnetic surveys of Canada and the United States, and surrounding waters, the compilation effort had been preceded by compilations of the United States (Zietz, 1982) and Canada (Hood et al., 1985). The North American compilation was released as a 2 km grid. The addition of aeromagnetic surveys over Mexico, and improved Canadian and US maps, led to a 2nd generation product (Bankey et al., 2002; Hernandez et al., 2001). The data grids comprising this map have a variety of wavelength content, 1-km grid spacing, and show the total field at 1 km above the terrain. They are projected using a spherical transverse Mercator with a central meridian of 100^{o} W, base latitude of 0^{o}, scale factor of 0.926 and Earth radius of 6,371,204 m. Wavelengths greater than 150 km are poorly represented in this compilation. A recent update (Ravat et al., 2009) using the NURE data set, in conjunction with the Comprehensive model (Sabaka et al, 2004), has now recovered much of the longer wavelength information.

Magnetic observations of the North Atlantic and Arctic oceans, and adjacent landmasses, were compiled as part of a Geological Survey of Canada program (Macnab et al., 1995; Verhoef et al. 1996, and Figure 4). The final data set, on a 5 km grid, was merged from three sub grids of 1) digital airborne observations, 2) digital ship borne observations, and 3) pre-existing grids or digitized maps. Only the ship borne observations showed some agreement with the satellite measurements of the crustal magnetic field, and as a consequence, all three sub grids were filtered to remove wavelengths greater than 400 km prior to merging. An update of the North Atlantic and Arctic region compilations, now including both magnetics and gravity, has recently been completed (Gaina et al., 2011). The updated compilation preserves smaller wavelength structures from the original surveys by using a 2 km grid, and includes updated data in the NE Atlantic, the high Arctic, and north of Greenland. It also utilizes the long wavelength component of the MF-6 satellite-based lithospheric magnetic model (Maus et al., 2007)

European magnetic observations, from northern, western, and Eastern Europe, were compiled by Wonik et al. (2001) on a 5 km grid at an altitude of 3 km above mean sea level (Figure 4). Long wavelengths were retained in this survey, although comparisons with satellite data suggest that wavelengths in excess of 300 km are poorly resolved. Questions have been raised about the reliability of the registration of this map.

A compilation of magnetic maps of onshore and offshore regions of China, Mongolia, and Russia with accompanying interpretation was produced by a team from the Geological Survey of Canada (1995). The data were on a 5 km grid, and wavelengths in

excess of 400 km have been removed from the map, which is displayed with a Transverse Mercator Projection.

A digital compilation of marine and aeromagnetic data over South Asia (Geol. Sur. Japan, 2002) was produced on a 2 km grid. A Lambert azimuthal equal-area projection was used with a central point at 15 ^{o} N 120 ^{o} E, and a terrestrial radius of 6377 km.

A digital compilation of aeromagnetic data over Australia and the surrounding oceans is now in its fifth edition (Milligan et al., 2009, Milligan and Franklin, 2004; Milligan et al., 2005). The associated database contains publicly available airborne magnetic grid data for on-shore and near-offshore Australia. Flight-line magnetic data for each survey have been optimally gridded and the grids matched in one inverse process. A composite grid at 80 m grid spacing is available. Aeromagnetic traverses flown around Australia during 1990 and 1994 are used in both quality control of the grids they intersect, and also to constrain grid merging by forcing grid data, where intersected, to the level of the traverse data. The map is displayed with a Lambert Conformal Conic Projection.

A sparse grid of aeromagnetic and marine magnetic data, supplemented by satellite magnetic coverage, is available for the Antarctic (Golynsky et al., 2002; Golynsky et al., 2013). The data set is publicly available as a 5 km grid, referenced to a polar stereographic projection.

The first compilation of onshore and offshore magnetic anomaly maps for China date from the late-1980s (Chinese National Aerogeophysics Survey and Remote Sensing Center, 1989), and has been updated(2004) in digital form.

Industry-led consortia have produced magnetic compilations of Africa (Barritt et al., 1993), Arabia, India and the Middle East (Reeves and Erren, 1994), and South America (Getech, 1996).

Oceanic data sets (, 1999) are held by the National Geophysical Data Center of NOAA. The most recent regional compilations are by Dyment et al. (2012), Quesnel et al. (2009), and Ishihara (2004), where the subtraction of non-crustal magnetic field sources was done using the CM4 model of Sabaka et al. (2004) (see section 6.01.5.2).

6.01.4.2 World Digital Magnetic Anomaly Map Compilation

Although aeromagnetic data have been collected for more than 70 years, no worldwide compilation of them existed until the production of the World Digital Magnetic Anomaly Map (Korhonen et al., 2007). This was an initiative of the International Association of Geomagnetism and Aeronomy, which had as its goal the production of a 5 km grid of the crustal magnetic field at an altitude of 5 km.

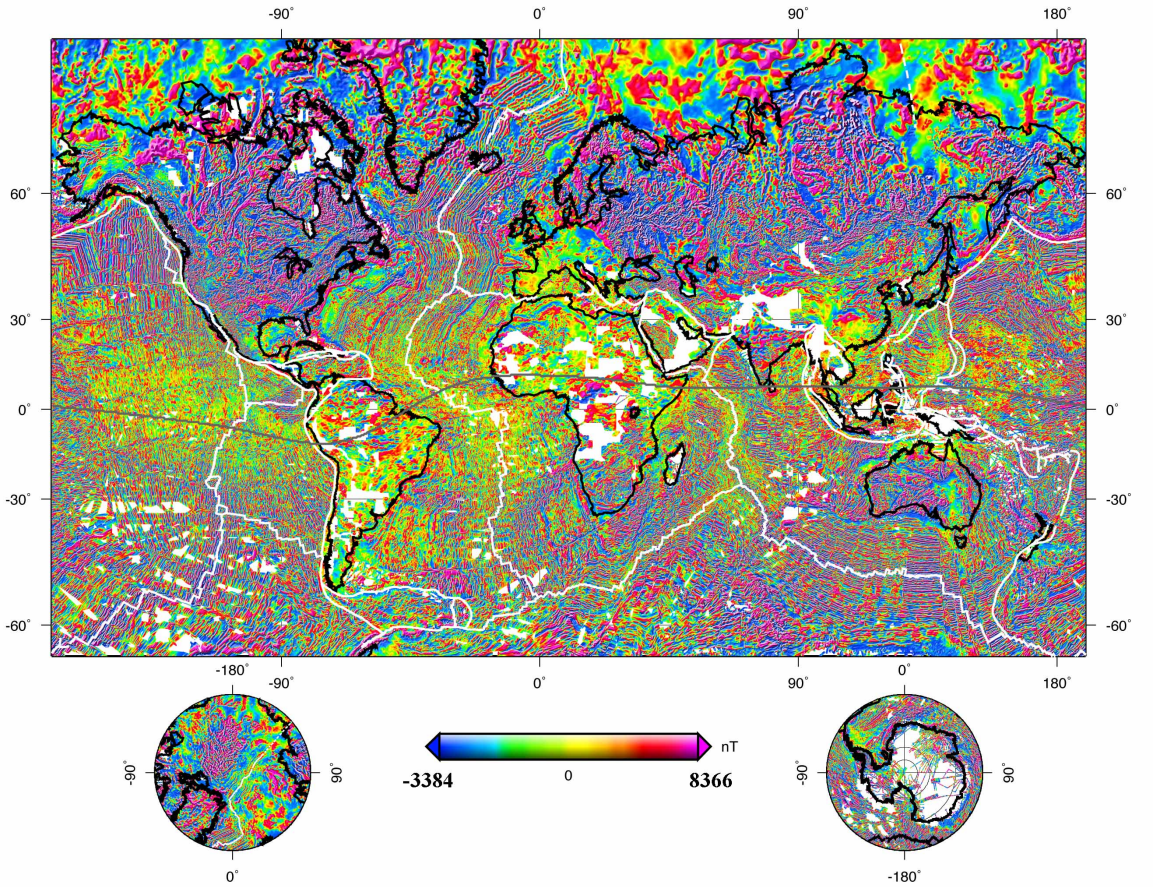

Figure 4. Total field anomaly map (ΔT) at 4 km above the WGS84 ellipsoid with Mercator and polar stereographic projections. Map is based on the EMAG2 model (Maus et al., 2009). Ridges, fracture zones, and trenches are shown as white lines. Continental outlines are shown in black. The compilation shows the absence of data from areas in white, either because the data does not exist, or because it has not been released. The magnetic dip equator is shown as a gray line extending across the entire equatorial region. The dip equator differs from the geographic equator because the magnetic field is not exactly aligned with the spin axis of the earth. The internal magnetic field is weakest, and horizontal, at the magnetic dip equator, and these facts produce a host of interesting features in both the magnetic field of the crust (Annihilators (section 6.01.5.6), induced magnetization (section 6.01.7) and that of the ionosphere (Equatorial Electrojet, see chapter 3).

The unveiling occurred at the General Assembly of IUGG/IAGA at Perugia, July 2007 (Korhonen et al., 2005; Ravat et al., 2003, Reeves et al., 1998). The map utilized airborne, marine, and satellite data to capture as many wavelengths as possible between 10 and 2200 km. It included all freely available major digital national and regional anomaly data sets: Arctic-North Atlantic, North America, Europe, South Asia, North East Asia, Eastern Indian Ocean, Australia, and the Antarctic. It also included lower resolution grids extracted from the proprietary coverage of Getech (1996) for Africa and South America. Getech's web page contains maps showing aeromagnetic coverage worldwide in their holdings. This global magnetic field may be quasi-static on a human time-scale, but maps of this field continue to improve. We expect that there will be updates to this map series, and releases of interim products from research groups. One such release, from the NOAA group (Maus et al., 2009) is shown as Figure 4.

6.01.4.3 Satellite compilations of crustal magnetic fields.

Satellite models of crustal magnetic fields are commonly spherical harmonic analyses of data often gathered during magnetically quiet times, but sometimes at all times. Two current models of this type are the MF series (MF-7 uses the approach of Maus et al., 2008 on CHAMP data between 2007 and 2010) and CM4 (Sabaka et al. 2004). The two models reflect somewhat different design philosophies, and hence have different strengths: MF-7 is an inversion of data from which estimates of other magnetic field sources have been removed, whilst CM4 solves for all sources, suitably parameterized, simultaneously. Thus MF-7 is a crustal field model only, and extends from degrees 16 to 133. The CHAMP magnetic field satellite input to MF-7 has had removed an internal field model to degree 15, a simple magnetospheric model, and the predicted signatures from eight main ocean tidal components. Additional external fields are subsequently removed in a track-by-track scheme. Because of its design philosophy, the MF-7 model can be considered a minimum estimate of the crustal magnetic field, one in which there will be some suppression of along-track magnetic fields. Regularization has been applied to degrees higher than 80 to extract clusters of spherical harmonic coefficients that are well-resolved by the data.

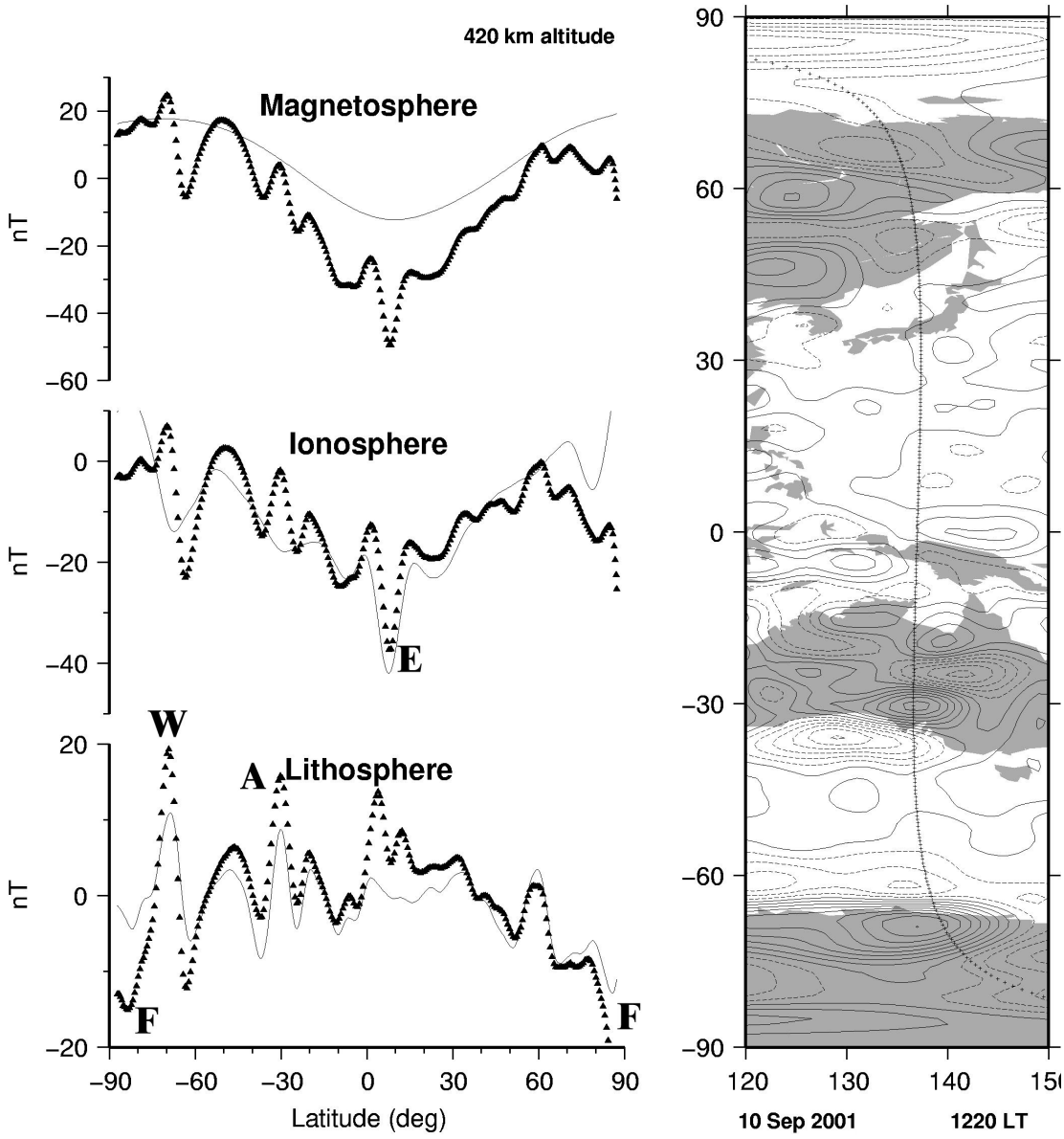

Figure 5. Residual progression versus geographic latitude as magnetic fields from the four main source regions (core, crust, ionosphere, and magnetosphere) are removed with the Comprehensive Model CM4 (Sabaka et al., 2004). This profile shows the total field T in the direction of the main field **F** of a CHAMP descending (South-going) satellite pass on 10 September 2001. The pass is centered at 0300 UT and crosses the Equator at 137° W and 1220 LT. Magnetically quiet conditions prevailed, with Kp = 1^+ for this period, Kp=0^+ for the previous three hour period, Dst=2 nT, and |d(Dst)/dt| < 2 nT/hr. Siebert and Meyer (1996) discuss magnetic indices, while Mandea and Purucker (2005) discuss their role in data selection (see also Appendix to Chapter 3). For a given panel, the symbols represent residuals with respect to a main field (to spherical harmonic degree 13) plus all fields labeled in the panels above; the line is the prediction from the field source labeled in the current panel. The figure on the right shows the location of the sub satellite point and includes a contour map of the total field anomaly (ΔT) originating in the crust (to spherical harmonic degree 60) from the Comprehensive Model (contour interval = 2 nT, dashed lines indicated negative ΔT). The data from this profile were not included in the construction of the Comprehensive model. The

equatorial electrojet (EE) can be seen (E) because it is most prominent around mid-day, following the magnetic dip equator. Although the amplitude of the EE in the model and profile is similar, a slight amplitude offset and latitudinal shift results in a residual anomaly that might be mistaken for a crustal anomaly. While the EE is a robust feature of the low-latitude ionosphere, it does exhibit significant variability on a day to day basis (Lühr et al., 2004; Langel et al., 1993), and includes wavelengths shorter than the resolution of CM4 (spherical harmonic degree 45 for the EE). The magnetic field originating in the distant magnetosphere exhibits variations, which are not entirely accounted for by the Dst index, and this may account for some of the mismatch. In contrast, the high-latitude current system (F) exhibits significant variability in time on a minute to minute basis, and in space, and CM4 does not attempt to model it. Two significant crustal anomalies, in Wilkes Land, Antarctica (W), and in southern Australia (A) are prominent in the profile. The frequency content of these anomalies again exceeds the cut-off of CM4 (spherical harmonic degree 65 for crustal fields). These two magnetic features (Purucker et al., 1999; Mayhew and Johnson, 1987) were adjacent (Von Frese et al., 1986) in pre-rift reconstructions of Gondwana.

CM4, in contrast, is a comprehensive model, i.e. it includes components of internal and external origin, and toroidal fields, in addition to the crustal field (Figure 5). It is based on data from all high-precision satellite magnetic field missions, beginning with the POGO missions of the 1960s. It uses an iteratively reweighted least squares approach to solve for all of the 25000+ parameters using more than 2 million observations. Because of its design philosophy, the CM4 crustal field component estimate is expected to have more power than that of the MF series, both because no direct damping is applied to the crustal field coefficients, and because of the along-track approach used in the MF series. CM4 has no suppression of along-track magnetic fields, and some of them, especially in the vicinity of the dip equator, are of uncertain origin.

6.01.4.4 Global magnetization models

Global magnetization models often represent an integration of compositional and thermal models of the crust and mantle with long wavelength crustal magnetic field measurements from satellite. Both forward (Hemant and Maus, 2005) and inverse (Fox Maule et al., 2005) approaches have been employed. For example, one approach (Purucker et al., 2007) has used the 3SMAC (Nataf and Ricard, 1996) compositional and thermal model of the crust and mantle as a starting model, which is then modified in an iterative fashion with the satellite data until the magnetic field predicted by the model (Figure 6) matches the observed magnetic field. A unique magnetic crustal thickness solution is obtained by assuming 1) that induced magnetizations dominate in continental crust, 2) the model of Dyment and Arkani-Hamed (1999) describes the oceanic remanence, and 3) that vertical thickness variations dominate over lateral susceptibility variations. A starting model is necessary for two reasons: 1) to constrain wavelengths obscured by overlap with the core field, and 2) to ensure that most magnetic crustal thicknesses will be non-negative. An approach (Figure 6) such as this has been used to define the thickness and thermal properties of cratonic North America (Purucker et al., 2002).

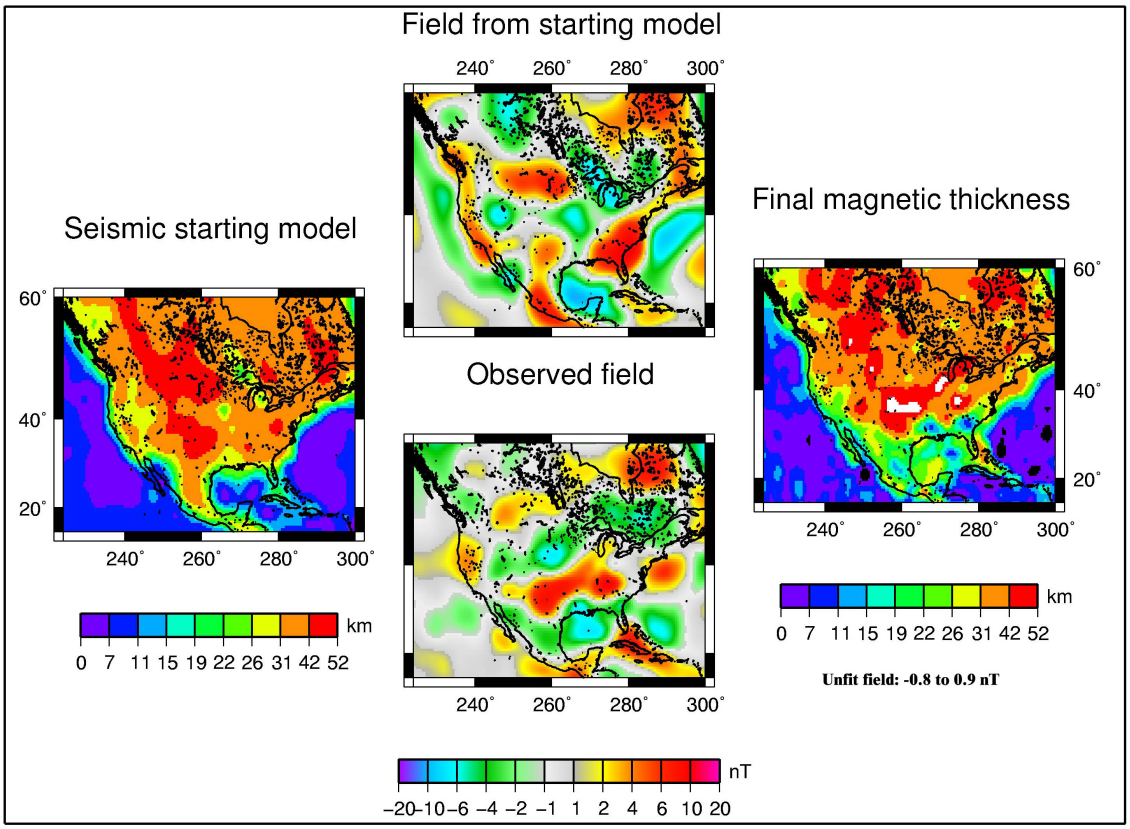

Figure 6. Magnetic crustal thickness map of North America (right), which reproduces satellite observations (bottom) from CHAMP, as represented by MF-4 (Maus et al., 2006). As a starting model the seismic crustal thicknesses (left) from Chulick and Mooney (2002) over North America are used instead of the global 3SMAC crustal and thermal model (Nataf and Ricard, 1996). The magnetic field is calculated from this starting model (top) under the assumption of a constant magnetic susceptibility (χ) of 0.04, and long wavelength fields (spherical harmonic degree < 15) are removed, simulating a main field subtraction. The observed (bottom) and modeled (top) fields are differenced, and the difference is inverted for a magnetic crustal thickness. The starting model is then updated to reflect this change, and the process continues until

convergence is achieved. The process is non-linear because the total anomaly field (ΔT) is used, and because of the high-pass filter. After three iterations of this technique the residuals to the observations are less than ± 1 nT. Negative magnetic crustal thickness (shown in black, the minimum is –6 km) over a few regions in the ocean could be a consequence of remanent magnetic fields. Large magnetic crustal thicknesses (shown in white, the maximum is 60 km) over parts of the mid-continent region could be a consequence of inaccuracies in the starting model. Purucker et al. (2002) applied this approach over North America, and found that if 3SMAC alone was used as a starting model, negative crustal thicknesses were found over the southeastern U.S. landmass. Modification of 3SMAC to place the major crustal thickness change near the Coastal Plain/Piedmont boundary resulted in more realistic crustal thicknesses.

A second approach (Hemant and Maus, 2005, based on earlier work of Hahn and Bosum, 1986) uses the available magnetic petrology, geological age, tectonic and seismic crustal thickness information of the Earth's crust and assigns magnetization strengths and directions to geological units based on their age and rock compositions. In this way a global magnetization model of the Earth's crust is computed. The model is used to predict the crustal magnetic field at satellite altitude and compared with the observed crustal field measurements. One can match the observed field by varying the boundaries and composition of lower-crustal structures.

6.01.5 The 'Tools of the Trade'

6.01.5.1 Survey Design and resolution

Although magnetic surveys are frequently conducted as 'missions of opportunity', where the mission design is largely dictated by the needs of the primary instrument, or the platform, there are many cases in which the collection of a magnetic survey is the primary goal, and consideration needs to be given to optimizing the return from the survey. A recent example of such a process, and its documentation, has been the planning for the Swarm magnetic field satellite constellation (Olsen et al., 2006b). Survey design of aeromagnetic surveys, including the spacing and orientation of flight lines, their altitude, and the inclusion of tie lines, is discussed by Reid (1980). For further details, refer to Chapter 4 on 'Observation and Measurement Techniques'.

6.01.5.2 Removal of non-crustal fields

An important part of obtaining crustal anomalies suitable for further processing, modeling and interpretation is adequate removal of non-crustal fields, primarily that arising from dynamo action in the core, and external fields due to solar-terrestrial interactions. The geodynamo-generated field, often referred to as the main field, has large amplitude but varies slowly, both temporally and spatially. External fields have much smaller amplitudes but have much more rapid temporal and spatial variations. Time-varying external fields also induce sub-surface magnetic fields throughout the crust and mantle, but their amplitudes are generally small compared to those of typical crustal anomalies.

The effect of external fields can be minimized by collecting data at magnetically quiet times, but this is frequently impractical, especially at higher magnetic latitudes. Many surveys are conducted with a continuously recording base station to monitor and correct for external variations. The base station is located at a site where the spatial field

gradients are low (i.e. not on a magnetic anomaly), ideally in roughly the center of the survey area. It can be used to alert surveyors to magnetic storms, when data acquisition will be suspended, and as a means to judge the quality of the survey data. In periods of normal activity, the temporal variations recorded at the base station will be a reasonable approximation to the external field throughout the survey area. External fields are a minimum at night in low and mid-latitudes. Over several days (or longer) it is usually possible to identify a 'night time quiet value' (NTQV) from the base station record. The difference between the NTQV and the base station value at a given time is an approximation to the external field at that time, and is removed from the survey data. The difficulty of this method lies in the complicated behavior of the external field, combined with the generally unknown conductivity structure of the Earth. A second approach to the correction of external fields is via a least-squares analysis of the mis-ties at intersecting survey lines (Ray, 1985). The two approaches are often used together, with the regression-type analysis used as a refinement, to remove errors not removed by the first approach.

After correcting for external fields, the method for removing the main field depends on the size and scope of the survey. For a small, ground-based survey, it is often sufficient to treat the main field as constant over the survey area. Its amplitude is likely to be well-approximated by the average field (data mean) or the NTQV. Airborne and satellite surveys typically cover much larger areas, over which it may not be reasonable to assume the main field is constant, and therefore more sophisticated main field removal methods are justified. An obvious extension is to remove the best-fitting line (for a 1D survey) or plane (2D survey) through the data. More commonly, the predictions of a main field model such as the International Geomagnetic Reference Field (IGRF) are subtracted. IGRFs consist of values for the spherical harmonic coefficients from which the field can be calculated at any point in space and time (see Chapter 2 for further details). Each IGRF consists of a set of main field and secular variation coefficients covering a five-year interval, thereby accounting for the temporal evolution of the main field. However, mis-matches can occur between crustal anomaly fields in overlapping or abutting areas obtained from surveys at different times because the IGRF representations are not perfect. This is a particular problem when trying to merge surveys to form larger compilations.

The most important data for IGRF modeling have been permanent magnetic observatory night-time values on magnetically quiet days, usually selected on the basis of geomagnetic activity indices (see the Appendix to Chapter 3, and Siebert and Meyer, 1996). Observatories are located in areas of low spatial magnetic field gradients, and where crustal fields are a minimum. With the incorporation of large numbers of data from orbiting satellites, and the availability of more powerful computational resources, different methods of analysis become appropriate. As described earlier, rather than attempting to remove certain field sources from the data on a point by point basis prior to main field modeling, they can now be solved for simultaneously. This approach has led to the series of 'comprehensive models' (e.g. Sabaka et al., 2004) in which large numbers of parameters expressing the main, crustal, external and induced fields are co-estimated (see Chapter 2). These models (Figure 7) should enable better estimates of the crustal field to

be obtained from survey data (Nabighian et al., 2005). The current version of the 'comprehensive model is CM4 (Sabaka et al., 2004) and the data envelope extends from 1960 through July of 2002. Usage of the model outside of this time range entails two steps. First, the user must update the values of Dst and F10.7, the indices used for characterizing the state of the ionopshere and magnetosphere. Second, the internal, time-varying low-degree part of the model must be replaced by a model that is valid over the time span considered. This would mean the IGRF for data collected prior to 1960, and a model such as the CHAOS model (Olsen et al., 2006a) for data collected after 2002.7

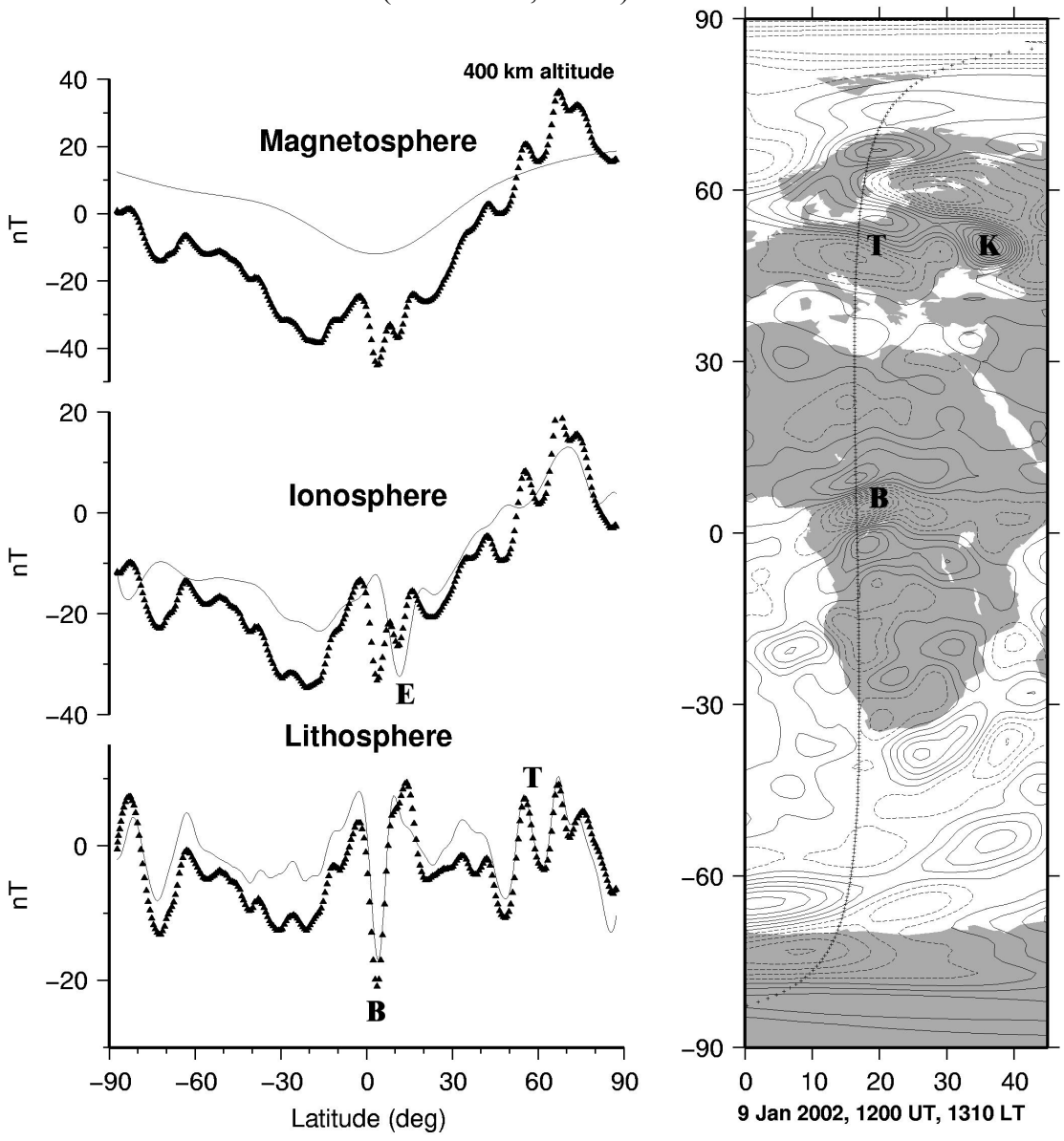

Figure 7. Residual progression versus geographic latitude as magnetic fields from the four main source regions (core, crust, ionosphere, and magnetosphere) are removed with the Comprehensive Model CM4 (Sabaka et al., 2004). This profile shows the total field T in the direction of the main field **F** of a CHAMP satellite pass on 9 January 2002, when the magnetic field was in a quiet state. The data from this profile were not included in the construction of the Comprehensive model. For a given panel, the symbols

represent residuals with respect to a main field (to spherical harmonic degree 13) plus all fields labeled in the panels above; the line is the prediction from the field source labeled in the current panel. The figure on the right shows the location of the sub satellite point and includes a contour map of the total field anomaly (ΔT) originating in the crust (to spherical harmonic degree 60) from the Comprehensive Model (contour interval = 2 nT, dashed lines indicated negative ΔT). This figure illustrates the ionospheric/lithospheric separation that is possible with a Comprehensive model approach with the equatorial electrojet (E) in close proximity to the Bangui (B) crustal anomaly (Girdler et al., 1992). Note also the Tornquist-Teisseyre zone (Taylor and Ravat, 1995) (T), a major litho-tectonic structure in Central Europe, and the Kursk (Taylor and Frawley, 1986) anomaly (K), associated with a substantial Banded Iron Formation.

The end result of this data reduction process should be point representations of our best estimates of the crustal magnetic field, often referred to as the crustal anomaly field.

6.01.5.3 Representations

Taking the cue from the way seismic trace information is displayed, crustal magnetic data collected along a profile, or even a series of profiles, can be represented as a set of 'wiggles', with areas above the zero line filled, or the areas above and below the line colored differently. More often, data collected over an area are interpolated onto a regular grid for display as a color image, and for further processing and modeling. Various algorithms are suitable for gridding crustal magnetic data, and which is employed in a particular instance will depend on how the data have been collected, and the form of the crustal anomalies encountered. For example, aeromagnetic data usually have a much smaller interval between data points along flight lines than between them (see Chapter 4), making bi-directional spline gridding (Bhattacharyya, 1969) appropriate. For more evenly spaced data, minimum curvature methods (Smith and Wessel, 1990) are often applied. Widely spaced tie lines are often flown perpendicular to the survey direction, and this facilitates the 'leveling' of the survey (Ray, 1985). If the anomalies have a particular directionality to them (e.g. they arise from a series of parallel dykes), interpolations of the crustal anomaly field can be improved by incorporating measured horizontal gradients (Reford, 2006). Besides offering a visual image of the data through imaging, these regular grids form the basis for all the transformations (mostly using wave number domain manipulation) discussed below that can be applied to the data. As a consequence this is an area of continuing research (O'Connell et al., 2005; Hansen, 1993; Cordell, 1992; Keating, 1993; Ridsdill-Smith and Dentith, 1999)

There are many methods of modeling the data that can be used to interpolate between data points and extrapolate beyond the survey area. Some of these are only useful for local modeling, others are only applicable to data sets covering all, or at least a large part of, the Earth's surface, and some can be used for both local and global modeling. Global methods are well summarized in Langel and Hinze's (1998) book, and they present most of the methods outlined below in a uniform notation.

6.01.5.3.1 Spherical Harmonic Analysis

The most commonly employed global method is spherical harmonic analysis (SHA), which has been described in chapter 2 in the context of main field modeling. The potential satisfying Laplace's equation in spherical polar coordinates is expressed as

$$V = a\sum_{n=1}^{N_{\max}}\left(\frac{a}{r}\right)^{n+1}\sum_{m=0}^{n}\left(g_n^m\cos(m\phi)+h_n^m\sin(m\phi)\right)P_n^m(\cos\theta) \qquad (6.1.6)$$

where a is the radius of the Earth, r is the radial distance of the observation from the center of the Earth, ϕ denotes longitude and θ colatitude, $P_n^m(\cos\theta)$ are the Schmidt quasi-normalized associated Legendre functions of degree n and order m, and the g_n^m and h_n^m are the spherical harmonic coefficients to be estimated. The difference for crustal field modeling is that the series needs to include much higher harmonic degree terms (N_{max}) to represent the anomaly field adequately. Spherical harmonics, $P_n^m(\cos\theta)$ cos(mϕ) or $P_n^m(\cos\theta)$ sin(mϕ) are orthogonal over the sphere. Spherical harmonic models of the crustal field from satellite data (Sabaka et al., 2004; Maus et al., 2008) now go to spherical harmonic degrees as high as N_{max}=133, corresponding to $N_{max}(N_{max}+2)$ coefficients. This creates computational difficulties (Cain *et al*, 1989; Lesur & Gubbins, 1999), and high resolution data sets require enormous numbers of spherical harmonic coefficients to represent them adequately. SHA is not particularly well-suited to global (or near-global) data sets of varying spatial density: since the basis functions are themselves global, the spherical harmonic series must extend up to the degree representing the shortest spatial wavelength in the data set (approximately c/n, where c is circumference, and n is spherical harmonic degree). The coefficients multiplying these degree terms will not be well constrained if only a limited area of the globe has coverage at the spatial sampling rate appropriate to determine them and, unless regularization is applied, their numerical values may generate ringing over other parts of the globe. Basis functions with more local support, such as harmonic splines (Shure et al., 1982), or wavelet-like functions (Lesur and Maus, 2006; Beggan et al. 2013) are better suited to data sets with variable resolution over the globe.

6.01.5.3.2 Spectral, Rectangular Harmonic and Cylindrical Harmonic Analysis

Spectral analysis can be applied to data collected along profiles or on a plane, with the usual techniques to avoid ringing, edge effects and spectral leakage (Parker and O'Brien, 1997, Lowe et al., 2001). This allows high resolution data sets to be represented by small numbers of model parameters. Alldredge (1981) introduced rectangular harmonic analysis, suitable when the area covered is small enough for the flat Earth approximation to be appropriate. The method is based on the solution to Laplace's equation in a Cartesian geometry. The data are first transformed into the local Cartesian coordinate system with origin at the center of the region, and then the coefficients are determined. They can be used to predict the field at any altitude, and can also be transformed back to a spherical Earth coordinate system. Malin et al. (1996) introduced extra coefficients to remove trends. In an analysis of main field data, they concluded the method was only suitable for interpolation, and not for extrapolation. Nakagawa and Yukutake (1985) used

a cosine function weight near the edges of the region subject to rectangular harmonic analysis to reduce edge effects.

Alldredge (1982) introduced the related concept of cylindrical harmonic analysis, where the equation to be solved is Laplace's equation in cylindrical polar coordinates. He advocated this when the observations displayed cylindrical symmetry. Again, the size of the area to be modeled and single-valuedness of the potential imposes constraints on the arguments.

6.01.5.3.3 Equivalent Source Modeling

A representation useful for both local and global modeling (typically in a Cartesian and spherical coordinate system respectively), is equivalent source (ES) dipoles, where again the basis support is local. The magnetized crust is divided into blocks, each of which is assumed to have a magnetic dipole at its center. In this case the potential can be expressed as

$$V = -\mathbf{M} \cdot \nabla \frac{1}{d} \tag{6.1.7}$$

where d is the distance between the dipole and the observation location, and **M** is the dipole moment. The conversion factor, $\mu_0 / 4\pi$, between SI and cgs units (cf. Blakely, 1995 p. 67) is implicitly assumed to be included within equation (6.1.7) and subsequent equations relating the potential V to the magnetization **M.** The model parameters of (6.1.7) are the direction and magnetization strength of the dipoles. However, magnetization is often assumed to be purely induced, meaning that the dipole directions are known (parallel to the main field); the problem of inferring strength from vector component anomaly data is then linear. The dipoles can be arranged with variable density according to the data distribution, retaining the resolution of the original data set. This can be a far more efficient (i.e. fewer parameter) modeling method than SHA when the spatial resolution of the data set is uneven. Although the distribution of magnetization in the crust reproducing the anomaly data is highly non-unique (Runcorn, 1975; see section 6.01.5.6), it can be interpreted geologically, especially if a priori information has been incorporated in the modeling, whether forward or inverse (see section 6.01.5.5). ES dipole models (Dyment and Arkani-Hamed 1998) are widely used for forward modeling since they are intuitively accessible. They can be used straight-forwardly to predict the magnetic field at any altitude on or above the Earth's surface, so also provide an excellent tool for upward and downward (analytic) continuation (see section 6.01.5.4.1).

The crustal anomaly field at or above the Earth's surface, even as high as typical orbiting satellite altitudes of a few hundred kilometers, depends on the magnetization of only a small volume of the crust directly beneath the observation point – the footprint of an anomaly measurement is small. Thus when a local basis is used to represent the anomaly field, the matrix relating observations to model parameters is sparse. Using numerical methods for solving sparse matrix systems then allows a large number of basis functions to be included, meaning that the resolution of the original data set can be retained. An application of this to crustal anomaly modeling was by Purucker et al. (1996), who

applied the iterative conjugate gradient algorithm to ES dipole modeling of a satellite crustal anomaly data set.

6.01.5.3.4 Magnetic Monopole Modeling

Although non-physical and therefore not suitable as an interpretation tool, crustal anomaly data can be represented by a sub-surface distribution of magnetic monopole sources (O'Brien and Parker 1994). The number and positions of the monopoles on the source sphere are chosen to provide a good representation of the data (again, a spatially variable monopole density can be used to represent spatially variable resolution of the original data); the model parameters are then simply the monopole amplitudes (no assumptions concerning directionality are required).

The potential is expressed as a sum of potential sources $\varphi_k(\mathbf{r}), k = 1,...,K$

$$V(\mathbf{r}) = \sum_{k=1}^{K} \alpha_k \varphi_k(\mathbf{r}) \tag{6.1.8}$$

where α_k are the monopole amplitudes to be determined. Monopoles at locations $\mathbf{s}_k$ are represented by functions

$$\varphi_k(\mathbf{r}) = \frac{1}{|\mathbf{r} - \mathbf{s}_k|} \tag{6.1.9}$$

The solution is calculated by minimizing

$$U = \left\| \mathbf{C}^{-1}(\mathbf{d} - \mathbf{G}\boldsymbol{\alpha}) \right\|^2 + \lambda \boldsymbol{\alpha}^T \boldsymbol{\Gamma} \boldsymbol{\alpha} \tag{6.1.10}$$

where **C** is the data covariance matrix, **d** is the data vector, **G** is the matrix of Green's functions relating the monopoles to the measurements, λ is a Lagrange multiplier and $\boldsymbol{\alpha}^T \boldsymbol{\Gamma} \boldsymbol{\alpha}$ is a quadratic form expressing the field complexity. $\|\cdot\|$ denotes the Euclidean norm or length. **Γ** is known as the Gram matrix; its (j,k)th element is the inner product of φ_j and φ_k. Thus the first term measures the fit to the data, and the second, the amount of structure in the resulting field model. This is an example of a regularized, or minimum norm, solution; by an appropriate choice of λ, we can relax slightly the fit to the data such that it does not attempt to model noise. The quadratic form (and definition of the inner product for the calculation of the Gram matrix) is chosen to measure some global property of the field such as its mean strength or lateral variability; useful measures lead to closed-form, or at least easily calculable, Gram matrix elements. The concept was introduced with main field modeling in mind (see chapter 2), where some quantities that are expressible as quadratic norms can be bounded theoretically or empirically. It is now widely used as a regularizing tool. For crustal modeling, it ensures that the models have minimum structure for a given fit to the data; if the fit is acceptable, we can then argue that the real Earth has at least as much structure as the model. Since (6.1.10) minimizes a global measure of complexity, it does not matter if the monopole sources are distributed unevenly over the surface to reflect the data coverage.

6.01.5.3.5 Harmonic Spline Modeling

Harmonic splines (HS) are local basis functions introduced by Shure et al. (1982) for global main field modeling. They were the first to apply minimum norm modeling to geomagnetism. Using the Green's function for the magnetostatic potential, the solution is constructed as a linear combination of the HS associated with each data point, leading to the solution of a linear system of dimension the number of data points. This is impractically large even for main field modeling, but naturally preserves the resolution of the original data set. To make the inversion of large data sets computationally tractable, Parker and Shure (1982) expanded the solution in terms of HS at only a subset of the data points, known as the depleted basis. The system then reduces to one of the dimension of the number of data points. Tests based on small data sets demonstrated that the depleted basis solution had only a slightly larger norm than the minimum value obtained by HS. The resolution of the depleted basis solution depends on the spacing between the basis points. The field can be constructed at any radius beyond which the solution converges, making analytic continuation straightforward.

HS is not used in crustal anomaly modeling because the number of points in practical data sets is too large, but Whaler (1994) inverted a 2º by 2º grid of MAGSAT satellite crustal anomaly vector data using depleted basis HS, using it to downward continue the field from satellite altitude to just above the Earth's surface. With the computational resources available then, she was only able to retain every other basis point in latitude and longitude even over a continental-sized area of the globe (an 80º by 80º area centered on Africa), with consequent loss of resolution. She also found that a sparse distribution of points was required over the remainder of the globe to avoid ringing. Another disadvantage of depleted basis HS is that the arrangement of depleted basis points is subjective. However, it simplifies the inversion of total field anomaly data, since the basis functions for their expansion can be chosen to be those for the vertical component (at a limited subset of the actual data points), in which case the matrix elements can be calculated straightforwardly (Langel and Whaler, 1996).

A more satisfactory application of HS uses sparse matrix techniques, allowing the full basis to be retained. Unpublished models using the conjugate gradient algorithm based on satellite anomaly data are very similar to those obtained using other global methods, and also compare favorably with Whaler's (1994) depleted basis models over Africa. HS (and depleted basis HS) coefficients can be converted into an infinite series of SH coefficients that give power spectra similar to those obtained from SHA at low degree, but typically have less power at higher degrees.

Achache et al. (1987) used the same basis functions to model satellite data, but reduced the size of the linear system by recognizing that they fall to negligibly small values quickly with lateral distance from the point at which the solution is being calculated. They thus included only those related to data points close to the point of interest, reducing the dimensions of the matrix to be inverted from the number of data to the number of 'nearby' data points. Their recommendation is that points within a horizontal distance 3h, where h is satellite altitude, be included. In addition, they used principal component analysis to stabilize the inversion of the resulting (smaller) matrix by including only those eigenvectors associated with the largest eigenvalues. The decision as

to how many eigenvectors to include is subjective, but the eigenvalue spectrum shows a rapid fall off for satellite data acquired above 200 km altitude, making the choice relatively clear-cut. Previously, Langel et al. (1984) used principal component analysis to stabilize the calculation of ES solutions.

6.01.5.3.6 Spherical Slepian Function Analysis

Another regional modelling method producing coefficients that can be converted to their SH counterparts uses spherical Slepian functions, which provide the optimal spatial and spectral localisation of a function on a region of the unit sphere (see Simons et al., 2006, for a review). Spherical Slepian functions can be used to model data over a region, or to localise an SH model onto a region. Like spherical harmonics, spherical Slepians are orthogonal over the sphere, but in addition they are orthogonal over the region. The formulation was developed and most problems tackled to date have been for potentials on a sphere including the monopole coefficient, such as the geoid and the cosmic microwave background. In that case, an existing SH model to degree and order N_{max} over a region of fractional area A (in steradians) of the unit sphere is optimally represented by $(N_{max} + 1)^2$ $A/4\pi$ spherical Slepian functions, a quantity known as the Shannon number, S. The spherical Slepian functions are obtained by the eigenvector-eigenvalue decomposition of the symmetric 'localisation' matrix formed from the integration over the region of interest of all possible products of spherical harmonics of degree and order up to N_{max}. For most regions, this must be undertaken numerically, and thus for large N_{max} it is a significant computational undertaking. Ranked by decreasing eigenvalue, the first S eigenvectors are the spherical Slepians that optimally project the SH coefficients onto the region of interest. These eigenvectors are used to decompose the original SH coefficients into those optimally concentrating the potential over the region of interest, and the remainder into its complement, concentrated over the rest of the unit sphere. The region of interest need not be connected, and Beggan et al. (2013) use the method to decompose optimally MF-7 up to degree and order 72 (beyond which regularization was applied) into the continental and oceanic domains. They extended the original algorithm, which produced low-pass spherical Slepian functions, to produce their band-pass counterparts, leading to a modified expression for the Shannon number. The band-pass spherical Slepian decomposition prevented energy in degrees 16 and above in MF-7 from leaking into the lower degree coefficients - set to zero - which represent the core field. Although the decomposition was performed on the potential representing the field, rather than field components, it produced a good localisation of the vertical field. Beggan et al. (2013) found that the field over the continents dominates, and that its power spectrum is significantly different from that of the oceanic anomaly field - the oceanic power spectrum is approximately flat, whereas the continental power increases with increasing harmonic degree. Current research is developing methods for spherical Slepian analysis of vector components, and producing optimal localisation at any radius from analysis at any other (i.e. on analytical continuation of spherical Slepians). Spherical Slepian analysis is most effective on quantities with significant power over a large range of spherical harmonic degrees and that have an approximately white spectrum, and is thus well-suited to crustal anomaly field modelling.

6.01.5.3.7 Minimum Norm Magnetization Modeling

Based on methods originally developed for modeling seamount magnetism (Parker et al., 1987), then adapted to account for crustal magnetization when modeling the main field (Jackson, 1990; 1994), Whaler and Langel (1996) used a depleted basis minimum norm method to model crustal magnetization from satellite anomaly field data sets. Data are related to magnetization varying continuously in a crust of assumed constant thickness through (6.1.1), and hence the solution is expressed as a linear combination of the Green's functions

$$-\hat{\mathbf{l}}_j^{(\eta)} \cdot \nabla_{\mathbf{r}_j} \left\{ \frac{\mu_0}{4\pi} \nabla_{\mathbf{s}} \frac{1}{\left|\mathbf{r}_j - \mathbf{s}\right|} \right\} \tag{6.1.11}$$

The resulting Gram matrix elements have closed form expressions involving elliptic integrals, but these can be approximated very accurately by expressions involving only elementary functions since the thickness of the magnetized layer is small in comparison to the Earth's radius. A similar simplification applies if depth-independent magnetization is assumed; this is more appropriate for satellite data modelling, since the thickness of the magnetized layer is very much smaller than satellite altitude, so it is indistinguishable from a thin sheet. The norm minimized was

$$\left\|\mathbf{M}\right\| = \sqrt{\int_v \mathbf{M} \cdot \mathbf{M} dv} \tag{6.1.12}$$

i.e. the root-mean-square (RMS) magnetization amplitude of the crust. The method makes no assumption about the magnetization direction, so allows both remanent and induced magnetization. Whaler and Langel (1996) chose the same data set and distribution of depleted basis points Whaler (1994) used to downward continue the magnetic field to produce a magnetization model for Africa. For ease of comparison with ES dipole models assuming purely induced magnetization, they displayed the model as components in the direction of the main field (consistent with induced magnetization, or remanent magnetization acquired in to-day's main field), perpendicular to the main field in the meridian plane, and perpendicular to the meridian plane. Whaler and Langel (1996) note that by damping least squares ES inversion, the solution minimizes the same norm as they employed, i.e. minimum RMS magnetization. The largest component of magnetization was in the direction of the current main field (or anti-parallel to it), but the component of magnetization perpendicular to the main field in the meridian plane was also significant in many areas. The smallest component (perpendicular to the meridian plane) requires rotation and translation of the magnetization vector from that which would be recorded by rocks acquiring a contemporary remanent magnetization.

A similar difficulty of loss of resolution of the solution and subjectivity of the choice of depleted basis points can be overcome in the same fashion as for HS: by employing the iterative conjugate gradient technique to solve the full data-by-data system of equations, taking advantage of the sparseness of the matrix relating data to model parameters. Again, comparisons between Whaler and Langel's (1996) depleted basis magnetization model for Africa and surrounds and the equivalent part of the global conjugate gradient model of Whaler et al. (1996) are favorable. Whaler and Purucker (2005) have applied

this technique to Martian orbiting satellite data, and compared the model to Langlais et al.'s (2004) ES dipole model. Mars no longer has an active dynamo so the magnetization direction is unknown. Langlais et al. (2004) developed an iterative technique that allowed them to solve for both the amplitude and direction of ES dipoles. Convergence was difficult to achieve, particularly as the dipole spacing was reduced, so their final model had a coarser spacing than the separation between the data points. Nonetheless, there was good agreement between their model and Purucker and Whaler's (2005) model, which was also derived from a slightly different data set.

6.01.5.3.8 Spherical Cap Harmonic Analysis

Spherical cap harmonic analysis (SCHA) (Haines, 1985), and the related translated origin spherical cap harmonic analysis (TOSCA) (de Santis, 1991), has been developed to model the field over small patches of the globe. As for global spherical harmonic analysis, the potential is expressed as a finite sum of spherical harmonics, but including harmonics of non-integer degree. Assuming the cap is centered on $\theta=0$ and subtends an angle θ_0 at the center of the Earth, the possible values of degree, n_k, which is a function of order, m, are those for which θ_0 is a zero of either $P_{n_k}^{m}(\theta)$ or $\frac{\partial P_{n_k}^{m}(\theta)}{\partial \theta}$. SCHA maps harmonics on the sphere to the spherical cap, so their effective wavelength is reduced accordingly. Thus smaller scale features can be represented over the cap with fewer coefficients than are required for global SHA. TOSCA moves the origin from the center of the Earth towards the surface along a line joining the Earth's center to the center of the cap. This adjusts the wavelength represented by a given harmonics to be smaller at the center of the cap than at the edge, an advantage if the data distribution is concentrated towards the center of the region. Korte and Holme (2003) present a method for regularizing SCHA, pointing out that, unlike SHA, the basis functions are not orthogonal. This means that it is not possible simultaneously to represent the potential for the vertical and horizontal field components exactly. Analytic continuation is prone to errors that increase with the upward or downward continuation distance, although Thébault et al. (2004) have re-posed SCHA as a boundary value problem within a cone extending above the reference surface in a method they call revised SCHA or R-SCHA, thereby allowing satellite data to be downward continued to the Earth's surface. In a further extension, Thébault et al. (2006) use both Neumann and Dirichlet boundary conditions in R-SCHA, and relate the resulting coefficients to their SHA counterparts. Vervelidou (2013) has derived approximations that enable spatial power spectra to be calculated directly from the R-SCHA coefficients, allowing it to be extended efficiently to the shorter wavelengths that an R-SCHA can represent.

6.01.5.4 Transformations

The transformations of the next few sub-sections are applicable to two-dimensional data sets expressible in a rectangular geometry, such as those recorded in regional aeromagnetic surveys. They are most easily considered and performed in the wave number domain. The development here follows that of Gunn (1975) closely, but beware of typographical errors in his manuscript. We begin with the expression for the magnetic

scalar potential V resulting from a distribution of magnetization **M** within an infinite half-space. Assuming a uniform direction of magnetization, the potential is (in Cartesian coordinates, with z positive downwards)

$$V(x,y,z) = \frac{\partial}{\partial k_0}\int_0^\infty \int_{-\infty}^{\infty}\int_{-\infty}^{\infty} \frac{M(\alpha,\beta,\gamma)}{d} d\alpha d\beta d\gamma \qquad (6.1.13)$$

where $\partial/\partial k_0$ is the derivative in the direction of **M**, and d is the source-observation distance:

$$d^2 = (x-\alpha)^2 + (y-\beta)^2 + (z-\gamma)^2 \qquad (6.1.14)$$

The α, β integral is a convolution, i.e.

$$\int_{-\infty}^{\infty}\int_{-\infty}^{\infty} \frac{M(\alpha,\beta,\gamma)}{d} d\alpha d\beta \equiv M(x,y,\gamma) * R(x,y,z-\gamma) \qquad (6.1.15)$$

where * denotes convolution and

$$R(x,y,z-\gamma) = \frac{1}{\sqrt{x^2+y^2+(z-\gamma)^2}} \qquad (6.1.16)$$

Hence the Fourier transform of V is

$$\tilde{V}(u,v,z) = \frac{\partial}{\partial k_0}\int_0^\infty \tilde{M}(u,v,\gamma)\cdot\tilde{R}(u,v,z-\gamma)d\gamma \qquad (6.1.17)$$

(6.1.17)

where

$$\tilde{M}(u,v,\gamma) = \int_{-\infty}^{\infty}\int_{-\infty}^{\infty} M(x,y,\gamma)e^{-i(ux+vy)}dxdy \qquad (6.1.18)$$

is the Fourier transform of M, using the tilde symbol to denote Fourier transformed quantities. The Fourier transform of R is

$$\int_{-\infty}^{\infty}\int_{-\infty}^{\infty} \frac{1}{\sqrt{x^2+y^2+(z-\gamma)^2}} e^{-i(ux+vy)}dxdy = 2\pi\frac{e^{(z-\gamma)\sqrt{u^2+v^2}}}{\sqrt{u^2+v^2}} \qquad (6.1.19)$$

and so

$$\tilde{V}(u,v,z) = 2\pi\frac{\partial}{\partial k_0}\int_0^\infty \tilde{M}(u,v,\gamma)\frac{e^{(z-\gamma)\sqrt{u^2+v^2}}}{\sqrt{u^2+v^2}}d\gamma \qquad (6.1.20)$$

Let (l,m,n) be the direction cosines of **M**. Then

$$\frac{\partial}{\partial k_0} = l\frac{\partial}{\partial x} + m\frac{\partial}{\partial y} + n\frac{\partial}{\partial z} \qquad (6.1.21)$$

But $\frac{\partial f}{\partial x} = iu\tilde{f}$ for any Fourier transform pair $f,\ \tilde{f}$ (and similarly for differentiation with respect to y). Hence

$$\tilde{V}(u,v,z) = 2\pi\frac{ilu+imv+n\sqrt{u^2+v^2}}{\sqrt{u^2+v^2}}\int_0^\infty \tilde{M}(u,v,\gamma)e^{(z-\gamma)\sqrt{u^2+v^2}}d\gamma \qquad (6.1.22)$$

We now need to relate the (Fourier transformed) potential V to the (Fourier transformed) component of the magnetic field being measured, usually that in the direction of **F**, which we take to have direction cosines (l',m',n'):

$$\Delta\tilde{T}(u,v,z) = 2\pi \frac{\left[ilu + imv + n\sqrt{u^2+v^2}\right]\left[il'u + im'v + n'\sqrt{u^2+v^2}\right]}{\sqrt{u^2+v^2}} \int_0^\infty \tilde{M}(u,v,\gamma) e^{(z-\gamma)\sqrt{u^2+v^2}} d\gamma \quad (6.1.23)$$

It is easily shown that $l = \cos I_F \cos D_F$, $m = \cos I_F \sin D_F$ and $n = \sin I_F$, where I_F and D_F denote the inclination and declination of the main field, respectively, and similarly for (l',m',n').

6.01.5.4.1 Analytic continuation

From (6.1.23) it follows straightforwardly that analytic (upward or downward) continuation involves convolving with a filter whose frequency response is e^{Hk}, i.e. multiplying by e^{Hk} in the wave number domain, where $k^2=u^2+v^2$ is the square of the wave number, and H is the continuation height or depth (also measured positive downwards). e^{Hk} is sometimes referred to as the analytic continuation operator. Thus downward continuation is an amplifying and roughening operation (conversely for upward continuation). This is analogous to the spherical case where the amplification factor is $\left(\frac{a}{r}\right)^{n+2}$, where here n is spherical harmonic degree. a is the reference radius of the spherical harmonic expansion, and r the analytic continuation radius. Examples of the uses of analytic continuation are to suppress or enhance short wavelength features, reduce data collected at a variety of altitudes (e.g. different flying heights for airborne surveys) to constant height, either above terrain or relative to mean sea level, compare ground and airborne observations, and estimate depth to sources (e.g. sections 6.01.5.4.6- 6.01.5.4.8 and 6.01.5.5.2).

6.01.5.4.2 Reduction to the pole

Reduction to the pole (RTP) is achieved by convolving with a filter whose frequency response is

$$\frac{\sqrt{u^2+v^2}}{ilu + imv + n\sqrt{u^2+v^2}} \cdot \frac{\sqrt{u^2+v^2}}{il'u + im'v + n'\sqrt{u^2+v^2}} \quad (6.1.24)$$

(the factor $\sqrt{u^2+v^2}$ in each term preserves dimensions), i.e. (6.1.24) is the RTP operator (or filter). It removes the factors in (6.1.23) associated with the direction of the main field and the direction of remanent magnetization. Its effect is to reduce the anomalies to those that would be observed at the magnetic North pole with a vertical remanent magnetization direction. If the remanent magnetization direction is unknown, or magnetization can be assumed to be purely induced, the direction cosines of

magnetization are replaced by those of the main field. RTP becomes unstable as the magnetic equator is approached since the numerator of (6.1.24) approaches zero (recall $n = \sin I_F$). At low magnetic latitudes, it is possible to perform reduction to the equator (RTE) instead, but the form of the resulting anomalies is not as simple as for RTP. In particular, anomalies are smeared in the east-west direction, making north-south trending boundaries or structures difficult to identify. Silva (1986) has treated reduction to the pole as an inverse problem, using methods designed for stabilizing inversion to stabilize RTP. Besides aiding interpretation through simplifying the form of the anomalies and centering them over their causative structures, RTP eases the comparison of oceanic magnetic anomalies at different latitudes.

6.01.5.4.3 Pseudogravity

The pseudogravity transformation follows from Poisson's relation between the magnetic potential and the gravitational field. Consider a body with uniform magnetization (both strength and direction) and density occupying a volume Ω. Then the magnetic scalar potential is

$$V(P) = -\mathbf{M} \cdot \nabla_P \int_\Omega \frac{1}{d} d\Omega \tag{6.1.25}$$

where P is the observation point, and d is distance from P, and the gravitational potential is

$$U(P) = G\rho \int_\Omega \frac{1}{d} d\Omega \tag{6.1.26}$$

where G is the gravitational constant. Combining the two,

$$V(P) = -\frac{1}{G\rho} \mathbf{M} \cdot \nabla_P U = -\frac{1}{G\rho} M g_M \tag{6.1.27}$$

where g_M is the component of gravity in the direction of **M**. (6.1.27) is Poisson's relation. In fact, it is not necessary for the potential and magnetization to be constant. We can consider a body to be composed of arbitrarily small volumes in which density and magnetization can be regarded as constant. Since potentials add, (6.1.27) applies to a body in which density and magnetization vary in proportion. However, pseudogravity is defined as the gravity anomaly that would be observed if the magnetization distribution were replaced by an identical density distribution, i.e. $\frac{M}{\rho}$ is a constant. In the wave number domain, this gives

$$\tilde{g}_M = C\tilde{V} \tag{6.1.28}$$

where $C = -\frac{G\rho}{M}$ is a constant. Converting from the magnetic potential to total field anomaly,

$$\tilde{g}_M = C \frac{1}{(il'u + im'v + n'\sqrt{u^2 + v^2})} \Delta\tilde{T} \tag{6.1.29}$$

Finally, converting from the component of gravity in the direction of **M** to the vertical component gives the Fourier-transformed pseudogravity, $\tilde{g}_{ps}$:

$$\tilde{g}_{ps} = C\frac{\sqrt{u^2+v^2}}{(ilu+imv+n\sqrt{u^2+v^2})(il'u+im'v+n'\sqrt{u^2+v^2})}\Delta\tilde{T} \qquad (6.1.30)$$

Thus the pseudogravity operator is

$$\frac{\sqrt{u^2+v^2}}{(ilu+imv+n\sqrt{u^2+v^2})(il'u+im'v+n'\sqrt{u^2+v^2})} \qquad (6.1.31)$$

Note that, unlike the expression for the RTP operator, there is only one factor $\sqrt{u^2+v^2}$ in the numerator of (6.1.31) because Poisson's relation (6.1.27) relates the magnetic scalar *potential* to the component of the gravitational *field* in the direction of magnetization. This means that the pseudogravity operator alters the frequency content of the signal, preferentially amplifying the longer wavelength components (in contrast to the spatial derivatives discussed in section 6.01.5.4.4, which preferentially amplify the shorter wavelength components). Like the RTP operator, it can run into problems at low magnetic field or magnetization inclinations. The constant C in (6.1.30) means we can predict the pattern (but not the amplitude) of the gravity anomalies that would be obtained over the same structure. The pseudogravity transformation aids the comparison of magnetic and gravity anomalies, allows gravity methods to be used to interpret magnetic anomalies, and can be used in conjunction with gravity data to determine the direction of magnetization and the ratio of magnetization to density (Cordell and Taylor, 1971). Note that Poisson's relationship provides an example of the ambiguity in magnetization modeling – there is no total field anomaly over a uniformly magnetized sheet (regardless of the direction of magnetization) since its gravity anomaly is constant. The result extends to a spherical geometry, where more complicated magnetization distributions can be shown to produce no external magnetic field (Runcorn, 1975). These magnetic annihilators are discussed more fully in section 6.01.5.6.

6.01.5.4.4 Spatial derivatives

Derivatives are useful for enhancing smaller scale features of a data set, and anomalies caused by shallow bodies, and directional derivatives for enhancing or suppressing features in a given direction. The second vertical derivative is valuable because it relates to second horizontal derivatives through Laplace's equation, which is satisfied by the total field anomaly as well as the scalar potential if the main field direction is constant. This involves multiplying $\Delta\tilde{T}$ by k^2 and is thus a significantly roughening operation. It is used to suppress regional gradients, and to aid in the determination of source depth and the attitude of interfaces. As noted above, differentiation with respect to x or y multiplies $\Delta\tilde{T}$ by iu or iv respectively. The horizontal derivative, i.e. the derivative in the direction of maximum change, therefore has a Fourier transform $k\Delta\tilde{T}$. This follows because

$$\nabla_H \Delta T = \frac{\partial \Delta T}{\partial x}\mathbf{i} + \frac{\partial \Delta T}{\partial y}\mathbf{j} \qquad (6.1.32)$$

where **i**, **j** are unit vectors in the x-, y-directions respectively. Thus in the wave number domain

$$\nabla_H \Delta\widetilde{T} = iu\Delta\widetilde{T}\mathbf{i} + iv\Delta\widetilde{T}\mathbf{j} \tag{6.1.33}$$

and hence

$$\left|\nabla_H \Delta\widetilde{T}\right| = \sqrt{\nabla_H \Delta\widetilde{T} * \nabla_H \Delta\widetilde{T}} = k\Delta\widetilde{T} \tag{6.1.34}$$

where here * denotes complex conjugate. First derivatives are also required in some methods of estimating depth to sources (see e.g. section 6.01.4.7). Directional derivatives, e.g. in the direction defined by an angle φ_0 with the x-axis, are obtained by taking the magnitude of $\cos\varphi_0$ times the x-derivative and $\sin\varphi_0$ times the y-derivative. Directions are preserved on Fourier transformation: since the wave vector **k** has components u and v in the x- and y-directions respectively, its magnitude is $\sqrt{u^2+v^2}$ and its phase is

$$\tan\varphi_0 = \frac{v}{u} = \frac{y}{x} \tag{6.1.35}$$

the latter by definition of φ_0. Thus the directional derivative enhances features making an angle φ_0 with the x-axis; to suppress them, but still improve the definition of smaller scale features, one could take the directional derivative in the orthogonal direction.

6.01.5.4.5 Pie-crust filter

An alternative method of eliminating anomalies in a particular direction is to use the pie-crust filter or operator, given by

$$W(\varphi) = \begin{cases} 0 & \left(\varphi_0 - \Delta\varphi < \varphi < \varphi_0 + \Delta\varphi\right) \\ 0 & \left(\varphi_0 - \Delta\varphi < \varphi + \pi < \varphi_0 + \Delta\varphi\right) \\ 1 & \left(otherwise\right) \end{cases} \tag{6.1.36}$$

This removes anomalies within an angle $\Delta\varphi$ either side of φ_0, and preserves those at all other angles, without altering the frequency content. Anomalies within this wedge can be preserved by swapping the values 0 and 1 in (6.1.36). A more sophisticated filter (with a taper between 0 and 1) would reduce ringing when the filtered anomalies are transformed back to the spatial domain.

6.01.5.4.6 Analytic signal

Another useful interpretational tool is the analytic signal, defined as

$$\mathbf{A}(x,y) = \frac{\partial\Delta T}{\partial x}\mathbf{i} + \frac{\partial\Delta T}{\partial y}\mathbf{j} + i\frac{\partial\Delta T}{\partial z}\mathbf{k} \tag{6.1.37}$$

where **i**, **j** and **k** are unit vectors in the x-, y- and z-directions respectively. The real and imaginary parts of its Fourier transform are the horizontal and vertical derivatives of ΔT, respectively. They form a Hilbert transform pair, as required for **A** to be an analytical signal, a property most easily demonstrated in the wave number domain (Roest et al., 1992). The amplitude of the analytic signal

$$\left|\mathbf{A}(x,y)\right|^2 = \sqrt{\left(\frac{\partial\Delta T}{\partial x}\right)^2 + \left(\frac{\partial\Delta T}{\partial y}\right)^2 + \left(\frac{\partial\Delta T}{\partial z}\right)^2} \tag{6.1.38}$$

is most often used for interpretation. It has maxima at magnetization contrasts, independent of the direction of the ambient magnetic field for 2-D sources and only weakly dependent on these directions for 3-D sources, offering a method for locating the edges of magnetized bodies. If the edges are assumed vertical, it can be used to determine depth to sources. Over a 2-D vertical contrast in magnetization at depth d, the amplitude of the analytic signal is proportional to $\frac{1}{x^2 + d^2}$ where x is the horizontal distance from the contact (Nabighian, 1972**)**. Thus the half-width of the curve gives *d*, the depth to the contrast. Automatic methods for finding the positions of maxima of quantities such as the analytic signal are given by Blakeley and Simpson (1986). Other boundary edge finding methods include the terracing operator of Cordell and McCafferty (1989) and the amplitude-of-horizontal-gradient method of Cordell and Grauch (1985).

6.01.5.4.7 Euler deconvolution

Euler's homogeneity equation can be written (e.g. Reid et al., 1990)

$$(x - x_0)\partial\Delta T / \partial x + (y - y_0)\partial\Delta T / \partial y + (z - z_0)\partial\Delta T / \partial z = -s_i \Delta T \qquad (6.1.39)$$

Here, (x,y,z) is the position at which the total field anomaly is ΔT, arising from a source at position (x_0,y_0,z_0). s_i is the 'structural index' (SI), a measure of the rate of fall-off of the field with distance, which therefore reflects the source geometry (Thompson, 1982). An SI of 3 corresponds to a point source (dipole), 2 is appropriate for extended line sources, such as pipes and cylinders, a value of 1 for a step, thin dike or sill edge, and values of 0.5 and 0 have been chosen for faults and other contacts. If s_i is set to zero, the right-hand side of (6.1.39) should be replaced by a constant, which depends on the amplitude of the contrast in magnetization, and the strike and dip of the contact (Reid et al., 1990).

Euler deconvolution (which is not strictly a deconvolution) has proved itself particularly useful in a regional context, when grids or profiles of data can be inverted systematically for source parameters and the background field (or the constant on the right-hand side of (6.1.39) when $s_i = 0$). As (6.1.39) shows, the method requires derivatives of ΔT, which are usually calculated in the wave number domain. These are treated as data (along with the SI) in an inversion for the source positions and background field (or right-hand side constant). Obtaining useful solutions depends on careful choice of the window size (i.e. how many adjacent points are included in a single least-squares type inversion). Each window produces a set of source parameters, and only those with standard deviations below a specified threshold are retained. Even these often plot as quasi-linear features ('strings of pearls'), i.e. the solutions tend to be defocused. This may be partly because a region often includes sources represented by more than one SI, and attempts have been made to develop a multiple source approach. Alternatively, it is possible to focus the solutions and determine appropriate structural indices, based on methods that apply similarity transforms to Euler's equation (e.g. Gerovska et al. 2010). Other approaches include methods of determining automatically, or also solving for, SI, e.g. wavelet-based

methods for estimating degree of homogeneity (Sailhac et al., 2000). The usual methods of damping and generalized inverses are useful in improving the performance of the method and interpretation of the results (e.g. Whaler et al., 1991; Mushayandebvu et al., 2004), but damping tends to bias depth estimates.

Several authors have pointed out that Euler deconvolution can be applied to any homogeneous field or function. This includes the horizontal gradient or analytic signal of a field that is itself homogeneous, e.g. the magnetic field, or its Hilbert transform; the appropriate SI for the horizontal gradient or analytic signal is then one larger than that of the original field source. The advantage of deconvolving the analytic signal rather than the magnetic field itself is that its calculation effectively removes the background field.

6.01.5.4.8. Tilt-depth method

Another popular interpretation techniqe providing both lateral and depth source information that depends only on first derivatives of the field is the tilt-depth method (Salem et al., 2008), a generalisation of the local phase (Miller and Singh, 1994; Verduzco et al., 2004). The tilt angle, or tilt derivative, is defined as

$$\theta = \tan^{-1}\left(\frac{\dfrac{\partial \Delta T}{\partial z}}{\dfrac{\partial \Delta T}{\partial H}}\right)$$

where $\dfrac{\partial \Delta T}{\partial H} = \sqrt{\left(\dfrac{\partial \Delta T}{\partial x}\right)^2 + \left(\dfrac{\partial \Delta T}{\partial y}\right)^2}$ denotes the horizontal derivative. It is independent of field strength and thus acts as an unbiased automatic-gain-control filter, preserving equally long and short wavelength anomalies. It is also independent of susceptibility contrast between the source and its surroundings but this (and strike) can be obtained by combined with e.g. the analytical signal. When applied to RTP anomaly fields to remove the inclination dependency, the tilt derivative vanishes over the edge of the source, and the depth can then be obtained from

$$\theta = \tan^{-1}\left(\frac{h}{z}\right)$$

where h is the distance from the contact (assumed vertical) and z is its depth. Thus, for instance, θ is ±45° at horizontal distances z from the source, and the two estimates can be averaged to account for non-vertical contacts and noise. Tilt-depth profiles for RTE data are the mirror image of their RTP equivalents (i.e. $\theta_{RTE} = -\theta_{RTP}$) so the same averaging provides the depth estimate in this case (Fairhead et al. 2011). However, whereas tilt angles calculated from RTP data are azimuthally symmetric, their RTE equivalents are more complex, making interpretation more difficult. Fairhead et al. (2011) caution against relying on zero tilt-depth contours of RTE anomalies to define the boundaries of structures or susceptibility contrasts.

6.01.5.5 Forward and inverse methods

Transformations assist in the characterization of certain features of the magnetic source, thereby facilitating interpretation. Forward and inverse methods take this characterization a step further, determining attributes of the magnetic source. Forward methods begin with one or more magnetic bodies whose salient features are selected a priori, on the basis of geologic or geophysical knowledge. Magnetic fields are then predicted for these bodies at the survey location, and model parameters are adjusted on the basis of the closeness of the fit to the observation. This process continues until a sufficiently close fit to the observations is achieved. Inverse methods, in contrast, allow for the direct determination of one or more attributes of the magnetic source, usually through least-squares or Fourier-transform techniques.

6.01.5.5.1 Forward models

Procedures for calculating magnetic forward models involve simplification of complex bodies into simpler ones, either as collections of rectangular prisms (Bhattacharyya, 1964), magnetic dipoles (Dyment and Arkani-Hamed, 1998), polygonal laminae (Talwani, 1965; Plouff, 1976), or polyhedrons (Bott, 1963). The calculation can be made either in the space or wave number domains. Parker (1973) gives a wave number domain based algorithm for the rapid calculation of the crustal magnetic field over sources defined by a magnetization contrast over a topographic surface.

6.01.5.5.2 Inverse approaches

Quantitative interpretations sought using an inverse approach aim to estimate the causative body's depth, dimension, and magnetization contrast. In many applications, depth to the magnetic source is the most important of these properties. Depth to source determinations are of two types, 1) based on the shape of individual anomalies (beginning with Peters, 1949), and 2) based on the statistical properties of ensembles of anomalies (beginning with Spector and Grant, 1970), and implemented in the spectral domain.

The first analytic approximation to determining the depth to source was by Werner (1955), who solved the problem under the assumption that the source was a thin dike. Subsequent work has relaxed that limitation, and allowed for other source geometries (Ku and Sharp, 1983). The exploitation of Euler's homogeneity relation (6.1.39) led to a second class of analytic approximations (Reid et al., 1990). This approximation allows for a variety of sources to be treated successfully, as outlined in section 6.01.5.4.7.

Wave number domain approaches to individual anomalies include the methods of Naudy (1971), applicable to a vertical dike or thin plate, and CompuDepth (O'Brien, 1972).

6.01.5.5.2.1 Fourier domain approaches to groups of anomalies

Matched Filters (Syberg, 1972; Phillips, 1997) use the Fourier-domain properties (Spector, 1968; Spector and Grant, 1970) of the magnetic field to estimate the depths of the principal sources. These depths are then used to design wavelength filters, which are in turn used to decompose observed magnetic anomalies into estimates of the anomalies

caused by sources at those principal depths. The original Spector and Grant (1970) method estimated the depth from the slope of the radially-averaged power spectrum.

6.01.5.6 Resolving interpretational ambiguity

Some of the ways for resolving or better understanding interpretational ambiguity include annihilators (Runcorn, 1975; Maus and Haak, 2003, Gubbins et al., 2011), ideal body analysis (Parker, 2003), Monte Carlo simulations (Sambridge and Mosegaard, 2002), and, of course, through the use of prior information.

It has long been known that an infinite sheet with constant magnetization produces no magnetic field outside of the sheet, although 2nd order effects usually ensure that some magnetic fields escape. Only magnetization contrasts produce magnetic fields. Runcorn (1975) demonstrated, in the case of the moon, that a spherical shell of constant susceptibility linearly magnetized by an arbitrary internal field also produces no field outside of the shell. More recently, Maus and Haak (2003) illustrated another class of magnetization solutions that produce no external fields. Their example, based on reasoning from spherical harmonics, is one defined by a magnetic susceptibility profile in a dipolar field that is symmetric about the magnetic equator. In the case of the Earth, South America and Africa are approximately bisected by the magnetic dipole equator, and their shape can be approximated fairly well by an annihilator. Thus, if these continents possess a large scale magnetic contrast with the surrounding ocean, much of that contrast may be invisible. Further inquiry (Gubbins et al., 2011) has revealed additional information on annihilators.

The theory of ideal bodies (Parker, 1974, 1975) systematizes the process of placing bounds on the parameters of the source region, such as the depth of burial (Grant and West, 1965). The process for doing this involves the minimization of the infinity norm of the magnetic intensity $|\mathbf{M}|$ within the source region. Parker (2003) showed how such a process could be used to determine the distribution of magnetization that has the smallest possible intensity, without any assumptions about its direction.

The Metropolis algorithm and the Gibbs sampler (Mosegaard and Sambridge, 2002) are Monte Carlo techniques for the exploration of the space of feasible solutions. They also provide measures of resolution and uncertainty. Although not widely used in the field of crustal magnetism, the Metropolis algorithm has been used by Rygaard-Hjalsted et al. (2000) to conduct resolution studies on fluid flow in the Earth's outer core from geomagnetic field observations. Monte Carlo techniques can also be used to find globally optimal solutions, and Dittmer and Szymanski (1995) have applied simulated annealing to magnetic and resistivity data.

6.01.6 Spectral Overlap with Other Fields

The transition from core-dominated to crust-dominated processes occurs as a relatively sharp break centered at spherical harmonic degree 14 (Alldredge et al., 1963; Cain et al.,

1974; Langel and Estes, 1982) corresponding to wavelengths of 40000/14 = 2860 km. This transition can be seen in a power spectrum

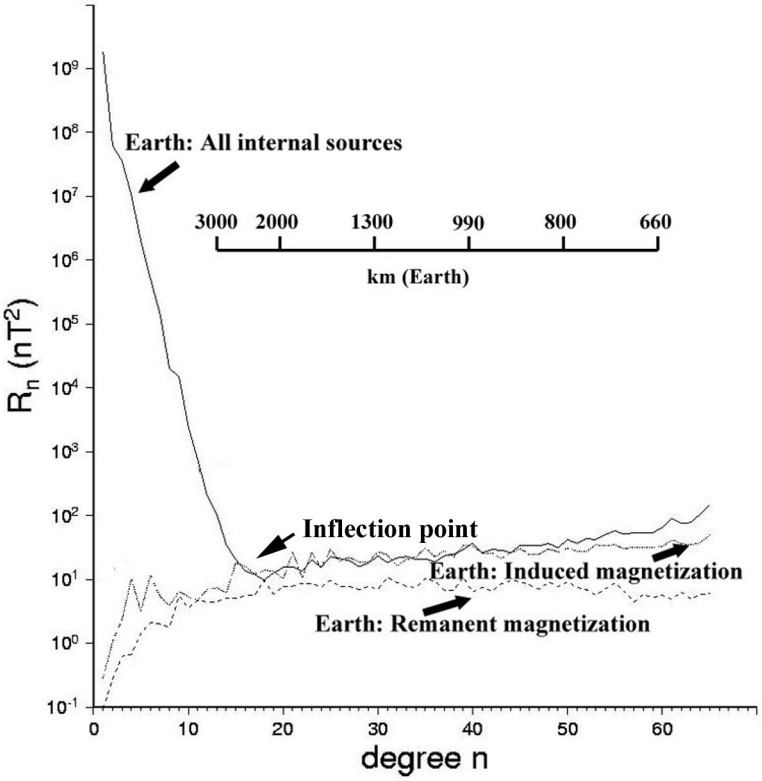

Figure 8. Comparison of the Lowes-Mauersberger (R_n) spectra at the surface of the Earth for a variety of internal fields. The inflection point in the terrestrial power spectra represents the sharp transition from core processes at low n to lithospheric processes at higher n. R_n is the mean square amplitude of the magnetic field over a sphere produced by harmonics of degree n. The spectrum of all internal sources comes from Sabaka et al. (2004), the induced spectrum is derived from Fox Maule et al. (2005), and the remanent magnetization spectrum (of the oceans, and hence a minimum value) was derived from Dyment and Arkani-Hamed (1998).

of the static field (Figure 8). The crustal field is much stronger over the continents than over the oceans (Arkani-Hamed and Strangway, 1986; Hinze et al., 1991, Beggan et al., 2013) and so we expect that the spectral overlap with the core field will be different for continental than for oceanic crust. The crustal field is expected to have power at wavelengths longer than degree 14 because of the markedly different characteristics of continental and oceanic crust (Meissner, 1986) and because of long-wavelength oceanic magnetic anomalies (Dyment and Arkani-Hamed, 1999). These longest wavelengths are masked by the dominant core fields (Hahn and Bosum, 1986), and various forward (Cohen, 1989) and inverse (Purucker et al, 1998, 2002) approaches have been developed in an attempt to include at least some notional idea of these fields. The longest wavelength crustal magnetic fields remain inaccessible to direct observation, although Mayhew and Estes (1983) suggest that simultaneous modeling of core and crustal fields using equivalent source dipole arrays located both within the core and crust might make possible the separation of the sources. The task they outlined is now computationally feasible (Purucker et al. 1996), but there are reasons for suspecting that a full separation may not be possible. For example, it is possible to represent magnetic fields of long

wavelength (say the dimension of a continent) by equivalent source dipoles placed either at the surface, or at the core-mantle boundary. A separation based solely on the radial position of the dipoles is thus likely to be ill-posed, and depend on details of the parameterization, such as the tessellation used, its spacing, and the distance over which the observations are expected to influence the crustal dipoles. The debate over the existence of field-aligned current systems (Dessler, 1986) shows the difficulty of interpreting physically an equivalent current/dipole system deduced solely from observations of the magnetic field.

On the other hand, coestimation of magnetic fields of internal and external origin through the 'comprehensive model' approach (Sabaka et al., 2002, 2004; Olsen et al., 2006a) has been successful because of the different decay characteristics of the internal and external fields (Langel et al., 1996). This approach utilizes magnetic field measurements from satellites (ionosphere, crust, and core are internal) and the surface (crust and core are internal), and does not separate the internal fields of core and crustal origin, lumping them instead into a spherical harmonic series from spherical harmonic degrees 1 through 60. These 'Comprehensive' models are now widely touted (Nabighian et al., 2005) to replace the existing International Geomagnetic Reference Field Models in many applications.

Another, qualitative, approach to separation is to characterize visually the field, and magnetization solutions deduced from that field, in the hope that features at small scales will provide clues into what is happening at the largest scales. Because of the wider spectral content of recent satellite crustal field models, Purucker and Whaler (2004) were able to recognize two patterns in the vertical component map (Figure 9) of the crustal field of the North American region.

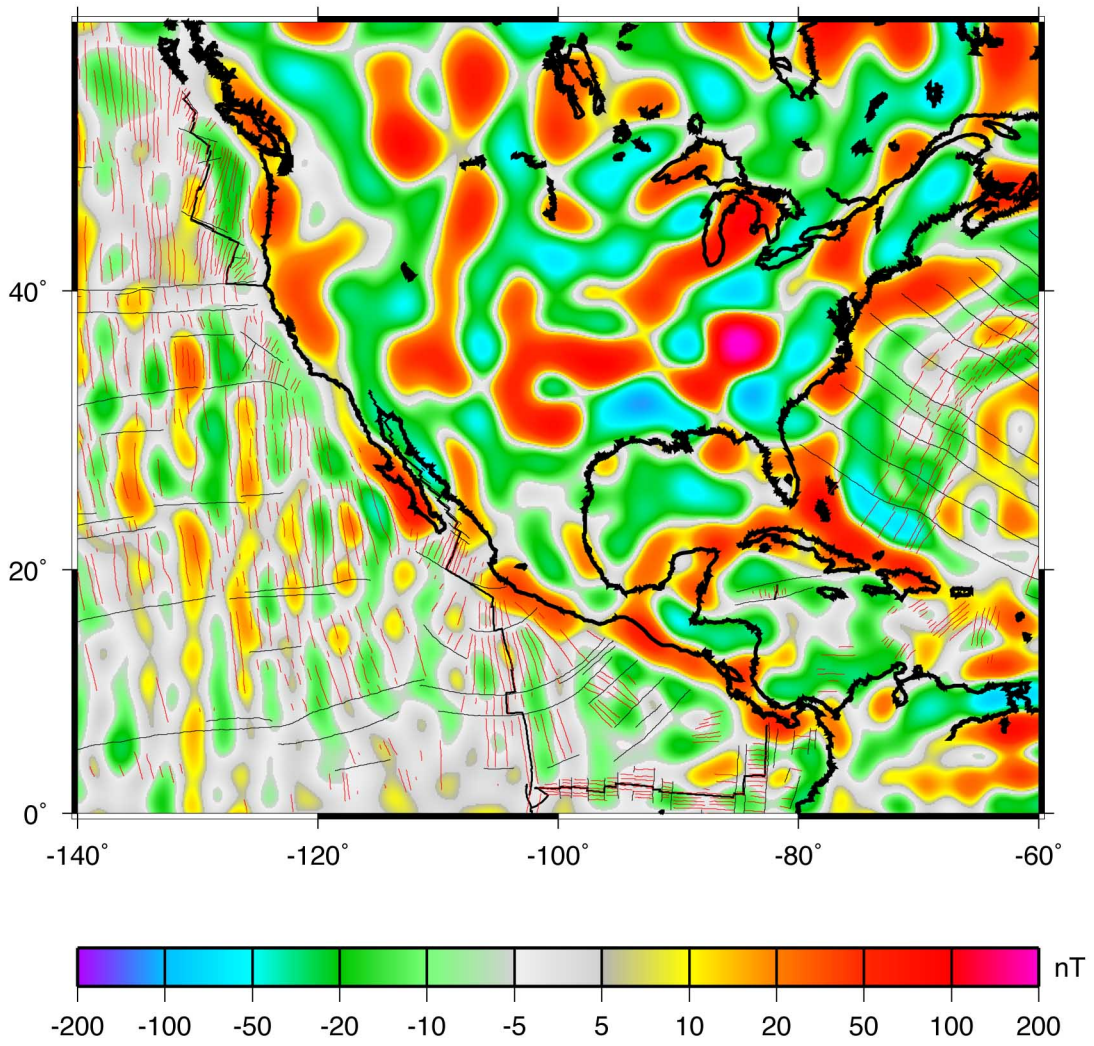

Figure 9. CHAOS-4**α** vertical field map of the crustal magnetic field (Olsen et al., 2006a; Olsen et al., 2010) over North America, evaluated at 50 km altitude.

The first pattern, which they refer to as 'C', encompasses the North American land mass, the Caribbean and Gulf of Mexico, and northernmost South America. The peak-to-trough magnitude of anomalies in 'C' typically exceeds 50 nT, and the anomalies are either equidimensional or oriented in a direction subparallel to the nearest coastline or tectonic element. The second pattern, which they refer to as 'O', encompasses the Eastern Pacific, the Cocos plate, and the western Atlantic away from continental North America. The peak-to-trough magnitude of anomalies in 'O' is typically less than 30 nT, and the anomalies are commonly narrow and elongate in the direction of the nearest spreading or subduction zone. The 'C' pattern can also be discerned on global maps of the field, when account is taken of the higher altitude. The 'C' pattern is characteristic of much of the Asian landmass, a region centered on but more extensive than Australia, and two broad regions within the African landmass. The 'O' pattern is seen in the eastern Pacific, the North and South Atlantic, and the Indian oceans. The 'C' and 'O' patterns are also

evident in a magnetization model based on these observations (Purucker and Whaler, 2004). A map of $|\mathbf{M}|$ shows these patterns best (Figure 10). Regions with magnetizations greater than 0.1 A/m (red regions on Figure 10 map) correspond to the 'C' pattern, and regions with magnetization less than 0.06 A/m (gray regions) correspond to the 'O' pattern.

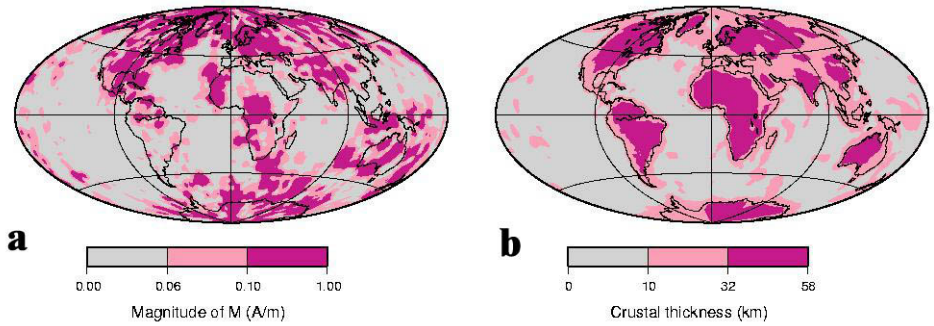

Figure 10. Map showing the magnitude (a) of the magnetization inferred from a model based on MF-3 (Maus et al., 2006), compared with a map of the magnetic crustal thickness (b) from Nataf and Ricard (1996).

Intermediate values of magnetization (between 0.06 and 0.1 A/m, pink on above map) generally envelop regions displaying the 'C' pattern. In a general way, the 'C' and 'O' patterns correspond to regions of thick and thin magnetic crustal thickness, as defined by temperature and seismology in the 3SMAC model (Nataf and Ricard, 1996). There are conspicuous exceptions to this generalization. Most of the South American landmass south of the Equator is characterized by the 'O' pattern, yet crustal thicknesses are typical of continental crust. The other major exception is the Sahara desert, again characterized by the 'O' pattern but with typical continental crustal thicknesses. In both of these regions, seismic crustal thickness and heat flow are poorly known.

Electrical conductivity contrasts (Grammatica and Tarits, 2002) and motional induction by ocean currents (Vivier et al., 2004) can also produce quasi-static magnetic fields that overlap with the crustal field. Specific time-variable features of these fields makes separation possible, but their low amplitude makes separation difficult in practice, and no separation has yet been achieved.

6.01.7 Separation of Induced and Remanent Magnetization

Separation of induced and remanent magnetization is a major outstanding issue. Induced magnetizations in the crust represent one of the largest time-variable geomagnetic fields of internal, non-core origin, and the separation of induced from remanent magnetization remains an area of active research. McLeod (1996) predicted that crustal-source secular variation should dominate core-source secular variation for spherical harmonic degrees in excess of 22. The separation of induced from remanent magnetization can be done without ambiguity only if the source material is available for rock magnetic tests (cf. Chapter 8), and if the time scale is specified. Although magnetizations are often

considered either remanent or induced, the distribution of magnetic coercivities in rocks is a continuous function, and viscous remanent magnetizations exist at all time scales.

Both the spatial variability of the static field as a function of inducing field, and an approach using time-variable geomagnetic fields as a probe, have been used to estimate induced magnetizations. Maus and Haak (2002) investigated the long-wavelength power of the crustal field as a function of magnetic dip latitude. Two of the crustal magnetic field models (Sabaka et al., 2002; Cain et al., 1989) they examined showed the strong trend with latitude expected for induced magnetization, while the third model (Arkani-Hamed et al., 1994) they examined was consistent with a purely remanent magnetization. It may be relevant that the models that were consistent with induced magnetization were models of both internal (core and crust) and external fields, while the model that was consistent with remanence was a crustal-only model that employed along-track filtering to remove non-crustal(?) long-wavelength trends. Maus and Haak (2002) also showed that, even in the case of a purely remanent magnetization, ΔT is expected to increase by a factor of two between the equator and the pole, while for a purely induced magnetization, ΔT is expected to increase by a factor of 32/3 (almost 11) between the equator and the pole. This is due to the preferential sampling of the weaker tangential part of the crustal field at the equator and the stronger radial part at the poles.

Approaches using time-variable geomagnetic fields can be either direct, using the change of the main geomagnetic field, or indirect, using an EM induction response (Goldstein and Ward, 1966; Yanovsky, 1938; Clark et al., 1998) to time variable fields like Sq or micropulsations. Lesur and Gubbins (2000) take a direct approach, with a regional study of 20 long-running European observatories. They calculate the difference between the observatory annual mean and the core field model of Bloxham and Jackson (1992). The variability with time of that difference, or observatory bias, was then examined to see if it was consistent with induced or remanent magnetization. They found that for nine observatories a time-dependent induced field fit the data better than a steady remanent field at the 99% confidence level. The other observatories yielded ambiguous results. Some external field signatures remain in observatory annual mean data, and only local distributions of induced and remanent magnetization were considered in the analysis. A global approach to observatory biases by Mandea and Langlais (2002), for observatories operating while the Magsat (1980) and Ørsted (2000) missions were in operation, while not attempting to isolate the remanent and induced components, illustrates some of the other difficulties that the direct approach entails. In addition to contamination by external fields, changes in observatory location or measurement practice add to the uncertainty. One can estimate the magnitude of the change in the observatory bias between the Magsat and Ørsted epochs, assuming that it is caused solely by changes in the induced magnetization. Values can be as large as 77 nT, with 14 of the 62 observatories having predicted changes in excess of 5 nT. Such a large signal over only 20 years should be measurable, assuming that it can be isolated. Although Mandea and Langlais (2002) determine the biases *a posteriori* the model generation, they could also be solved for in a model, as for example in the Comprehensive model of Sabaka et al. (2002).

The separation of induced and remanent magnetization can also be attempted from the spatial distribution of ΔT over isolated magnetic bodies (Zietz and Andreasen, 1967). Zietz and Andreasen (1967) used the position and relative intensity of the maximum and minimum anomaly to infer the declination and inclination of the magnetization vector in the causative body. Schnetzler and Taylor (1984) evaluated this technique globally, and found that the method was more sensitive at higher magnetic latitudes, and that due to zero level uncertainties, inclination was very difficult to estimate.

Glossary

Analytic Signal. A transformation formed through the combination of the horizontal and vertical gradients of a magnetic anomaly.

CHAMP. A low-earth orbiting satellite launched in 2001 designed to map the vector crustal magnetic field.

Crust (Lithosphere). The outer shell of the Earth formed by differentiation under the influence of temperature and gravity. The crust overlies the mantle, and the distinction can be expressed in terms of seismic velocities, rock density, rock type, mineralogy, chemical composition, or magnetic properties. The lithosphere, a rheological term, includes the crust, and the uppermost mantle.

Curie depth. The depth at which rocks lose their permanent and induced magnetism by virtue of their elevated temperature. The Curie depth is a function of the geothermal gradient within the Earth, and the magnetic mineralogy.

Curie temperature. The temperature at which a rock loses its permanent and induced magnetism.

Euler deconvolution method. A technique for estimating source positions for magnetic anomalies, which relates the magnetic field to its gradient through the specification of the arrangement of the magnetic sources.

Green's function. Used here to denote the relation of magnetization to magnetostatic potential.

Harmonic Spline. A local basis function employed in modeling the magnetic field.

International Geomagnetic Reference Field (IGRF). Values for the spherical harmonic coefficients from which the magnetic field can be calculated at any point in space and time. Each IGRF consists of a set of main field and secular variation coefficients covering a five-year interval, thereby accounting for the temporal evolution of the main field.

Koenigsberger ratio, Q, or Q-ratio. Expresses the relation between the strength of the induced and remanent magnetizations. It is given by $|\mathbf{M}_r| \div |\mathbf{M}_i|$. Hence, Q's greater than unity indicate dominance by remanent magnetization; Q's less than unity indicate dominance by induced magnetization.

Induced magnetization. One of two types of magnetization, the other being remanent. Induced magnetizations are proportional in magnitude and generally parallel to the ambient field **H.**

Magnetic basement. The top of a layer of more strongly magnetized rocks, usually igneous and/or metamorphic rocks, underlying more weakly magnetized sediments.

Magnetic susceptibility. Expresses the proportionality factor relating ambient field **H** to the induced magnetization.

Magnetite. Dominant magnetic mineral, often with some Ti, in the Earth's crust.

MAGSAT. The first satellite mission to map the Earth's vector magnetic field, including the long-wavelength crustal magnetic field.

Matched filter. Filter(s) that can then be used to decompose observed magnetic anomalies into estimates of the anomalies caused by sources at various depths. These depths are determined by a Fourier domain decomposition of the magnetic anomaly signal.

Observatory bias. The difference between the magnetic components measured at a magnetic observatory and those predicted by a geomagnetic model truncated at degree 13. This quantity is thought to reflect the higher degree crustal magnetic field contribution, in part.

Pseudogravity transformation. Converts a magnetic anomaly into the gravity anomaly that would be caused by a density distribution exactly proportional to the magnetization distribution.

Remanent magnetization. One of two types of magnetization, the other being induced. The direction and intensity of a remanent magnetization is dependent on the origin and history of a rock.

Reduction to pole (RTP). Transforms magnetic anomalies into the anomalies that would be caused by identical magnetic sources but with vertical magnetization and with measurement in a vertical magnetic field.

Spherical Slepian function. A local basis function employed in modeling the magnetic field.

Structural Index (SI). Expresses the rate of attenuation of a magnetic anomaly. This attenuation is a function of the source geometry.

Tilt angle. Inverse tangent of the ratio of vertical to horizontal field derivatives, used to solve for the lateral positions and depths of sources.

Total field anomaly. The signed scalar quantity, which is the most common measure of the Earth's crustal magnetic field.

Upward (downward) continuation. Transforms observed anomalies into the anomalies that would be observed at a higher (lower) altitude.

Werner deconvolution. A depth to basement technique that assumes the magnetic body has a specific geometry (dike-like), and solves for the depth to the top of the body based on four or more observations of the magnetic field over the body.

List of relevant websites

Software and Models

USGS potential field software http://pubs.usgs.gov/fs/fs-0076-95/FS076-95.html
Magnetic field models, Denmark http://www.dnsc.dk/Oested/Field_models
DTU field models at http://www.spacecenter.dk/files/magnetic-models/CHAOS-4
NGDC Magnetic field models at http://www.ngdc.noaa.gov/geomag .
SHTOOLS, at http://www.ipgp.fr/~wieczor/SHTOOLS/SHTOOLS.html.
Spherepack, at http://www.cisl.ucar.edu/css/software/spherepack.
GMT at http://gmt.soest.hawaii.edu.
Numerical Recipes at http://www.nr.com.
Spherical Slepian function software at
http://geoweb.princeton.edu/people/simons/software.html

Online applications

Planetary magnetic field evaluation at http://planetary-mag.net
IGRF at http://geomag.org
Atlas of Structural Geophysics at at http://virtualexplorer.com.au/special/noddyatlas

Acknowledgments

David Clark, Richard Gibson, Terence Sabaka, and an anonymous reviewer provided feedback through their edits. We further thank Terence Sabaka for discussions about the Comprehensive model, and Misac Nabighian, for providing additional references. We appreciate the patience of our editor, Masaru Kono. All graphs and maps have been plotted using the Generic Mapping Tools (GMT) software (Wessel and Smith 1998)

References

Achache J A, Abtout A, Le Mouël J L (1987). The downward continuation of MAGSAT crustal anomaly field over Southeast Asia. *J. Geophys. Res*. **92**, 11584-11596

Adams J C, Swarztrauber P N (1997). Spherepack 2.0: A model development facility, *NCAR Technical Note NCAR/TN-436-STR*

Alldredge L R, Vanvoorhis G D. Davis TM (1963). A magnetic profile around the world., *J. Geophys. Res*. **68** 3679-3692

Alldredge L R (1981). Rectangular harmonic analysis applied to the geomagnetic field. *J Geophys Res **86*** 3021-3026

Alldredge L R (1982). Geomagnetic local and regional harmonic analysis. *J Geophys Res* **87** 1921-1926

Andreasen G E, Zietz I (1969). Magnetic fields for a 4 X 6 prismatic model. *U. S. Geological Survey Professional Paper 666,* Washington DC

Arctic Gravity Project (2002). [http://earth-info.nga.mil/GandG/wgs84/agp/readme.html] 5' x 5' grids compiled by the International Association of Geodesy from airborne, survey, and submarine surveys.

Arkani-Hamed J, Strangway D (1986). Band-limited global scalar magnetic anomaly map of the Earth derived from Magsat data *J Geophys Res* **91** 8193-8203

Arkani-Hamed J, Langel R, Purucker M (1994). Scalar magnetic anomaly maps of Earth derived from POGO and Magsat data *J Geophys Res* **99** 24075-24090

Aspler L B Pilkington M Miles W F (2003). Interpretations of Precambrian basement based on recent aeromagnetic data, Mackenzie Valley, Northwest Territories. *Geol Sur. Of Canada Curr Research* **2003-C2,** 11 pp.

Aydin I Karat H I Kocak A (2005). Curie-point depth map of Turkey. *Geophys J Int* **162** 633-640

Bankey V Cuevas A Daniels D Finn C A Hernandez I Hill P Kucks R Miles W Pilkington M Roberts C Roest W Rystrom V Shearer S Snyder S Sweeney R Velez J (2002). Digital data grids for the magnetic anomaly map of North America, *USGS Open File Report 02-414* [http://pubs.usgs.gov/of/2002/ofr-02-414] [http://crustal.usgs.gov/geophysics]

Baranov V 1957 A new method for interpretation of aeromagnetic maps; pseudo-gravimetric anomalies. *Geophysics* **22** 359-383.

Baranov V Naudy H 1964 Numerical calculation of the formula of reduction to the magnetic pole. *Geophysics* **29,** 67-79.

Barbosa V C F Silva, J B C Medeiros W E 1999 Stability analysis and improvement of structural index estimation in Euler deconvolution. Geophysics **64**, 48-60.

Barritt S A Fairhead J D Misener D J (1993). The African Magnetic Mapping Project. *ITC Journal* 122-131

Bean R J (1966). A rapid graphing solution for the aeromagnetic anomaly of a two-dimensional tabular body. *Geophysics* **31** 963-970

Beggan, C.D., Saarimäki, J., Whaler, K.A, and Simons, F.J. (2013). Spectral and spatial decomposition of lithospheric magnetic field models using spherical Slepian functions, *Geophys. J. Int.* **193**, 136-148, doi:10.1093/gji/ggs122.

Bhattacharyya B K (1964). Magnetic anomalies due to prism-shaped bodies with arbitrary polarization. *Geophysics* **29**, 517-531.

Bhattacharyya B K (1965). Two-dimensional harmonic analysis as a tool for magnetic interpretation. *Geophysics* **30**, 829-857

Bhattacharyya B K (1966). Continuous spectrum of the total-magnetic-field anomaly due to a rectangular prismatic body. *Geophysics* **31**, 97-121

Bhattacharyya B K (1969). Bicubic spline interpolation as a method for treatment of potential field data. *Geophysics* **34**, 402-423.

Bhattacharyya B K (1980). A generalized multibody model for inversion of magnetic anomalies. *Geophysics* **45,** 255-270

Bhattacharyya B K Chan K C (1977a)., Reduction of magnetic and gravity data on an arbitrary surface acquired in a region of high topographic relief. *Geophysics* **42**, 1411-1430

Bhattacharyya B K Chan K C (1977b). Computation of gravity and magnetic anomalies due to inhomogeneous distribution of magnetization and density in a localized region. *Geophysics* **42,** 602-609

Blakely R J (1995) *Potential theory in gravity and magnetic applications,* Cambridge University Press, New York, NY

Blakely R J Connard G G (1989). Crustal studies using magnetic data. In: Pakiser L C, Mooney W D (eds.) *Geophysical framework of the continental United States*. Geological Society of America Memoir **172**, Boulder, Chap. 4, pp. 45-60

Blakely R J Wells R E Yelin T S Madin I P Beeson M H (1995). Tectonic setting of the Portland-Vancouver area, Oregon and Washington: Constraints from low-altitude aeromagnetic data: *Geological Society of America Bulletin*, **107**,1051-1062

Blakely R J Wells R E Tolan T L Beeson M H Trehu A M Liberty L M (2000). New aeromagnetic data reveal large strike-slip faults in the northern Willamette Valley, Oregon. *Geological Society of America Bulleti*n **112**, 1225-1233

Blakely R J Wells R E Weaver C S Johnson S Y (2002). Location, structure, and seismicity of the Seattle fault zone, Washington: Evidence from aeromagnetic anomalies, geologic mapping, and seismic-reflection data. *Geological Society of America Bulletin* **114**,169-177.

Blakely R J (1981). A program for rapidly computing the magnetic anomaly over digital topography. *U.S. Geological Survey Open File Report 81-298*.
Blakely R J (1988). Curie-temperature isotherm analysis and tectonic implications of aeromagnetic data from Nevada. *Journal of Geophysical Research* **93**, 11,817-11,832

Blakely R J Simpson R W (1986). Approximating edges of source bodies from magnetic or gravity anomalies. *Geophysics* **51** 1494-1498

Blakely R J Grauch V J S (1983). Magnetic models of crystalline terrane: Accounting for the effect of topography *Geophysics* **48**, 1551-1557
Blakely R J Jachens R C Simpson R W Couch R W (1985)., Tectonic setting of the southern Cascade Range as interpreted from its magnetic and gravity fields: *Geological Society of America Bulletin* **96**, 43-48
Blakely R J, Brocher T M, Wells R E (2005). Subduction zone magnetic anomalies and implications for hydrated forearc mantle, *Geol. Soc of Amer. Bull*. **33** 445-448.

Bloxham J, Jackson A (1992). Time-dependent mapping of the magnetic field at the core-mantle boundary. *J Geophys Res*. **97** 19537-19563

Bosum W Pucher R Roeser H (1985) Crustal anomalies and their causes. In: Fuchs K, Soffel H (eds.) *Geophysics of the Solid Earth, the Moon and the Planets*, Springer-Verlag, Berlin, Vol V2, Subvolume B, Chap 4.2.1, pp. 74-99

Bott M H P (1963). Two methods applicable to computers for evaluating magnetic anomalies due to finite three dimensional bodies. *Geophysical Prospecting* **11,** 292-299

Bouligand C, Glen J, Blakely R (2009). Mapping Curie temperature depth in the western United States with a fractal model for crustal magnetization. *J Geophys Res.* 114, B11104, doi:10.1029/2009JB006494.

Bucknam R C Hemphill-Haley E Leopold E B (1992). Abrupt uplift withn the past 1700 yr at southern Puget Sound. *Science* **258** 1611-1614.

Cain J C *et al.* (1974). An N=22 model of the geomagnetic feld. *EOS, Trans of the American Geophysical Union*, **56** 1108.

Cain J C *et al*. (1989). Derivation of a geomagnetic model to n=63. *Geophys. J.* **97**, 431-441

Cady, J.W (1980)., Calculation of gravity and magnetic anomalies of finite-length right polygonal prisms: Geophysics, **45**, 1507-1512.
Campos-Enriquez J O et al. Chicxulub - Subsurface structure of impact crater inferred from gravity and magnetic data. *The Leading Edge* **15** 357-359.

Caress D W, Parker R L (1989). Spectral interpolation and downward continuation of marine magnetic anomaly data. *J Geophys Res* **94** 17393-17407
Chavez Gomez S (2001). A catalogue of dykes from aeromagnetic surveys in eastern and southern Africa. *ITC publication # 80*.

Chenot D, Debeglia N (1990). Three-dimensional gravity or magnetic constrained depth inversion with lateral and vertical variation of contrast. *Geophysics* **55** 327-335.
Chinese National Aerogeophysics Survey and Remote Sensing Center (1989). Aeromagnetic Anomaly Map of China and Adjacent Sea, Geological Publishing House: Beijing (2nd digital edition in 2004)

Chulick G S, Mooney W D (2002). Seismic structure of the crust and uppermost mantle of North America and adjacent oceanic basins: a synthesis. *Bull. Seis. Soc. Am*. **92,** 2478-2492.

Clark D A (1997). Magnetic petrophysics and magnetic petrology; aids to geological interpretation of magnetic surveys. *AGSO Journal of Australian Geology and Geophysics* **17**, 83-103

Clark D A et al. (1998). Remote determination of magnetic properties and improved drill targeting of magnetic anomaly sources by differential vector magnetometry. *Expl. Geophy*. **29** 312-312

Clark D A (1999). Magnetic petrology of igneous intrusions: implications for exploration and magnetic interpretation. *Exploration Geophysics* **30**, 5-26

Clark S C, Frey H, Thomas H H (1985). Satellite magnetic anomalies over subduction zones *Geophys Res Lett* **12** 41-44

Cohen, Y. (1989). Traitements et interpretations de donnees spatiales in geomagnetisme: etude des variations laterales d'aimantation de la lithosphere terrestre, Docteur es sciences physiques thèse, Paris, 95 pp.

Coleman R. (1992). Project Magnet High-Level Vector Survey Data Reduction, in NASA Conf. Pub. 3153, Types and Characteristics of Data for Geomagnetic field modelling (Langel, R and Baldwin R, eds.), 1992, pp. 215-248.

Constable C G, Parker R. L (1988). Smoothing, splines and smoothing splines, *J. Comp. Phys.* **78**, 493-508
Cooper G R J, Cowan D R (2003). Sunshading geophysical data using fractional order horizontal gradients. *The Leading Edge* **22**, 204.

Cooper G R J (2003). Feature detection using sun shading. *Computers and Geosciences* **29** 941-948.

Cordell L Taylor P T (1971). Investigation of magnetization and density of a North Atlantic Seamount using Poisson's Theorem. *Geophysics* **36**, p. 919-937.

Cordell L (1992). A scattered equivalent-source method for the interpolation and gridding of potential-field data in three dimensions. *Geophysics* **57**, p.629-636.

Cordell L, McCafferty A E (1989). A terracing operator for physical property mapping with potential field data. *Geophysics* **54**, 621-634.

Cordell L, Grauch VJS (1985). Mapping basement magnetization zones from aeromagnetic data in the San Juan basin, New Mexico. In: Hinze W J (ed) *The utility of regional gravity and magnetic anomaly maps*. Society of Exploration Geophysicists, Tulsa, OK, pp. 181-197

Cowan D R, Cowan S (1993). Separation filtering applied to aeromagnetic data: Exploration Geophysics **24**, 429-436.
Cowan D R, Cooper G R J (2005). Enhancement of magnetic signatures of impact structures. In: Kenkmann T, Horz, F, Deutsch A (eds.) *Large Meteorite Impacts*. GSA Special Paper 384, Geol Soc of America., pp. 51-65.

Craig M 1996 Analytic signals for multivariate data. *Mathematical Geology*, **28**, 315-329.

Criss R E, Champion D E (1984). Magnetic properties of granitic rocks from the southern half of the Idaho Batholith: Influences of hydrothermal alteration and implications for aeromagnetic interpretations. *J. Geophys Res*. **89** 7061-7076.

Davies J, Mushayandebvu M.F, Smith R (2004). Magnetic detection and characterization of Tertiary and Quaternary buried channels: *SEG Expanded Abstracts*, **23**, 734.

Dentith M, Cowan D, Tompkins L (2000). Enhancement of subtle features in aeromagnetic data. *Exploration Geophysics*, **31**, 104-108.

De Santis, A (1991) Translated original spherical cap harmonic analysis, *Geophys. J. Int.*, **106**, 253-263

Dessler A J (1986). The evolution of arguments regarding the existence of field-aligned currents. In: Potemra T (ed) *Magnetospheric Currents*, Geophysical Monograph 28, American Geophysical Union, Washington, DC. 22-28

Dimri V P (1998)., Fractal behaviour and detectability limits of geophysical surveys, Geophysics **63**, 1943-1946.
Dittmer J K, Szymanski J E (1995). The stochastic inversion of magnetics and resistivity data using the simulated annealing algorithm. *Geophys. Prosp*. **43**(3), 397-416

Driscoll, J.R. and Healy, D.M. (1994). Computing Fourier transforms and convolutions on the 2-sphere. *Adv. Appl. Math* **15**, 202-250.

Dyment J, Arkani-Hamed J (1999). Contibution of lithospheric remanent magnetization to satellite magnetic anomalies over the world's oceans. *J. Geophys. Res* **103** 15423-15441.

Dyment J Arkani-Hamed, J. (1998). Equivalent source magnetic dipoles revisited. *Geophys Res. Lett* **25** 2003-2006.

Dyment, J., Hamoudi, M., Choi, Y. et al. (2012). Equivalent magnetization over the World Ocean. *EOS Fall meeting Abstracts*. T42B-01

Eaton D Vasudevan K. (2004). Skeletonization of aeromagnetic data. *Geophysics* **69,** 478-488.Elkins-Tanton L, Bowring S (2006). Report on the workshop on the Siberian flood basalts and the end-Permian extinction, NSF-sponsored workshop, Sept. 2005.

Ernst R E *et al*. (1996). Diabase (dolerite) dike swarms of the world: first edition, 1:35,000,000 map, 104 pp. *Geol. Surv. Can. Open File 3241*

Ernst R E, Buchan K L (1997). Giant radiating Dyke Swarms: Their Use in Identifying Pre-Mesozoic Large Igneous Provinces and Mantle Plumes. In: Mahoney J J, Coffin M F (eds.) *Large igneous provinces: continental, oceanic, and planetary flood volcanism*. Amer. Geophy. Union Monograph 100. Washington DC, pp. 297-333.

Ernst R E, Buchan K L (2001). The use of mafic dike swarms in identifiying and locating mantle plumes. In: Ernst R E, Buchan K L (eds). *Mantle Plumes: Their identification through time.* Geol Soc Amer. Spec. Paper 352, Boulder CO, pp. 247-265.

Erwin D E (1994). The Permo-Triassic extinction. *Nature* **367** 231-236.

Fairhead J D, Salem A, Cascone, L, Hammill, M, Masterton, S and Samson, E (2011). New developments of the magnetic tilt-depth method to improve structural mapping of sedimentary basins. *Geophysical Prospecting* **59**, 1072-1086.

Finn C. (1990). Geophysical Constraints on Washington Convergent Margin Structure, *Jour. Geophys. Res*. **95**, 19533-19546.

Fox Maule C, Purucker M, Olsen N, Mosegaard K (2005). Heat flux anomalies in Antarctica revealed by satellite magnetic data. *Science* **309**, 464-467

Fox Maule C, Purucker M, Olsen N, (2009). Inferring magnetic crustal thickness and geothermal heat flux from crustal magnetic field models, *Danish Climate Centre Report 09-09*, Danish Meteorological Institute, 33 pp.

Friis-Christensen E, Lühr H, Hulot G, Haagmans R, Purucker M (2009). Geomagnetic Research from Space, *EOS,* 90, 25, 213-214.

Frost B R, Shive P N (1989). Comment on "Limiting Depth of Magnetization in Cratonic Lithosphere". *Geophy Res Lett* **16** 477-479

Frost B R (1991a). Magnetic Petrology: Factors that control the occurrence of magnetite in crustal rocks. In: Lindsley D H (ed). *Oxide Minerals: Petrologic and Magnetic Significance*, v. 25. Mineralogical Society of America, Blacksburg, VA., Chap 14, pp. 489-509

Frost B R (1991b). Stability of Oxide Minerals in Metamorphic Rocks. In: Lindsley D H (ed). *Oxide Minerals: Petrologic and Magnetic Significance*, v. 25. Mineralogical Society of America, Blacksburg, VA, Chap 13, pp 469-488

Frost B R (1991c). Introduction to Oxygen Fugacity and its Petrologic Importance. In: Lindsley D H (ed). *Oxide Minerals: Petrologic and Magnetic Significance*, v. 25. Mineralogical Society of America, Blacksburg, VA., Chap 1., pp1-8

Gaina C, Werner SC, Saltus R, Maus S, and the CAMP-GM group, (2011). Circum-arctic mapping project: new magnetic and gravity anomaly maps of the Arctic, *Geol. Soc, London, Memoirs*, 35, 39-48, doi:10.1144/M35.3

Geol. Sur. of Canada (1995). Magnetic anomalies and tectonic elements of Northeast Eurasia. GSC Open-file report 2574

Geol. Sur. of Japan (2002). Magnetic anomaly map of East Asia. *Geol.Sur.Japan Digital Geoscience Map P-3, 2nd ed.*

Gerovska, D, Araúzo-Bravo, M J, Whaler, K, Stavrev, P and Reid, A (2010). Three-dimensional interpretation of magnetic and gravity anomalies using the finite difference similarity transform, *Geophysics*, **75**, L79 - L90

Getech (1996). [http://www.getech.com/data]

Gibson R I, Millegan P S (eds.) (1998) *Geologic applications of gravity and magnetics: case histories*. Soc. Expl. Geophy. Geophysical Reference Series 8, Tulsa, OK.

Gibson R I (1998a). Interpretation of Rift-stage Faulting in the West Siberian Basin from Magnetic Data. In: Gibson R I, Millegan P S (eds.) *Geologic applications of gravity and magnetics*. Expl. Geophy. Geophysical Reference Series 8, Tulsa, OK pp. 79-81.

Gibson R I (1998b). Gravity and Magnetics in Oil Exploration: A Historical Perspective. In:*Geologic applications of gravity and magnetics: case histories*. Soc. Expl. Geophy. Geophysical Reference Series 8, Tulsa, OK.

Girdler R W, Taylor P T, Frawley J J (1992). A possible impact origin for the Bangui magnetic anomaly (Central Africa). *Tectonophysics* **212** 45-58

Goldhaber MB Reynolds R L (1991). Relations among hydrocarbon reservoirs, epigenetic sulfidization, and rock magnetization: Examples from the south Texas coastal plain. *Geophysics* **56**, 748-757.

Goldstein N E Ward S H (1966). The separation of remanent from induced magnetism in situ. *Geophysics* **31** 779-796.

Golynsky A M *et al.* (2001). "ADMAP – Magnetic Anomaly Map of the Antarctic," 1:10 000 000 scale map, in Morris, P R, von Frese R, (eds.), BAS (Misc.) 10, Cambridge, British Antarctic Survey.

Golynsky, A.M., Bell, R., Blankenship, D., et al. (2013). Air and shipborne magnetic surveys of the Antarctic into the 21st century. *Tectonophysics* **585**, 3-12.

Goussev, S.A. Charters, R.A. Peirce, J.W.Glenn, W.E (2003). The Meter Reader - Jackpine magnetic anomaly: Identification of a buried meteorite impact structure. *The Leading Edge*, **22**, 740-741.

Grace J D, Hart G F (1990). Urengoy gas field—USSR West Siberian basin, Tyumen District. In: Beaumont E A, Foster N H (eds.) *Structural traps III, tectonic old and fault traps*. AAPG Treatise of Petroleum Geology, Atlas of Oil and Gas fields, Tulsa, Ok, A-109, p. 309-335.

Grant F S (1985). Aeromagnetics, geology and ore environments: In: Magnetite in igneous, sedimentary and metamorphic rocks: An overview: *Geoexploration* **23** 303-333.

Grant F S, West G F (1965). *Interpretation theory in applied geophysics*. McGraw-Hill, New York.

Grammatica N, Tarits P (2002). Contribution at satellite altitude of electromagnetically induced anomalies from a three-dimensional heterogeneously conducting Earth, using Sq as an inducing source field*: Geophys. J. Int*. **151** 913-923.

Grauch V J S (1987). A new variable-magnetization terrain correction method for aeromagnetic data. *Geophysics*, **52**, 94-107.

Grieve R, Therriault A (2000). Vredefort, Sudbury, Chicxulub: Three of a kind? *Annu. Rev. Earth Planet. Sci* **28** 305-338.

Grieve R, Reimold W, Morgan J, Riller U, Pilkington M (2008). Meteoritics and Planetary Science 43(5), 855-882.

Gubbins D and Herrero-Bervera E (eds) (2007). *Encyclopedia of Geomagnetism and Paleomagnetism*, Springer, Berlin, Germany, 1054 pp.

Gubbins, D., Ivers, D, Masterton, S.M., and Winch, D.E. (2011). Analysis of lithospheric magnetization in vector spherical harmonics. *Geophys. J. Int*, doi:10.1111/j.1365-246X.2011.5153.x.

Gunn P J (1975). Linear transformations of gravity and magnetic fields. *Geophys. Pros*. **23** 300-312.

Gunn P J (ed) (1997). Airborne magnetic and radiometric sureys. *AGSO J.* **17** #2.

Haggerty S E (1976). Opaque mineral oxides in terrestrial igneous rocks. In: Rumble D (ed.) *Oxide Minerals*, Mineralogical Society of America, Blacksburg, Vol 3., Chap 4., pp. 1-98.

Haggerty S E (1979). The aeromagnetic mineralogy of igneous rocks: Canadian Journal of Earth Sciences **16** 1281-1293.

Hahn, A., Ahrendt, H., Meyer, J Hufen J.H. (1984). A model of magnetic sources within the Earth's crust compatible with the field measured by the satellite Magsat, Geol. Jb., **A75**, 125-156.

Hahn A, Bosum W (1986). *Geomagnetics: Selected Examples and Case Histories*, Geopublication Associates, Berlin, Germany

Haines, G V (1985) Spherical cap harmonic analysis, *J. Geophys. Res.*, **90**, 2583-2591, doi: 10.1029/JB090iB03p02583

Hanna W F (ed) (1987). Geologic applications of modern aeromagnetic surveys. *USGS Bull. 1924*.

Hansen R O (1993). Interpretative gridding by anisotropic kriging. *Geophysics* **58**, 1491-1497.

Hansen, R. O. Miyazaki, Y (1984)., Continuation of potential fields between arbitrary surfaces: *Geophysics* **49,** 787-795.

Hansen, R. O., Suciu, L., (2002). Multiple-source Euler deconvolution. *Geophysics* **67,** 525-535.

Hansen R O (2005). 3D multiple-source Werner deconvolution for magnetic data. *Geophysics* **70** L45-L51

Hansen, R. O., and Pawlowski, R. S., (1989), Reduction to the pole at low latitudes by Wiener filtering, *Geophysics*, **54**, 1607-1613.

Hansen, R. O., and Simmonds, M., (1993) Multiple-source Werner deconvolution: Geophysics, **58**, 1792-1800.

Hansen, R. O.Wang, X. (1988) Simplified frequency-domain expressions for potential fields of arbitrary three-dimensional bodies. *Geophysics* **53**, 365-374.

Harrison C (1987). The crustal field. In: Jacobs J (ed.) *Geomagnetism,* Academic Press, London, Vol 1, Chap. 5, pp. 513-610

Heirtzler J R, Dickson G O, Herron E M, Pitman W C, Le Pichon X (1968). Marine magnetic anomalies, geomagnetic field reversals, and motions of the ocean floor and continents. *Jour Geophys Res* **73** 2119-2136

Hemant K, S. Maus (2005). Geological modeling of the new CHAMP magnetic anomaly maps using a Geographical Information System technique, *J. Geophys. Res.* **110** B12, doi:10.1029/2005JB003837

Hemant, K. Maus, S. (2005). Why no anomaly is visible over most of the continent-ocean boundary in the global crustal magnetic field, *Phys. Earth Plan. Int.* **149**, 321–333

Hernandez I, et al. (2001). Aeromagnetic map of Mexico: an exploration approach for the new millennium—A progress report. *Revista Geofisica* Instituto Panamericano de Geografia e Historia 55, 33 pp.

Hildebrand A R *et al*. (1991). Chicxulub crater: a possible Cretaceous-Tertiary boundary impact crater on the Yucatan peninsula. *Geology* **19** 867-871

Hill, P L (1991). Bibliographies and location maps of publications on aeromagnetic and aeroradiometric surveys. *U.S. Geological Survey Open-File Report 91-370A-F*, Reston, Virginia

Hinze W (1979). Continental magnetic anomalies. *Reviews of Geophysics and Space Physics* **17,** 257-273**.**

Hinze W J (ed) (1985). *The utility of regional gravity and magnetic anomaly maps*. Society of Exploration Geophysicists, Tulsa, OK.

Hinze W J, Zietz I (1985). The composite magnetic-anomaly map of the conterminous United States. In: Hinze W J (ed) *The utility of regional gravity and magnetic anomaly maps*. Society of Exploration Geophysicists, Tulsa, OK, pp. 1-24.

Hinze W *et al.* (1988). Magnetic anomaly map of North America. *The Leading Edge* **7** 19-21.

Hinze W, Von Frese R, Ravat D (1991). Mean magnetic contrast between oceans and continents. *Tectonophysics* **192** 117-127

Hinze W., Von Frese, R.B., Saad, A.H. (2013). *Gravity and Magnetic Exploration: Principles, Practices, and Application.* Cambridge, Cambridge University Press.

Hitzman M W, Oreskes N, Einaudi M T (1992). Geological characteristics and tectonic setting of Proterozoic iron oxide (Cu-U-Au-REE) deposits, *Precambrian Research* **58** 241-287.

Hood P J, McGrath P H, Teskey, D J (1985). Evolution of Geological Survey of Canada magnetic-anomaly maps: A Canadian perspective. In: Hinze W J (ed) *The utility of regional gravity and magnetic anomaly maps*. Society of Exploration Geophysicists, Tulsa, OK, pp. 62-87

Hornby, P., Boschetti, F.Horowitz, F. G., (1999). Analysis of Potential Field Data in the Wavelet Domain, *Geophys. Jour. Internat*., **137**, 175-196.

Hsu S-K, Sibuet J-C, Shyu C-T (1996). High-resolution detection of geologic boundaries from potential-field anomalies: An enhanced analytic signal technique. *Geophysics* **61**, 373-386.

Hsu S-K, Coppens D, Shyu C-T, (1998). Depth to magnetic source using the generalized analytic signal. *Geophysics* **63**, 1947-1957.

Hyndman R D, Peacock S M (2003). Serpentinization of the forearc mantle. *Earth and Plan. Sci. Lett.* **212** 417-432.

Ishihara S (1981). The granitoid series and mineralization. *Economic Geology 75th Anniversary Issue*, 458-484.

Ishihara T (2004). Application of CM3 model in compilation of marine magnetic anomaly data of North Pacific. *EOS Trans.AGU* **85** (47), Fall Meet. Suppl. Abstract GP11D-0882

Jackson, A (1990). Accounting for crustal magnetization in models of the core magnetic field. *Geophys. J. Int*. **103**, 657-673

Jackson A (1994). Statistical treatment of crustal magnetization *Geophys. J. Int*. **119**, 991-998

Jackson A (1996). Bounding the long wavelength crustal magnetic field *Phys. Earth Plan. Int*. **98**, 283-302

Jackson, D. D., (1972). Interpretation of inaccurate, insufficient and inconsistent data: *Geophys. Jour. Roy. Astr. Soc*., **28**, 97-109.

Jansen J, Witherly K (2004). The Tli Kwi Cho Kimberlite Complex, Northwest Territories, Canada: A Geophysical Case Study. *Soc. Expl. Geophy. 74st Annual Mtg Tech Prog* (Ext. Abstr), Denver, CO. **23** 1147-1149

Jessell, M.W., (2001). Three-dimensional modeling of potential-field data: *Computers & Geosciences*, **27**, 455-465.

Jessell, M.W., and Fractal Geophysics Pty Ltd, (2002). An atlas of structural geophysics II: Journal of the Virtual Explorer, **5**.

Johnson, S.Y., Dadisman, S.V., Mosher, D.C., Blakely, R.J. Childs, J.R., (2001). Active tectonics of the Devils Mountain fault and related structures, northern Puget Lowland and eastern Strait of Juan de Fuca region, Pacific Northwest: *U.S. Geological Survey Professional Paper 1643*, 45 p., 2 plates.

Johnson S Y et al. (1996) The southern Whidbey Island fault: An active structure in the Puget Lowland. *Geol Soc Amer. Bull*. **108** 334-354

Jourdan F, Fraud G, Bertrand H, Watkeys M K, Kampunzu A B, Le Gall B (2006). Basement control on dyke distribution in Large Igneous Provinces: Case study of the Karoo triple junction. *Earth Planet. Sci. Lett*. **241**, 307-322

Kanasewich., E. R. Agarwal, (1970). Analysis of combined gravity and magnetic fields in wavenumber domain: *Jour Geophys. Res*., **75**, 5702-5712.

Keating P, (1993). The fractal dimension of gravity data sets and its implication for gridding. *Geophysical Prospecting* **41**,983-994

Keating, P., (1995). A simple technique to identify magnetic anomalies due to kimberlite pipes: *Exploration Mining Geology*, **4**, 121-125.

Keating P Sailhac P, (2004). Use of the analytic signal to identify magnetic anomalies due to kimberlite pipes. *Geophysics* **69** 180-190.

Keating, P Zerbo, L., (1996). An improved technique for reduction-to-the-pole at low latitudes. *Geophysics*, **61,** 131-137.

Keller G R (1988). The development of gravity and magnetic studies, emphasizing articles published in the GSA Bulletin. *Geol. Soc. Amer. Bull*. **100** 469-478.

Kellogg, O.D., (1953). Foundations of Potential Theory: Dover.

Korhonen *et al*. (1993). One hundred seventy eight thousand petrophysical parameter determinations from the regional Petrophysical Programme . In: Autio, S. (ed.) Geological Survey of Finland, Current Research 1991-1992. Geological Survey of Finland. Special Paper 18, 137-141.

Korhonen et al. (2007). Magnetic anomaly map of the world, and associated DVD, Commission for the Geological Map of the World, UNESCO, Paris, France, Scale: 1:50,000,000.

Korte, M, Holme, R (2003). Regularization of spherical cap harmonics. *Geophys. J. Int.* **153**, 253-262.

Koulomzine T, Lamontagne Y, Nadeau A (1970). New methods for the direct interpretation of magnetic anomalies caused by inclined dikes of infinite length. *Geophysics* **35,** 812-830.

Krajick, K (2001). *Barren Lands: An epic search for diamonds in the North American Arctic*. Henry Hold, New York, NY

Ku C C, Sharp J A (1983). Werner deconvolution for automated magnetic interpretation and its refinement using Marquardt inverse modeling. *Geophysics* **48,** 754-774.

LaBrecque J L Ghidella M E (1997). Depth of magnetic basement, and sediment thickness estimates from aerogeophysical data over the western Weddell Basin. *J Geophys Res.* **102** 7929-7945

LaBrecque J L, Raymond C A, (1985). Seafloor spreading anomalies in the MAGSAT field of the North Atlantic, *J Geophys Res*. **90** 2565-2575.

Langel, R.A., Estes, R.H., (1982). A geomagnetic field spectrum, *Geophys. Res. Lett*., **9**, 250-253, 1982.

Langel R A, Slud V E, Smith P J (1984). Reduction of satellite magnetic anomaly data. *J Geophys*. **54** 207-212.

Langel R A *et al.* (1996). The near-Earth magnetic field from magnetospheric and quiet-day ionospheric sources and how it is modelled. *Phys. Earth Plan Int*. **98** 235-267

Langel R A et al (1993). The equatorial electrojet and associated currents as seen in the Magsat data. *Jour Atm. Terr. Phy*. **55**, 1233-1269

Langel R, Hinze W (1998). *The magnetic field of the Earth's lithosphere*, Cambridge University Press, Cambridge, UK

Langel R, Benson B V (1987). The Magsat bibliography. *NASA Tech Memo*. TM 87822.

Langlais B, Purucker M, Mandea M (2004). Crustal magnetic field of Mars. *J. Geophys Res*. **109** E02008 doi:10.1029/2003JE002048

Langlais B, Lesur V., Purucker M, Connerney J, Mandea M, (2009). Crustal magnetic field of terrestrial planets, *Space Science Reviews*, doi:10.1007/s11214-009-9557-y

Leaman D E (1994). Criteria for evaluation of potential field interpretations. *First Break* **12** 181-191.

LeSchack L A, Van Alstine D R (2002). High-resolution ground-magnetic (HRGM) and radiometric surveys for hydrocarbon exploration: Six case histories in Western Canada. In: Schumacher D, LeSchack L A (eds.) *Surface exploration case histories: Applications of geochemistry, magnetics, and remote sensing*. AAPG Studies in Geology No. 48 and SEG Geophysical Reference Series No. 11, Tulsa, Ok, pp. 67-156

Lesur V, Gubbins D (1999). Evaluation of fast spherical transforms for geophysical applications *Geophys J Int* **139** 547-555

Lesur V, Gubbins D (2000). Using geomagnetic secular variation to separate remanent and induced sources of the crustal magnetic field. *Geophys J Int*. **142** 889-897.

Lesur V, Maus S (2006). A global lithospheric magnetic field model with reduced noise in the Polar regions, *Geophys Res. Lett*. **33** doi:10.1029/2006GL025826

Li, Y. and Oldenburg, D. W., (1996). 3-D inversion of magnetic data. *Geophysics* **61,** 394-408.

Li, Y Oldenburg, D. W., (2003). Fast inversion of large-scale magnetic data using wavelet transforms and logarithmic barrier method. *Geophysical Journal International*, **152**, 251-265.

Li X (2003). On the use of different methods for estimating magnetic depth. *The Leading Edge* **22** 1090-1099

Lühr H, Maus S, Rother M (2004). Noon-time equatorial electrojet: Its spatial features as determined by the CHAMP satellite. *Journal of Geophysical Research* **109**, A01306, doi: 10.1029/2002JA009656

Lindsley D H (ed.) (1991). *Oxide Minerals: Petrologic and Magnetic Significance*, v. 25. Mineralogical Society of America, Blacksburg, VA.

Lowe, D.A.J., Parker, R.L., Purucker, M,E. Constable, C.G. (2001). Estimating the crustal power spectrum from vector Magsat data, *J. Geophys. Res.* **106**, 8589-8598

Machel H G, Burton E A (1991) Chemical and microbial processes causing anomalous magnetization in environments affected by hydrocarbon seepage. *Geophysics* **56** 598-605.

Makarova, Z. A. (Ed.). (1974). Map of the anomalous magnetic field of the Territory of the U.S.S.R. and adjacent marine areas, scale 1:2,500,000 (18 sheets), *U.S.S.R. Ministry of Geology*, VSEGEI, Leningrad.

Macnab R *et al.* (1995). New database documents the magnetic character of the Arctic and North Atlantic. *EOS, Transactions of the American Geophysical Union* **76** (45) 449-458

Macnae, J. C (1979). Kimberlites and exploration geophysics. *Geophysics*, **44**, 1395-1416.

Malin S R C, Duzgit Z, Baydemir N (1996). Rectangular harmonic analysis revisited. *J Geophys. Res.* **101** 28205-28209.

Mandea M, Langlais B, (2002). Observatory crustal magnetic biases during MAGSAT and Orsted satellite missions. *Geophys Res Lett* **29,** http**://**dx.doi.org/10.1029/2001GL013693

Mandea M, Purucker M (2005). Observing, Modeling, and Interpreting Magnetic Fields of the Solid Earth, *Surveys in Geophysics* http://dx.doi.org/10.1007/s10712-005-3857-x

Marsh J S (2005). DISCUSSION: The geophysical mapping of Mesozoic dyke swarms in southern Africa and their origin in the disruption of Gondwana. *J. Afr. Earth Sci* **35,** 525-527

Masterton, S.M., Gubbins, D., Muller, R.D., and Singh, K.H. (2013). Forward modelling of oceanic lithospheric magnetization, *Geophys. J. Int*, **192**, 951-962, doi:10.1093/gji/ggs063.

Maus, S. Haak, V. (2003) Magnetic field annihilators: invisible magnetisation at the magnetic equator. *Geophys. J. Int*. **155**, 509-513

Maus, S. Haak, V. (2002). Is the long wavelength crustal magnetic field dominated by induced or by remanent magnetisation? *J. Ind. Geophys. Union*, Vol. **6**,1-5

Maus, S., Gordon, D., Fairhead, J.D (1997). Curie temperature depth estimation using a self-similar magnetisation model, *Geophys. J. Int.* **129**,163-168

Maus, S., & Dimri, V.P (1996). Depth estimation from the scaling power spectrum of potential fields?, *Geophys. J. Int.* **124**,113-120

Maus, S., and Macmillan, S., (2005). 10th generation International Geomagnetic Reference Field: *EOS Transactions of the American Geophysical Union*, **86**, 159.

Maus, S et al. (2006). Earth's lithospheric magnetic field determined to spherical harmonic degree 90 from CHAMP satellite measurements. *Geophys. J. Int.* **164**, 319-330.

Maus, S et al. (2007). Fifth-generation lithospheric magnetic field model from CHAMP satellite measurements. *Geochem Geophys Geosyst* 8: doi: 10.1029/2006GC001521

Maus, S., Yin, F., Luhr, H., Manoj, C., Rother, M. et al. (2008). Resolution of direction of oceanic magnetic lineations by the sixth generation lithospheric magnetic field model from CHAMP satellite magnetic measurements. *Geochem. Geophys. Geosyst.* **9**: doi: 10.1029/2008GC001949.

Maus, S., Barckhausen, U., Berkenbosch, H. et al. (2009). EMAG2: A 2-arc min resolution Earth Magnetic Anomaly Grid compiled from satellite, airborne, and marine magnetic measurements, *Geochem. Geophys. Geosyst.* **10** (8), doi:10.1029/2009GC002471.

May P R (1971). Pattern of Triassic-Jurassic diabase dyks around the North Atlantic in context of predrift position of the continents. *Geol. Soc. Amer. Bull*. **82** 1285-1292.

Mayhew M (1982). Application of satellite magnetic anomaly data to Curie isotherm mapping. *J. Geophys. Res* **87**, 4846-4854

Mayhew M, LaBrecque J (1987). Crustal geologic studies with Magsat and surface magnetic data. *Reviews of Geophysics* **25**, 971-981

Mayhew M, Johnson B D, Wasilewski P J (1985). A review of problems and progress in studies of satellite magnetic anomalies. *J. Geophys. Res*. **90**, 2511-2522

Mayhew M, Johnson B D (1987). An equivalent layer magnetization model for Australia based on Magsat data. *Earth Planet. Sci. Lett*. **83**, 167-174

Mayhew M, Estes R (1983). Equivalent source modeling of the core magnetic field using Magsat data. *J Geomag. Geoelec.* **35**, 119-130

McEnroe S A, Brown L L (2000). A closer look at remanence-dominated anomalies: Rock-magnetic properties and magnetic mineralogy of the Russell Belt microcline-

sillmanite gneisses, Northwest Adirondacks Mountains, New York. *Journal of Geophysical Research* ***105*** 16,437-16,456.

McEnroe S A, Robinson P, Panish P (2001a). Aeromagnetic anomalies, magnetic petrology and rock magnetism of hemo-ilmenite- and magnetite-rich cumulates from the Sokndal Region, South Rogaland, Norway, *American Mineralogist* **86,** 1447-1468.

McEnroe S A *et al*. (2001b). Effect of fine-scale microstructures in titanohematite on the acquisition and stability of natural remanent magnetization in granulite facies metamorphic rocks, southwest Sweden: Implications for crustal magnetism, *J. Geophys. Res.* **106** 30523-30546.

McLeod M G (1996). Spatial and temporal power spectra of the geomagnetic field. *J Geophys. Res.* **101** 2745-2763.

Meissner R (1986). *The Continental Crust-A Geophysical Approach*, **Int. Geophys. Ser, 34**, Academic, San Diego, CA

Miller H.G. and Singh V. (1994). Potential field tilt: A new concept for location of potential field sources. *Journal of Applied Geophysics*, **32**, 213–217

Milligan P R, et al. (2005). Fourth edition Magnetic Anomaly Map of Australia, derived from a new-generation Magnetic Anomaly Grid Database of Australia (MAGDA), Int. Assoc. Geomag Aeronomy, IAGA2005-A-01186, Toulouse, France.

Milligan P R, Franklin R (2004). Magnetic anomaly map of Australia, Geoscience Australia, 1:25000000

Milligan PI, Minty BRS, Richardson M, Franklin R, (2009). The Australia-wide Airborne Geophysical Survey- accurate continental magnetic coverage, *Preview*, 138, 70.

Modisi, M.P., Atekwana, E.A., Kampunzu, A.B Ngwisanyi, T.H., (2000). Rift kinematics during the incipient stages of continental extension: Evidence from the nascent Okavango rift basin, northwest Botswana. *Geology*, **28**, 939-942.

Mooney W D, Laske G, Masters T G, (1998). Crust 5.1: A global crustal model at 5 x 5. *J. Geophys. Res*. **103** 727-748

Moreau, F., Gibert, D., Holschneider, M. Saracco, G., (1997). Wavelet analysis of potential fields: *Inverse Problems*, **13**, 165-178

Mosegaard K, Sambridge M (2002). Monte Carlo analysis of Inverse Problems. *Inverse Problems* **18**, R29-R54.

Mubu M S (1995). Aeromagnetic mapping and interpretation of mafic dyke swarms in southern Africa. MSc thesis, ITC Delft, Netherlands, 63 pp.

Mushayandebvu M F, van Driel P, Reid A B, Fairhead J D (2001). Magnetic source parameters of two-dimensional structures using extended Euler deconvolution. *Geophysics* **66,** 814-823.

Mushayandebvu, M F, Lesur V, Reid A B and Fairhead J D (2004). Grid Euler deconvolution with constraints for 2D structures. *Geophysics* **69**, 489-496.

Nabighian M N *et al* (2005). The historical development of the magnetic method in exploration. *Geophysics **70**, 33-61*

Nabighian M N, Asten M W (2002). Metalliferous mining geophysics-State of the art in the last decade of the century and the beginning of the new millennium. *Geophysics* **67** 964-978

Nabighian, M. N., (1972). The analytic signal of two-dimensional magnetic bodies with polygonal cross-section: Its properties and use for automated interpretation. *Geophysics*, **37**, 507-517.

Nabighian, M. N., (1984). Toward a three-dimensional automatic interpretation of potential field data via generalized Hilbert transforms: Fundamental relations: *Geophysics*, **49**, 780-786.

Nabighian, M. N. Hansen, R. O., (2001). Unification of Euler and Werner deconvolution in three dimensions via the generalized Hilbert transform: *Geophysics*, **66**, 1805-1810.

Nakagawa I, Yukutake T, (1985). Rectangular harmonic analysis of geomagnetic anomalies derived from Magsat data over the area of the Japanese islands. *J. Geomag. Geoelec* **37** 957-977

Naidu P. S., (1970). Fourier transform of large scale aeromagnetic field using a modified version of Fast Fourier Transform: *Pure and Applied Geophysics*, **81**, 17-25.

Nataf H, Ricard Y (1996). An a priori tomographic model of the upper mantle based on geophysical modelling. *Phys. Earth Planet. Int*. **95** 101-122.

Naudy H (1971). Automatic determination of depth on aeromagnetic profiles. *Geophysics* **36,** 717-722.

Nelson, J. B., (1988). Calculation of the magnetic gradient tensor from total field gradient measurements and its application to geophysical interpretation: *Geophysics*, **53**, 957-966.

Nicholas JB, Purucker ME, Johnson CL, Sabaka TJ, Olsen N, Sun Z, Al Asad M, Anderson BJ, Korth H, Slavin JA, Alexeev II, Belenkaya ES, Phillips RJ, Solomon SC, Lillis RJ, Langlais B, Winslow R, Russell CT, Dougherty MK, Zuber MT, (2011).

Magnetic fields of the solar system: A comparative planetology toolkit, GP21B-0992, Fall AGU meeting.

NGDC (1996). *Magnetic anomaly data of the former U.S.S.R.*, U.S. Naval Oceanographic Office, in collaboration with the Ministry of Geology of the U.S.S.R, 1 CD-ROM

O'Brien D P (1973) CompuDepth – new method for depth-to-magnetic-basement computation, *Geophysics*, **38**, 187, *Soc. Expl. Geophy. 42nd Annual Mtg Tech Prog* (Abstr), Anaheim, CA

O'Brien M S, Parker R L (1994). Regularized geomagnetic field modeling using monopoles, *Geophys. J. Internat* **118***,* 566-578

O'Connell MD *et al*. (2005). Gridding aeromagnetic data using longitudinal and transverse gradients with the minimum curvature operator. *The Leading Edge* **24**, 142-145.

Olsen KB, Stephenson WJ, Geisselmeyer A, (2007). 3D crustal structure and long-period ground motions from a M9.0 megathrust earthquake in the Pacific Northwest region, J Seismol., DOI: 10.1007/s10950-007-9082-y.

Olsen N, Lühr H, Sabaka T J, Mandea M, Rother M, Toffner-Clausen, L, Choi, S, *(*2006a). CHAOS-A model of Earth's magnetic field derived from CHAMP, Orsted, and SAC-C magnetic field data, *Geophys. J. Int*, **166** 67-75

Olsen N *et al.* (2006b). The Swarm end-to-end mission simulator study: A demonstration of separating the various contributions to Earth's magnetic field using synthetic data, *Earth Planets Space*, **58** 359-370

Olsen N, Luehr H, Sabaka T, Michaelis I, Rauberg J, Toffner-Clausen, L, (2010). CHAOS-4 – A high resolution geomagnetic field model derived from low-altitude CHAMP data, *AGU Fall Meeting 2010*, San Francisco, Poster GP21A-0992.

Parker R L, O'Brien M S (1997). Spectral analysis of vector magnetic field profiles *J. Geophys. Res.* **102**, 24815-24822

Parker R L (1997). Coherence of signals from magnetometers on parallel paths. *J. Geophys. Res* **102**, 5111-5117

Parker, R. L (1988). A statistical theory of seamount magnetism. *J. Geophys. Res.* **93**, 3105-3115

Parker R L, Shure L, Hildebrand J (1987). The application of inverse theory to seamount magnetism. *Rev. Geophys.,* **25**, 17-40

Parker R L, Shure L (1985). Gravitational and magnetic fields of some simple solids of revolution. *Geophys. J. R. Astron. Soc.* **80**, 631-647

Parker R L, Shure L (1982). Efficient modeling of the earth's magnetic field with harmonic splines. *Geophysical Research Letters* **9**, 812-815

Parker R L (1986). Harmonic splines in geomagnetism, in *Function Estimation, Am. Math. Soc. Proc., Contemporary Mathematics.* **59**, 63-76

Parker R L (1991). A theory of ideal bodies for seamount magnetism, *J. Geophys. Res.* **96** 16101-16112

Parker R L (1973). The rapid calculation of potential anomalies. *Geophys. J. Roy. Astr. Soc.*, **31**, 447-455.

Parker R L (1972). Inverse theory with grossly inadequate data. *Geophys. J. R. astr. Soc.,* ***29*****,** 123-138

Parker R L (1974). Best bounds on density and depth from gravity data, *Geophysics* **39**, 644-649.

Parker R L (1975). The theory of ideal bodies for gravity interpretation. *Geophys. J. Roy. Astro. Soc* **42** 315-334

Parker R L (2003). Ideal bodies for Mars magnetics. *J. Geophys. Res.* **108**, E1, 5006, doi:10.1029/2001JE001760

Parker R L, Huestis S P (1974). Inversion of magnetic anomalies in the presence of topography. *Journal of Geophysical Research*, **79,** 1587-1593.

Parker R L, Klitgord K D (1972). Magnetic upward continuation from an uneven track: *Geophysics* **37**, 662-668.

Paterson N R, Reeves C V (1985). Applications of gravity and magnetic surveys: The state-of-the-art in 1985 *Geophysics* **50** 2558-2594

Pedersen, L.B., (1977). Interpretation of potential field data - A generalized inverse approach: *Geophysical Prospecting*, **25,** 199-230.

Pedersen, L. B., (1979). Constrained inversion of potential field data: *Geophysical Prospecting,* **27,** 726-748

Pedersen, L. B., (1978). Wavenumber domain expressions for potential fields from arbitrary 2-, 2½-, and 3-dimensional bodies: *Geophysics*, **43**, 626-630.

Pedersen, L. B.Rasmussen, T. M., (1990). The gradient tensor of potential field anomalies: Some implications on data collection and data processing of maps: *Geophysics*, **55**, 1558-1566.

Pedersen, L. B., (1991). Relations between potential fields and some equivalent sources: *Geophysics*, **56**, 961-971.

Penfield G T, Camargo Z A (1981). Definition of a major igneous zone in the central Yucatan with aeromagnetics and gravity. *Soc. Expl. Geophy. 51st Annual Mtg Tech Prog* (Abstr), 37 Los Angeles, CA.

Peters L J (1949). The direct approach to magnetic interpretation and its practical application. *Geophysics* **14** 290-320

Phillips JD Reynolds RL Frey H (1991). Crustal structure interpreted from magnetic anomalies *Reviews of Geophysics Supplement* 416-427.

Phillips J D (1997). Potential-field geophysical software for the PC-version 2.2. U.S. Geological Survey Open-File Report 97-725, 34 pp

Pilkington M, Grieve R A F (1992). The geophysical signature of terrestrial impact craters *Reviews of Geophysics* **30** 161-181

Pilkington, M, Todoeschuck J P (1995). Scaling nature of crustal susceptibilities *Geophys. Res. Lett* **22** 779-782

Pilkington, M., (1997). 3-D magnetic imaging using conjugate gradients: *Geophysics*, **62,** 1132-1142.

Pilkington, M. Crossley, D. J., (1986). Determination of crustal interface topography from potential fields: *Geophysics*, **51**, 1277-1284.

Pilkington, M. Keating, P., (2004). Contact mapping from gridded magnetic data - a comparison of techniques: *Exploration Geophysics*, **35**, 306-311

Pilkington M, Hildebrand A R (2000). Three-dimensional magnetic imaging of the Chicxulub crater *J Geophys Res **105** 23,479-23,491*

Plouff, D., (1976). Gravity and magnetic fields of polygonal prisms and application to magnetic terrain corrections: *Geophysics*, **41**, 727-741.

Power M, Belcourt G, Rockel E (2004). Geophysical methods for kimberlite exploration in northern Canada. *The Leading Edge*, **23**, 1124-1129

Press W H, Teukolsky S A, Vetterling W T, Flannery B P (1992). Numerical Recipes in Fortran. The Art of Scientific Computing, 2nd edn. Cambridge Press, Cambridge, UK

Press W H, Teukolsky S A, Vetterling W T, Flannery B P (1996). Numerical Recipes in Fortran 90. The Art of Scientific Computing, Cambridge Press, Cambridge, UK

Press W H, Teukolsky S A, Vetterling W T, Flannery B P (1997). Numerical Recipes in C. The Art of Scientific Computing, 2nd edn. Cambridge Press, Cambridge, UK

Prieto, C. Morton G., (2003). New insights from a 3D earth model, deepwater Gulf of Mexico: *The Leading Edge*, **22**, 356-360

Primdahl F (2000). Resonance magnetometers In: Ripka P (ed), *Magnetic sensors and magnetometers*, Artech, Boston, p. 267-304

Prodehl C, Mooney WD (2012). Exploring the Earth's Crust: History and results of controlled source seismology, *Geol Soc. Of America Memoir 208*, 764 pp.

Purucker, M., R. Langel, M. Rajaram, and C. Raymond (1998). Global magnetization models with a priori information, *Journal of Geophysical Research*.**103**, 2563-2584

Purucker M, Von Frese R R B, Taylor P T (1999). Mapping and interpretation of satellite magnetic anomalies from POGO data over the Antarctic region. *Annali Di Geofisica* **42** 215-228

Purucker, M. Ishihara, T (2005). Magnetic images of the Sumatran region crust, *Transactions of the American Geophysical Union*, **86** (10) 101-102.

Purucker, M., Langlais, B., Olsen, N., Hulot, G., Mandea, M. (2002). The southern edge of cratonic North America: Evidence from new satellite magnetometer observations, *Geophys.Res.Lett*., **29**(15),8000, doi:10.1029/2001GL013645

Purucker, M., T. Sabaka, and R. Langel (1996). Conjugate Gradient Analysis: A New Tool For Studying Satellite Magnetic Data Sets, *Geophy Res Let*, **23**, 507-510

Purucker, M. (1990). The Computation of Vector Magnetic Anomalies: A Comparison of Techniques and Errors, *Physics of the Earth and Planetary Interiors*, **62**, 231-245

Purucker M, Mandea M (2005). New research directions based on the World Digital Magnetic Anomaly Map, and Swarm, Int. Assoc Geomag. Aeronomy Int. Meeting, Toulouse, France, 18-29 July 2005.

Purucker M, Whaler K (2004). Recognizing and interpreting the longest wavelength lithospheric magnetic fields obscured by overlap with the core field. *Eos Trans. AGU*, **85**(47), Fall Meeting Suppl. Abstract GP31A-0821

Purucker M, Clark D, (2011). Interpretation and mapping of the lithospheric magnetic field, (Mandea, M. and Korte, M., eds), in *Geomagnetic Observations and models*, IAGA Special Sopron book series 5, Springer, pp 311-338.

Purucker M, Head J, Wilson L, (2012). Magnetic signature of the lunar South Pole-Aitken basin: Character, origin and age, *J. Geophys. Res.* 117, E05001: doi: 10.1029/2011JE003922.

Purucker, M.E., Sabaka, T., Le, G., Slavin, J.A., Strangeway, R.J., and Busby, C. (2007). Magnetic field gradients from the ST-5 constellation: Improving magnetic and thermal models of the lithosphere, *Geophys. Res. Lett.* **34**, doi:10.1029/2007GL031739.

Quesnel, Y., Catalan, M. and Ishihara, T. (2009). A new global marine magnetic anomaly data set. *J. Geophys. Res.* **114**, B04106, doi:10.1029/2008JB006144.

Rasmussen, R Pedersen, L.B., (1979). End corrections in potential field modeling: *Geophysical Prospecting*, **27**, 749-760.

Ravat D (1996). Analysis of the Euler method and its applicability in environmental magnetic applications. *Journal of Environmental Engineering and Geophysics* **1** 229-238

Ravat, D., Whaler, K., Pilkington, M., Sabaka, T. Purucker, M. (2002). Compatibility of high-altitude aeromagnetic and satellite altitude magnetic anomalies over Canada, Geophysics, **67**, 546-554

Ravat, D., Hildenbrand, T.G. Roest, W., (2003). New way of processing near-surface magnetic data: The utility of the Comprehensive Model of the magnetic field: *The Leading Edge*, **22**, 784-785.

Ravat D, Finn C, Hill P, Kucks R, Phillips J, Blakely R, Bouligand C, Sabaka T, Elshayat A, Aref A, Elawadi E, (2009). A preliminary, full spectrum, magnetic anomaly grid of the United States with improved long wavelengths for studying continental dynamics: A website for distribution of data, USGS OF09-1258.

Ray R D (1985). Correction of systematic error in magnetic surveys: An application of ridge regression and sparse matrix theory. *Geophysics* **50**, 1721-1731

Reed LE, Witherly KE, (2007). 50 Years of Kimberlite Geophysics, A Review, Proceedings of Exploration 07: Fifth Decennial International Conference on Mineral Exploration (Milkereit, B, ed), 679-689.

Reeves C V, Erren H (1994). AAIME: Aeromagnetics of Arabia, India, and the Middle East, International Institute for Aerospace Survey and Earth Science, unpublished.

Reeves C V, Macnab R, Maschenkov S (1998). Compiling all the world' magnetic anomalies, *Eos Trans. AGU* **79** (28) 338-339

Reeves C V (2000). The geophysical mapping of Mesozoic dyke swarms in southern Africa and their origin in the disruption of Gondwana. *J. Afr. Earth Sci*. **30** 499-513

Reford S (2006). Gradient enhancement of the total magnetic field. *The Leading Edge* **25***,* 59-66.

Reichow M K et al. (2002). Ar-Ar Dates from the West Siberian Basin: Siberian Flood Basalt Province Doubled. *Science* **296** 1846-1849

Reid, A. B., (1980). Aeromagnetic survey design: *Geophysics*, **45**, 973-976.

Reid A B, Allsop J M, Granser H, Millett A J, Somerton I W (1990). Magnetic interpretation in three dimensions using Euler deconvolution. *Geophysics* **55**, 80-91.

Reynolds, R. L. *et al*., (1990a) Iron sulphide minerals at Cement oilfield, Oklahoma: implications for magnetic detection of oilfields: *Geol. Soc. Am. Bull*., **102**, 368-380.

Reynolds, R. L., *et al*., (1990b) Magnetic forward models of Cement oil field, Oklahoma, based on rock magnetic, geochemical and petrological constraints: *Geophysics*, **55**, 344-353.

Reynolds R L *et al*., (1990c) Rock magnetism, the distribution of magnetic minerals in the earth's crust, and aeromagnetic anomalies In: Hanna W F (ed), *Geologic Applications of Modern Aeromagnetic Surveys*, U S Geological Survey Bulletin 1924, Denver, CO, p. 24-45

Reynolds, R.L., Fishman, N.S. Hudson, M.R., (1991) Sources of aeromagnetic anomalies over Cement oil field (Oklahoma), Simpson oil field (Alaska), and the Wyoming-Idaho-Utah thrust belt: *Geophysics*, **56**, 606-617.

Reynolds R L et al. (1994). Magnetization and geochemistry of greigite-bearing Cretaceous strata, North Slope Basin, Alaska, *Amer. J. Sci*., **294** 485-528.

Ridsdill-Smith T A, Dentith M C (1999). The wavelet transform in aeromagnetic processing. *Geophysics* **64**, 1003-1013.

Rigoti, A., Padilha, A. L., Chamalaun, F. H., Trivedi, N. B., (2000). Effects of the equatorial electrojet on aeromagnetic data acquisition: *Geophysics*, **65**, 553-558.

Ripka P (2000). Fluxgate magnetometers In: Ripka P (ed), *Magnetic sensors and magnetometers*, Artech, Boston, p. 75-128

Robinson D et al, (2008). Advancing process-based watershed hydrological rsearch using near-surface geophysics: a vision for, and review of, electrical and magnetic geophysical methods, *Hydrol Process*, 22:3604-3635.

Roest, W.R., Verhoef, J.Pilkington, M., (1992). Magnetic interpretation using the 3-D analytic signal: *Geophysics*, **57**, 116-125.

Roest, W.R., Pilkington, M., (1993). Identifying remanent magnetization effects in magnetic data: *Geophysics*, **58**, 653-659.

Runcorn S K (1975). On the interpretation of lunar magnetism. *Phys Earth Plan. Int*. **10** 327-335

Rygaard-Hjalsted C, Mosegaard K, Olsen N (2000). Resolution studies of fluid flow models near the core-mantle boundary through Bayesian inversion of geomagnetic data. In: *Methods and Applications of Invrsion: Proc. IIC98 Conf. (Copenhagen, 1998)* eds. Hansen P C, Jacobsen B H, Mosegaard K, 255-275

Saad A H (1969). Magnetic properties of ultramafic rocks from Red Mountain, California. *Geophysics* **34** 974-987.

Sabaka, T.J., Olsen, N., Langel, R.A., (2002). A comprehensive model of the quiet-time, near-the-earth magnetic field: Phase 3: *Geophysical Journal International*, **151**, 32-68**.**

Sabaka, T.J., Olsen, N., Purucker, M.E., (2004). Extending Comprehensive Models of the Earth's magnetic field with Orsted and Champ data: *Geophysical Journal International*, **159**, 521-547.

Sailhac., P., Galdeano, A., Gibert, D., Moreau, F., Delor, C., (2000). Identification of sources of potential fields with the continuous wavelet transform: Complex wavelets and application to aeromagnetic profiles in French Guiana: *Jour. Geophys. Res*., **105,** 19455-19475.

Salem A, Ravat, D (2003). A combined analytic signal and Euler method (AN-EUL) for automatic interpretation of magnetic data. *Geophysics* **68,** 1952-1961.

Salem, A et al. (2008). Interpretation of magnetic data using tilt-angle derivatives, *Geophysics*, **73**, doi: 10.1190/1.2799992

Saltus R W et al., (2005). Utility of aeromagnetic studies for mapping of potentially active faults in two forearc basins: Puget Sound, Washington, and Cook Inlet, Alaska. *Earth Planets Space* **57** 781-793

Sambridge M, Mosegaard K (2002). Monte Carlo methods in geophysical inverse problems. *Rev. Geophysics* **40**, 1009, doi:10.1029/200RG00089

Schlinger CM (1985). Magnetization of lower crust and interpretation of regional magnetic anomalies-Example from Lofoten and Vesteraen, Norway. *J Geophys Res* **90** 1484-1504

Schnetzler C C, Taylor P T (1984). Evaluation of an observational method for estimation of remanent magnetization. *Geophysics* **49** 282-290.

Schnetzler C C, Taylor P T, Langel R A, Hinze W J, Phillips J D (1985). Comparison between the recent U.S. composite magnetic anomaly map and Magsat anomaly data. *J. Geophys Res* **90** 2543-2548.

Schott J J, Thébault E (2011). Modeling the earth's magnetic field from global to regional scales. (Mandea, M. and Korte, M., eds), in *Geomagnetic Observations and models*, IAGA Special Sopron book series 5, Springer, pp 229-264.

Sexton MA et al. (1995). The Mt Leyshon magnetic anomaly. *Expl. Geophy*. **26** 84-91

Shah A K *et al*. (2005). New surveys of the Chesapeake Bay impact structure suggest melt pockets and target-structure effect. *Geology* **33**, 417-420

Sharpton V L *et al*. (1992). New links between the Chicxulub impact structure and the Cretaceous/Tertiary boundary. *Nature* **359** 819-821

Shive PN *et al*. (1992). Magnetic properties of the lower crust in Fountain DM Arculus R Kay RW (eds)., **Continental Lower Crust**, Developments in Geotectonics 23 Elsevier, New York, 145-178.

Shuey, R.T. Pasquale, A.S., (1973). End corrections in magnetic profile interpretation: *Geophysics*, **38**, 507-512.

Shure L. Parker R L, Backus G E (1982). Harmonic splines for geomagnetic modelling. *Phys. Earth Planet. Inter.* **28**, 215-229

Siebert M, Meyer J (1996). Geomagnetic Activity Indices. In: Dieminger W, Hartmann G K, Leitinger R (eds.) *The Upper Atmosphere: Data Analysis and Interpretation*. Springer, Berlin, Chap V.3, pp. 887-911.

Silva J B C (1986). Reduction to the pole as an inverse problem and its application to low-latitude anomalies. *Geophysics* **51**, 369-382.

Silva J B C, Barbosa V C F, Medeiros W E (2001). Scattering, symmetry, and bias analysis of source position estimates in Euler deconvolution and its practical implications. *Geophysics* **66**, 1149-1156.

Silva J B C, Barbosa V C F (2003). 3D Euler deconvolution: Theoretical basis for automatically selecting good solutions. *Geophysics* **68**, 1962-1968.

Simons, F J, Dahlen, F A, Wieczorek, M A (2006). Spatiospectral concentration on a sphere. *SIAM Rev.*, **48**, 504-536

Sleep N H (2005). Evolution of the continental lithosphere. *Annu. Rev. Earth Planet. Sci*. **33** 369-393.

Smith W H F, Wessel P (1990). Griding with continuous curvature splines in tension. *Geophysics* **55,** 293-305

Snyder D B, Hobbs R W, Chicxulub Working Group, (1999). Ringed structural zones with deep roots formed by the Chicxulub impact. *J Geophys Res* **104** 10743-10755

Soederlund U, Hofmann A, Klausen M, Olsson J, Ernst R, Persson P (2010). Towards a complete magmatic barcode for the Zimbabwe craton: Baddeleyite U-Pb dating of regional dolerite dyke swarms and sill complexes, *Precambrian Research* **183**, 388-398.

Spector, A., (1968). *Spectral analysis of aeromagnetic data*: Ph.D. Thesis, University of Toronto.

Spector A, Grant F S (1970). Statistical models for interpreting aeromagnetic data. *Geophysics* **35** 293-302

Stockmann R, Finlay C C, Jackson A (2009) Imaging Earth's crustal magnetic field with satellite data: a regularized spherical triangle tesselation approach. *Geophys. J. Int.* **179** 929-944.

Syberg F G R (1972). A Fourier method for the regional-residual problem of potential fields. *Geophysical Prospecting* **20** 47-75.

Talwani M (1965). Computation with the aid of a digital computer of magnetic anomalies caused by bodies of arbitrary shape. *Geophysics* **30**, 797-817

Tanaka A, Okubo Y, Matsubayashi O (1999). Curie point depth based on spectrum analysis of the magnetic anomaly data in East and Southeast Asia. *Tectonophysics* **306** 461-470

Tarlowski C et al. (1996). Dewarping the composite aeromagnetic anomaly map of Australia using control traverses and base stations. *Geophysics* **61** 696-705

Taylor P T, Frawley J J (1986). Magsat anomaly data over the Kursk region, USSR. *Phys. Earth Plan. Int*. **45**, 5-15

Taylor P T, Ravat D (1995). An interpretation of the Magsat anomalies of central Europe. *Appl. Geophys*. **34**, 83-91

Teskey, D.J., Hood, P.J., Morley, L.W., Gibb, R.A., Sawatzky, P., Bower, M. Ready, E.E., (1993). The aeromagnetic survey program of the Geological Survey of Canada;

contribution to regional geological mapping and mineral exploration: *Canadian Journal of Earth Sciences*, **30**, 243-260.

Thébault, E., J. J. Schott, M. Mandea, and J. P. Hoffbeck (2004), A new proposal for spherical cap harmonic modelling, *Geophys. J. Int.*, **159**, 83–103.

Thébault E *et al*. (2006). Revised spherical cap harmonic analysis (R-SCHA): Validation and properties. *J Geophys Res* **111** doi:10.1029/2005JB003836.

Thébault E, Purucker M, Whaler K, Langlais B, Sabaka T, (2010). The magnetic field of the Earth's lithosphere, Space Science Reviews, 155:95-127, doi:10.1007/s11214-010-9667-6.

Thompson D T (1982). EULDPH-A technique for making computer-assisted depth estimates for magnetic data. *Geophysics* **47** 31-37

Thurston J B, Smith R S (1997). Automatic conversion of magnetic data to depth, dip, and susceptibility contrast using the SPI ™ method. *Geophysics* **62** 807-813.

Thurston, J. B., Smith, R. S. and Guillon, J-C., (2002). A multimodel method for depth estimation from magnetic data: *Geophysics*, **67,** 555-561.

Toft P B Haggerty S E (1988). Limiting depth of magnetization in cratonic lithosphere. *Geophys. Res. Lett*. **15** 530-533

Toft P B Haggerty S E (1989). Reply:Limiting depth of magnetization in cratonic lithosphere. *Geophys Res. Lett* **16** 480-482

Treitel, S., Clement, W.G. Kaul, R.K., (1971). The spectral determination of depths to buried magnetic basement rocks: *Geophysical Journal of the Royal Astronomical Society*, **24**, 415-428.

Trumbull, R B *et al*. (2004). Aeromagnetic mapping and reconnaissance geochemistry of the Earth Cretaceous Henties Bay-Outjo dike swarm, Etendeka Igneous Province. *J. Afr. Earth Sci* **40** 17-29

Vacquier, V., Steenland, N.C., Henderson, R.G. Zietz, I., (1951). Interpretation of aeromagnetic maps: Geological Society of America, Memoir 47.

Vallée, M. A., Keating, P., Smith, R. S., St-Hilaire, C., (2004). Estimating depth and model type using the continuous wavelet transform of magnetic data: *Geophysics*, **69** 191-199.

Vasicek J M, Frey H V, Thomas H H (1988). Satellite magnetic anomalies and the Middle America trench. *Tectonophysics* **154** 19-24

Verduzco B., Fairhead J.D., Green C.M. and MacKenzie C. (2004). New insights into magnetic derivatives for structural mapping. *The Leading Edge* **23**, 116–119

Vervelidou, F. (2013). Contribution à la modélisation et à l'interprétation multi-échelle du champ magnétique de la lithosphère terrestre, PhD thesis, Université Paris Diderot

Verhoef J *et al.* (1996). Magnetic anomalies of the Arctic and North Atlantic Oceans and adjacent land areas. *Geol Sur.Canada Open file Report 3125*, Dartmouth, Nova Scotia.

Verrier V, Rochette P (2002). Estimating peak currents at ground lightning impacts using remanent magnetization. *Geophys. Res. Lett*. **29** doi:10.1029/2002GL015207

Vine F J, Matthews D H (1963). Magnetic anomalies over oceanic ridges. *Nature* **199** 947-949

Vivier F, Maier-Reimer E, Tyler R H (2004). Simulations of magnetic fields generated by the Antarctic circumpolar current at satellite altitude: Can geomagnetic measurements be used to monitor the flow? *Geophys Res. Lett*. L10306, doi: 10.1029/2004GL019804

Von Frese R R B, Hinze W J, Olivier R, Bentley C R (1986). Regional magnetic anomaly constraints on continental breakup. *Geology* **14**, 68-71

Voorhies, C.V., Sabaka, T.J., Purucker, M. (2002). On magnetic spectra of Earth and Mars, *Journal of Geophysical Research-Planets*, **107**(E6), 5034, doi:10.1029/2001JE001534

Wang, X. Hansen, R. O., (1990). Inversion for magnetic anomalies of arbitrary three-dimensional bodies. *Geophysics*, **55,** 1321-1326.

Warner R D, Wasilewski P J (1997). Magnetic petrology of arc xenoliths from Japan and Aleutian Islands. *J Geophys Res* **102** 20225-20244

Wasilewski P J, Mayhew M A (1992). The Moho as a Magnetic Boundary Revisited. *Geophys. Res. Lett*. **19,** 2259-2262.

Weinberg R F, Hodkiewicz P F, Groves D I (2004). What controls gold distribution in Archean cratons? *Geology* **32**, 545-548

Wells R E, Weaver C S, Blakely R J (1998). Fore-arc migration in Cascadia and its neotectonic significance. *Geology* **26** 759-762

Werner, S., (1955). Interpretation of magnetic anomalies of sheet-like bodies, Sver. Geol. Undersok. Serv. C, Arsbok **43,** No. 6.

Wessell P, Smith W (1998). New, improved version of Generic Mapping Tools released. *EOS Trans AGU* **79**, 579

Whaler KA, Neil C and Reid, A B (1991). Extension to Euler's method for three-dimensional potential field interpretation, EAEG 53rd Meeting and Technical Exhibition, Florence, Italy. Expanded Abstracts, 416-417.
Whaler K A (1994). Downward continuation of Magsat lithospheric anomalies to the Earth's surface, *Geophys. J. Int*., **116** 267-278.

Whaler KA Langel RA (1996). Minimal crustal magnetizations from satellite data. *Phys. Earth Plan Int*. **48** 303-319

Whaler, K A, Langel, R A, Jackson, A & Purucker, M E, (1996). Non-uniqueness in magnetization: Crustal models from satellite magnetic data, *EOS Trans*. *AGU*, **77**, F172.

Whaler, K. Purucker, M. (2005). A spatially continuous magnetization model for Mars, *J. Geophys. Res*., Vol. **110**, No. E9, E09001, http://dx.doi.org/10.1029/2004JE002393

Wieczorek, M.A., Weiss, B.P, and Stewart, S.T. (2012). An Impactor Origin for Lunar Magnetic Anomalies, *Science* **335**, 1212-1215.

Wonik T *et al.* (2001). Magnetic anomaly map for northern, western, and eastern Europe. *Terra Nova* **13** 203-213

Yanovsky B M (1938). Variations in elements of terrestrial magnetism in an anomalous field. Trans (Trudy) Main Geophysical Observatory. **17(3)**

Zietz I, Andreasen G E (1967). Remanent magnetization and aeromagnetic interpretation: in Mining Geophysics, v. 2, Society of Expl. Geophys., Tulsa, OK, 569-590.

Zietz I, Bhattacharyya B K (1975). Magnetic anomalies over the continents and their analyses. *Reviews of Geophysics and Space Physics* **13** 176-215

Zietz I (1982). Composite magnetic anomaly map of the United States; Part A, conterminous United States: U.S. Geological Survey Geophysical Investigations Map GP-954-A, 59 pp, 2 sheets, scale 1:2,500,000.